Russian Original Vol. 39, No. 6, December, 1975

June, 1976

SATEAZ 39(6) 1035–1148 (1975)

SOVIET ATOMIC ENERGY

АТОМНАЯ ЭНЕРГИЯ
(ATOMNAYA ÉNERGIYA)

TRANSLATED FROM RUSSIAN

CONSULTANTS BUREAU, NEW YORK

SOVIET ATOMIC ENERGY

Soviet Atomic Energy is a cover-to-cover translation of *Atomnaya Énergiya*, a publication of the Academy of Sciences of the USSR.

An agreement with the Copyright Agency of the USSR (VAAP) makes available both advance copies of the Russian journal and original glossy photographs and artwork. This serves to decrease the necessary time lag between publication of the original and publication of the translation and helps to improve the quality of the latter. The translation began with the first issue of the Russian journal.

Consultants Bureau journals appear about six months after the publication of the original Russian issue. For bibliographic accuracy, the English issue published by Consultants Bureau carries the same number and date as the original Russian from which it was translated. For example, a Russian issue published in December will appear in a Consultants Bureau English translation about the following June, but the translation issue will carry the December date. When ordering any volume or particular issue of a Consultants Bureau journal, please specify the date and, where applicable, the volume and issue numbers of the original Russian. The material you will receive will be a translation of that Russian volume or issue.

Subscription
$87.50 per volume (6 Issues)

Single Issue: $50
Single Article: $15

Prices somewhat higher outside the United States.

CONSULTANTS BUREAU, NEW YORK AND LONDON

227 West 17th Street
New York, New York 10011

Published monthly. Second-class postage paid at Jamaica, New York 11431.

Soviet Atomic Energy is abstracted or indexed in *Applied Mechanics Reviews, Chemical Abstracts, Engineering Index, INSPEC—Physics Abstracts and Electrical and Electronics Abstracts, Current Contents,* and *Nuclear Science Abstracts.*

SOVIET ATOMIC ENERGY

A translation of *Atomnaya Énergiya*

June, 1976

Volume 39, Number 6 December, 1975

CONTENTS

CONTENTS

(continued)

The Russian press date (podpisano k pechati) of this issue was 11/25/1975. Publication therefore did not occur prior to this date, but must be assumed to have taken place reasonably soon thereafter.

ARTICLES

THE POSITION OF HYBRID REACTORS IN POWER-GENERATION SYSTEMS

I. N. Golovin

UDC 620.91

Thermonuclear reactors with a magnetic plasma containment, just like fission reactors, will produce electric power only in a thermal cycle. But in contrast from a fission reactor, a thermonuclear reactor requires electrical energy consumed not only on auxiliary needs. In a number of schemes, it is advantageous to expend a considerable part of all the electric power produced by a thermonuclear power station on sustaining the reaction. In the latter case, it is not possible to speak of a power station in the normal sense of the word, for the product of such a facility sold to the consumer is not electric power but plutonium or some other type of fuel, for example, hydrogen or chemical substances produced in intense neutron fields. Thermonuclear reactors containing uranium or thorium in the blanket and producing ^{239}Pu or ^{233}U are called hybrid reactors.

Thermonuclear reactors could occupy an important place in power generation only under the conditions that their utilization gives an economic advantage in comparison with the use of a few fission reactors.

Preliminary estimates of the capital costs on thermonuclear power station plants made in various countries, and in more detail in the USA, show their competitive capability with nuclear power stations. However, these estimates will remain incomplete and unreliable until the lapse of a considerable period of operation of the first experimental thermonuclear reactor. It can be shown that the advantages of thermonuclear reactors over nuclear reactors (lower total radioactivity, negligible fuel component cost of electric power, absence of the necessity for transporting fuel for reprocessing by regeneration for the removal of plutonium, short doubling period, etc.) will be insufficient for widespread industrial application in consequence of the significantly greater complexity. Actually, in nuclear reactors there are no such costly and "delicate" parts as, for example, superconducting magnet windings or fast atom injectors. However, only by installing and comparing in operation fusion and fission reactors can it be recognized which will predominate: merits or shortcomings. Therefore, the necessity for installing experimental thermonuclear reactors does not give rise to doubts.

"Pure" Reactors

The Steady-State Reactors. The fusion reactor most resembling a fission reactor in operating characteristics and which is the most suitable for industrial application would be one in which a once-ignited thermonuclear reaction would continue to "burn" for an unlimited length of time, with a continuous supply of cold fuel and with the continuous take-off of the "ash" – helium and protium. In principle, this is possible for a classical or neoclassical model of plasma containment with a magnetic field in closed magnetic traps when, in the gas blanket cycle and with a density near the wall of the gas mixture of deuterium and tritium (DT) equal to or greater than the plasma density on the axis of the trap, the heavy impurities and helium drift outside of the plasma, but the deuterons and tritons are fed toward the inside of the plasma by the same friction mechanism. However, this cycle has not yet been studied experimentally and it implies that the magnetic configuration exists in the steady state. For Tokamaks, this means that the steady maintenance of a current in the plasma has been achieved.

Such a reactor, first and foremost a steady-state Tokamak reactor, would be a brilliant solution to the thermonuclear problem. Unfortunately, on route to its creation there remains the greatest number of insolvable problems of physical principles.

Translated from Atomnaya Énergiya, Vol. 39, No. 6, pp. 379-386, December, 1975. Original article submitted May 16, 1975.

TABLE 1. Tokamak Reactors with Ignition ($n\tau_E = 3 \cdot 10^{14}$ sec/cm^3; $A = R/a = 4$; $T = 15$ keV; $\beta_\varphi = 1$; $q = 2.2$)

Parameters	Neoclassical		Empiricism		One-hundred Bohm periods	
Plasma density n, cm^{-3}	$3 \cdot 10^{13}$	$1 \cdot 10^{14}$	$3 \cdot 10^{13}$	$1 \cdot 10^{14}$	$3 \cdot 10^{13}$	$1 \cdot 10^{14}$
Plasma current I, MA	1,6	1,6	6,5	4,8	28	21
Plasma radius a, m	0,5	0,3	2,2	0,9	9,5	3,8
Reactor power P_T, MW	2,2	1,7	180	140	10 000	7600
Plasma volume V, m^3	10	0,8	800	70	44 000	3700
Neutron flux Φ, cm$^{-2} \cdot$ sec^{-1}	$0,15 \cdot 10^{13}$	$0,07 \cdot 10^{13}$	$0,6 \cdot 10^{13}$	$0,26 \cdot 10^{13}$	$2,4 \cdot 10^{13}$	$1,1 \cdot 10^{13}$
Toroidal field H, kOe	53	97	53	97	53	97

The major ones are:

1. The laws of extrapolation of $n\tau_E$ to the reactor temperature and plasma density ($n \approx 3 \cdot 10^{13}$-$3 \cdot 10^{14}$ cm^{-3} and $T \approx 10$-20 keV) are not known, and therefore it is not known what will be the dimensions of the reactor, the strength of the magnetic field, and the current in the plasma.

2. It is not known how the contamination of the plasma by impurities can be kept low, whether achieved in the gas blanket cycle, and some means of removing the impurities from the plasma, or blocking their path of penetration into the plasma.

3. There are only theoretical concepts for steady-state maintenance of current in the Tokamak plasma. There is no experimental verification. The third problem does not exist for Stellerators. The first two are common for any closed systems. For open traps, only the first problem has not been solved and there is no second and third problem.

If the Tokamak reactor operates by cycles, in which the DT mixture is ionized, heated up to ignition, and combustion takes place until the reaction is extinguished in consequence of fuel burnup or cooling of the plasma by the accumulated impurities, then the second problem is simplified and there is no requirement for a solution of the third problem.

Cyclic Tokamak Reactor. Construction of this reactor appears to be the simplest if the law of extrapolation of $n\tau_E$ is favorable.

Let us consider what the various laws of extrapolation of $n\tau_E$ give. Neoclassical theory gives the value of $n\tau_E$ which is most possible in principle. However, the theory of plasma stability predicts the development of instabilities in reactor cycles. There are theoretical discussions about the fact that the worst possible containment corresponds to τ_E of the order of one-hundred Bohm periods. As a third possibility, although unfounded, extrapolation of one of the empirical relations can be taken and verified in an accessible range of parameters on existing installations. These three laws of extrapolation are expressed by the formulas:

$$n\tau_E = \frac{1}{2} A^{1/2} T^{1/2} I^2 \text{ (neoclassical);}$$

$$n\tau_E = 0.7 \cdot 10^{-8} aIn \text{ (empirical);}$$

$$n\tau_E = 6.3 \cdot 10^{-7} aIn \frac{qA}{T} \text{ (hundred Bohm periods).}$$

(Here and in the future, current will be expressed in amperes, dimensions in cm, temperature and energy in electron volts, and time in seconds.) It is usually assumed that for ignition of the reaction, it is necessary that $n\tau_E > 1.5 \cdot 10^{14}$ sec/cm^3. However, assuming that the values given for n and T mean the average values over the cross section of the plasma, we can use for ignition, $n\tau_E = 3 \cdot 10^{14}$ sec/cm^3, as small impurities or accentuated density and temperature profiles reduce the value of $n\tau_E$ twofold. Therefore, the values of I, a, V, Φ, and P_T given in Table 1 must be considered as the minimum possible for each of the laws of extrapolation. Let us discuss the data in Table 1.

Neoclassical. If this law of extrapolation were valid, then it should be possible to achieve ignition on the currently existing installations T-10 (USSR) and PLT (USA), by raising the current in the plasma to the values shown in Table 1. However, with such small values of a and R, it is not possible to surround the vacuum chamber with a blanket and a shield of superconducting windings. By increasing a and keeping R/a and n unchanged, the current in the plasma should be increased many times in order to maintain equilibrium of the plasma. But this, in its turn, leads to an increase of $n\tau_E \sim I^2$. When $n\tau_E \gg 1.5 \cdot 10^{14}$, the plasma

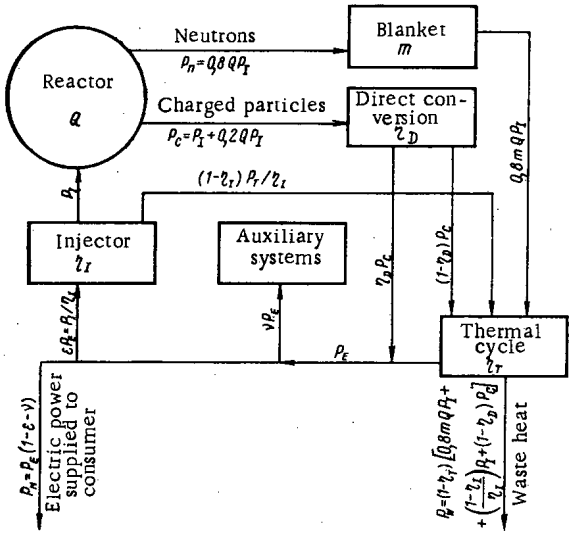

Fig. 1. Schematic diagram of a thermonuclear power station.

is thermally unstable. It is not known to what this instability can lead. Either with an increase of temperature and β_φ the loss of equilibrium will lead to such a reduction of $n\tau_E$ that thermal stability is automatically established, or the plasma will pass over to the relaxation cycle. In order to avoid these obscure phenomena, impurities can be mixed with the plasma at the start of heating in such quantity that $n\tau_E$ would not significantly exceed $1.5 \cdot 10^{14}$ sec/cm^3. In the explicit case with neoclassical containment, there is a free choice for the construction of a reactor and the probability that a technically sound reactor can be constructed in the not too distant future is high.

Empiricism. A reactor of impressive dimensions, but still a possibility, is obtained without falling outside the limits attainable with modern technology and the technology of the next decade, if its size is increased by a factor of two to three, so that there will be some reserve in $n\tau_E$ for ensuring combustion in the case of entry of impurities. The probability of building the reactor during the next two decades is less than in the first case.

One-Hundred Bohm Periods. The size and plasma current are so large that their increase exceeds the bounds of possibility technically achieved in the 20th century. Impurities in such a reactor are very dangerous. Thus, an impurity of 7% helium or 5% carbon will certainly extinguish the reaction. Incidentally, we note that in all experiments on Tokamaks, the plasma is considerably more contaminated and we do not yet know how to purify it. The probability of constructing such a reactor in the next decade is very low. In fact, in addition to the difficulties due to the dimensions and the danger of impurities in such a reactor, it is a very complicated problem to heat up the plasma to ignition, as a power of hundreds of megawatts must be injected into the plasma during a few seconds. There are no high-frequency generators with these parameters. In order to heat up the injections, injectors would have to be designed with atom energies in the megawatt range at a current of hundreds of amperes. The construction of such high-frequency generators or injectors would occupy many years.

Thus, if experiments confirm the feasibility of containment close to the empirical extrapolation or even better, then a cyclic reactor with ignition is achievable by means of modern technology. Under conditions of unimpeded entry of impurities or with diverters of the type discussed in the literature, this is a bad reactor as the time of buildup of the impurities, leading to extinction of the reaction, and the time of fuel burnup in it amounts to tens of seconds and these short cycles make difficult the construction of economically favorable thermonuclear power stations.

In the gas blanket cycle (if it exists), the duration of the working cycle is not limited by impurities of fuel burnup, which is supplied simply in the form of a gas with the surface of the plasma. The duration of the cycle, limited by the change of magnetic flux in the inductor, can reach at least thousands of seconds. Such a reactor already shows promise for industrial application.

Thus, if the laws of nature are favorable to us and the first two problems are solved successfully, then a cyclic Tokamak reactor can be constructed. With these same conditions, the Stellerator gives a steady-state reactor. The question as to whether a steady-state Stellerator reactor is a more profitable solution than a cyclic Tokamak reactor requires detailed analysis. The windings of the Stellerator are more expensive than in the Tokamak, but a power station with a Tokamak increases the cost of its cyclic operation at least because of the cost of the electrotechnical plant feeding the inductor. Cyclic operation of a Tokamak can be very costly if the first wall, which is subjected to intense radiation damage, will be destroyed rapidly because of thermal fatigue.

Reactors with Injection

Let us consider the feasibility of constructing reactors if the second and third problems are solved successfully, but the containment proves to be poor, i.e., worse than the empirical extrapolation. First of

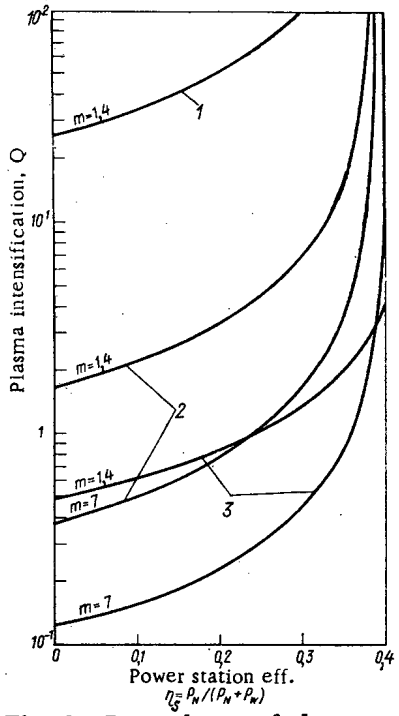

Fig. 2. Dependence of plasma intensification Q on the thermonuclear power station efficiency η_S for different types of reactors: 1, 2, 3) laser for closed and open reactors ($\eta_D = 0$, 0, 0.7 and $\eta_I =$ 0.05, 0.7, and 0.88, respectively); for all systems $\eta_T = 0.4$ and $\nu = 0.03$.

all, we recall that there is no third problem for Stellerators and there is no second or third problem for open reactors. The following analysis will be valid for all three versions: Tokamaks, Stellerators, and open reactors. It has already been mentioned repeatedly [1-3], that even with plasma containment at $n\tau_E < 1.5 \cdot 10^{14}$ sec/cm^3 the production of useful power nevertheless is possible in reactors with fast atom injection.

The schematic diagram of a power station with such a reactor is shown in Fig. 1. A power of P_I is injected into the plasma of the reactor by a beam of atoms. The thermonuclear reaction, with the release of 17.6 MeV/fission event increases the power by a factor Q, so that the neutrons carry a power of $0.8P_IQ$ from the plasma and in the blanket it is multiplied by a factor m, and a power of $P_I + 0.2P_IQ$ remains with the charged particles. The power $0.8P_IQm$ can be converted to electricity only in a thermal cycle with an efficiency of η_T via a stream generator and a turbine. The energy of the charged particles can be partially converted to electricity in a direct converter with efficiency η_D and part of it $(1-\eta_D)$ is converted to electricity in the thermal cycle with efficiency η_T. A fraction ε of electric power is expended on injection and a fraction ν on other inherent requirements of the power station.

A reactor with injection operates as a power booster. The plasma intensification Q depends on the containment of the plasma by the magnetic field. Formulas from which the intensification Q can be calculated are given in the appendix.

The most important characteristic of a power station is its total efficiency:

$$\eta_S = \frac{P_N}{P_N + P_W}, \tag{1}$$

where P_N is the electric power supplied to the consumer and P_W is the waste heat. It follows from Fig. 1 that

$$\begin{aligned} P_N &= (1-\varepsilon-\nu)\frac{P_I}{\eta_I}\{\eta_T + \eta_D\eta_I(1-\eta_T) + \\ &+ Q\eta_I[0.2(\eta_T + \eta_D - \eta_D\eta_T) + 0.8m\eta_T]\}, \\ P_W &= (1-\eta_T)\{1-\eta_D\eta_I + \\ &+ Q\eta_I[0.8m + 0.2(1-\eta_D)]\}P_I/\eta_I, \end{aligned} \tag{2}$$

and Q and ε are connected by the relation

$$\varepsilon^{-1} = \eta_I(\eta_D + \eta_T - \eta_T\eta_D)(1 + 0.2Q) + 0.8mQ\eta_T\eta_I + \eta_T(1-\eta_I). \tag{3}$$

If there is no direct conversion of the energy of the charged particles and all the conversion goes through the thermal cycle, then it must be assumed that $\eta_D = 0$.

If $\varepsilon > 1 - \nu$, then the power station does not distribute and requires electric power from the grid, but due to the total of the energy required and that developed in its reactor, valuable products such as tritium, plutonium, hydrogen or other chemical substances which are synthesized in the intense neutron fluxes can be produced in the blanket.

We shall discuss only the production of plutonium. For a pure thermonuclear reactor $m \approx 1.4$.

With the presence in the blanket of ^{238}U, an energy release of 100 MeV/fusion event can be achieved. In this case $m \approx 7.0$ and, together with the increased release of heat in the blanket, ^{239}Pu will be accumulated.

Some examples of calculations by formulas (1)-(3) are given in Fig. 2. Before discussing the general conclusions from these calculations, we shall consider examples of hybrid closed and open reactors.

Examples of Hybrid Reactors

Hybrid Tokamak Reactors. We shall suppose that the second and third problems have been solved successfully, i.e., an infinitely long maintenance of the necessary pure plasma and current in the plasma is possible. We shall suppose also that the first problem is solved in the worst way, i.e., containment of longer than one-hundred Bohm periods is not possible. The conclusions about the reactor with ignition, under these conditions were found to be unacceptable. Let us consider how the use of injection changes it.

When considering a reactor with ignition, the dimensions of the reactor are discouraging. Ignition corresponds to $Q=\infty$. Taking the first values of Q in order to maintain a high plasma temperature, it is necessary to introduce additional power into the plasma by injection. For this, we are bound to the range of parameters stated in Fig. 2 if we do not wish to consume energy from the grid.

The parameters of a hybrid Tokamak reactor with injection are shown below. The extrapolation formula is the empirical one or the one-hundred Bohm periods one ($\tau_E \sim aI$ and $n\tau_E = 1 \cdot 10^{13}$ sec/cm^3). The magnitude of $n\tau_E$ is reduced by instabilities or by impurities. Retardation of the injected beam is Coulomb retardation ($n_T = 0.4$, $n_I = 0.7$, and $\tau_c = 3\tau_E$).

Plasma density n, cm^{-3}	$3 \cdot 10^{13}$
Plasma current I, MA	2.9
Radius of plasma a, m	1.3
Reactor power (E_{nu} =100 MeV), MW	270
Plasma volume V, m^3	177
Neutron flux Φ, cm$^{-2} \cdot$ sec^{-1}	$0.3 \cdot 10^{13}$
Toroidality A	4
Plasma temperature T, keV	8.5
Plasma pressure β_φ	1
Injection current of deuterons and tritons I_d and I_t, A	300; 600
Energy of deuterons and tritons E_d and E_t, keV	150; 40
Plasma intensification Q	0.6
Electric power of injectors P_I, MW	98
Power station efficiency η_S	0.12
Plutonium production M, kg/y	270
Electric power P_N, fed into grid, MW	32

Hence, it can be seen how far the reactor parameters can be reduced for the worst law of extrapolation of $n\tau_E$, and yet remaining in the range of positive values of η_S. If the containment is better, then for the same parameters the injection current is less and $n\tau_E$, Q and the magnitude of η_S corresponding to Fig. 2 are larger. A more favorable containment and an increase of the reactor dimensions brings η_S closer to η_T, but for a hybrid reactor with injection, $\eta_S < \eta_T$ always.

Hybrid Open Reactors. There is no second or third problem for open reactors. However, possible solutions of the first problem limit their range of application. In closed reactors with sufficiently large dimensions and magnetic-field strength of the reactor, ignition is possible in principle ($Q=\infty$). For open reactors Q depends neither on the dimensions nor on the magnetic field strength and the maximum plasma intensification corresponding to E_{TN}= 17.6 MeV amounts to 1.4 $\log_{10}$R [4] and is achieved at an injection energy of about 200 keV. The screwplug ratio, taking into account the diamagnetism of the plasma, with present-day niobium–titanium superconductors obviously cannot be considered above R = 4, and in the future R > 8 will prove to be barely achievable, as we shall be limited always by the durability of the materials, during attempts to increase the field in plugs of large dimensions to higher than 100 kOe. Thus, the limit of plasma intensification, in principle, of open DT reactors amounts to $Q_{max} \sim 1.0$.

The efficiency of a power station with a hybrid reactor, according to Fig. 2, in this case is found to be close to η_T and therefore this solution would be completely acceptable on a large scale for world power generation systems. At the same time, a power station with a pure open reactor will have an efficiency of not more than 0.23 and could not compete with nuclear power stations.

However, the probability that the maximum value of Q = 1 will be achieved is very small. Obviously, the really achievable values of Q will be several times less. In order to produce useful power from a pure reactor, an increase of the injection efficiency η_I and of the direct conversion η_D above the values shown in Fig. 2 would be required. The probability of success in this respect in the next decade is small. But a hybrid reactor might serve for the production of plutonium without the requirement for external electric

TABLE 2. Open Hybrid Reactor with E_{nu} = 100 MeV/fusion Event (maximum plasma intensification $Q = 1.14 \log_{10} R$; field at center of trap 25 kOe)

Plasma press. β	0,72			
Inject. energy E_I, keV	200			
Plasma den. n, cm^{-3}	$4 \cdot 10^{13}$			
Plasma vol. V, m^3	100			
Direct conversion eff. η_D	0,7			
Thermal cycle eff. η_T	0,4			
Vacuum screwplug ratio R_0	2		4	
Plasma screwplug ratio R	3,8		7,5	
Plasma inten. Q	0,67		1,0	
Coulomb containment $n\tau$, sec/cm^3	$4,3 \cdot 10^{13}$		$6,5 \cdot 10^{13}$	
Inject. eff. η_I	0,88	0,70	0,88	0,70
Plasma inten. Q_{suf}, suff. for breeding when $\eta_S = 0$	0,12	0,20	0,12	0,20
Containment can be less than Coulomb by the stated factor	5,5	3,3	8,3	5,0
Permissible containment $n\tau$, 10^{13} sec/cm^3	0,78	1,3	0,78	1,3
Inject. curr. I_i, A	3300	2000	3300	2000
Thermal power P_T, MW	460			
Neutron flux at first wall Φ, $cm^{-2} \cdot sec^{-1}$	$2 \cdot 10^{13}$			
Electric power P_N, sent out to consumers	0			
Plutonium production $\dot{M}$, kg/y	460			

power right up to $Q = 0.12$. At present, it is impossible to estimate the probability of this occurrence, as the probability of one or other law of extrapolation of $n\tau_E$ for Tokamaks cannot be estimated. Only the general tendency in both cases is certain. Small values of Q are more probable.

Table 2 shows examples of possible open hybrid reactors for which $\eta_S = 0$ and all the electric power is consumed by injection. The plasma volume is taken arbitrarily without studying the design of the winding. The stated screwplug ratio can hardly be possible for a thick blanket combined with a shield of 1.5 m, with a smaller plasma volume.

The Position of Hybrid Reactors in Power-Generation Systems

Thermonuclear reactors of any type will acquire industrial importance only in the so-called distant phase of the power-generation problem [5], starting in the 1990's, when fast fission reactors will be widespread. Despite this, the production of additional plutonium by hybrid thermonuclear reactors can still be useful.

Hybrid Reactors with Ignition. Let us compare a fast breeder reactor and a thermonuclear reactor with ignition, in the blanket of which plutonium is formed from ^{238}U. The thermal efficiencies of both reactors are identical and, from the point of view of the thermal effect on the surroundings are equivalent. In the first, the plutonium breeding factor is equal to 1.5 and, consequently, for every megawatt of its thermal power, 200 g of plutonium are produced per annum. In the hybrid thermonuclear reactor, it is possible that plutonium up to 1 kg/annum will be produced for each megawatt of thermal power [3]. If the price of plutonium is \$20/g and power stations are to recover their money over 8 years, then only the sale of plutonium will allow the capital costs on the power station plant at \$400/kW of installed electric power to be generated for an efficiency of $\eta_T = 40\%$. By adding the sale of electric power at 0.5 cent/kW·h, we obtain additionally the permissible capital costs of \$360/kW. Thus, a hybrid power station with an efficiency of $\eta_S = 40\%$ will recover its money over 8 years, with capital costs of up to \$760/kW. According to estimates carried out, the capital costs on thermonuclear Tokamak reactors will be considerably lower. The addition of plutonium to the reactor blanket with ignition is still advantageous because, with given dimensions and power of the reactor, the loading of the first wall is reduced and its radiation damage is reduced.

Thus, the thermonuclear hybrid reactors with ignition will enable after the year 2000 A.D., less expensive breeder reactors and larger relatively cheap thermal fission reactors to be constructed. The same thermonuclear hybrid reactors, most likely, will be more expensive than fast breeder reactors of equal power but, as the estimates carried out show, they will be economically advantageous and will produce approximately five times more plutonium per unit of thermal power than the fast breeder reactor.

Hybrid Reactors with Injection. Hybrid reactors with injection might be used either only for the production of plutonium ($\eta_S = 0$), or for the simultaneous production of plutonium and electric power.

Let us consider some alternatives for their utilization prospects.

A. Extrapolation of $n\tau_E$ to the reactor parameters in Tokamaks or Stellerators is favorable and a reactor with ignition is obtained which is technically feasible and economically justifiable. The use of injection, nevertheless, may prove to be favorable if the reactors with ignition will have capacities of a few thousands of megawatts. In this case, the accessibility of strongly radioactive parts, capable of failure, is considerably restricted in a closed reactor. This leads to a significant probability of undesirable inter-

ruptions in the use of high capacities. Reactors with injection can be made with a lower capacity, and therefore their shutdown for maintenance will cause less hindrance to the power output. Hybridizing, i.e., the production of plutonium, in this case has a favorable effect on the design of a thermonuclear reactor. It allows, for example, less modern injectors to be avoided for the maintenance of the same output efficiency η_S. Hybrid reactors with injection in this case could be useful for replacing a part of costly fast breeder reactors, as well as hybrid reactors with ignition as discussed.

B. Reactors with ignition cannot be built, but a closed reactor (Tokamak or Stellerator) with injection or an open reactor are feasible. For a closed reactor with injection, the intensification Q is the greater, the closer $n\tau_E$ is to $1.5 \cdot 10^{14}$ sec/cm^2. Therefore, pure as well as hybrid closed reactors with injection might find industrial application. The probability of using hybrid reactors is greater, as they might be more costly although remaining economically favorable. The situation is otherwise for open reactors. If we assume that $Q = 1$, the upper limit for open reactors, then pure open reactors are of no interest for the commercial production of electric power. According to Fig. 2, for this value of Q, $\eta_S = 0.22$. With these same values of Q, the efficiency of a hybrid power station with an open reactor can be equal to 0.35.

The economic advisability of building hybrid reactors is discussed above. However, all hybrid power stations with injection have $\eta_S < \eta_T$. One questions: whether contamination of the habitable surroundings will be acceptable, if a large part of the electric power and plutonium is produced by these hybrid reactors?

In order to assess the situation arising, let us consider the following limiting case: all the power generation system of the world is constructed only on thermal fission reactors and on hybrid fusion reactors with injection, producing a shortage of plutonium and electric power with an efficiency of η_S. Suppose that the capacity of the power generation system of the world is constant in time. In this case, the efficiency of all the world's power generation system will be expressed by the formula

$$\eta_{MS} = \frac{\eta_T + 0.4\eta_S}{1.4},$$

for the derivation of which it is assumed that in hybrid reactors, plutonium is produced to the amount of 1 kg/yr MW(ton). Thus, the efficiency of a hybrid power station can be within the limits of $0 \leq \eta_S < \eta_T$. It is easy to be convinced that if $\eta_T = 0.4$ and $\eta_S = 0.3$, then $\eta_{MS} = 0.37$.

Obviously, such an insignificant reduction of the total efficiency of the power-generation system cannot be a strong argument against the use of hybrid reactors with injection, and their fate resolves not the problem of heat wastage, but the economical and technical arguments.

CONCLUSION

The range of application of hybrid reactors in power generation depends on laws of plasma physics with reactor parameters which have not yet been studied experimentally. If the plasma containment is close to the empirical law, or better, then the production of plutonium in the blanket of a fusion reactor with ignition justifies the capital expenditure on the construction of a power station of up to \$700/kW.

If ignition of the reaction is technically or economically unprofitable, closed reactors with injection might serve for the commercial production of electric power and might be pure, as well as in the form of hybrids, and open reactors only in the form of hybrids. At the present-day level of knowledge, the least number of unsolved problems for the design of hybrid reactors has remained for open magnetic traps (problem of containment). Stellerators occupy the second place (the problem of contaminants is added) and in third place are the Tokamaks (the problem of steady-state maintenance of the current in the plasma still must be solved).

We note that containment in one-hundred Bohm periods, assumed to be the worst for Tokamaks and Stellerators, has not yet been achieved in a single experiment. Therefore, all forecasts on the possibility of better containment in reactor cycles up to now have no experimental foundation whatsoever. The next five year period must bear some clarification of this most important question.

APPENDIX

A Method of Calculating the Parameters of Reactors with Injection

Tokamak Reactor. It is assumed that the steady state is maintained at deuterium and tritium concentrations of n_d and n_t respectively, and that $\gamma = n_t/n_d = 2$. It will be assumed that the lifetime of particles τ_c is twice as large as the energy time τ_E.

From the conditions of the balance of pressures

$$\left(\frac{I}{a}\right)^2 = 2.0 \cdot 10^{-9} nT/\beta_\varphi,$$

the expressions for $n\tau_E$ given in the text, and the formula

$$T = \frac{E_d + \gamma E_t}{3(\gamma+1)\frac{\tau_c}{\tau_E}} = \frac{E_d + 2E_t}{27}; \quad q = \frac{5aII}{AI}; \quad I_d = \frac{nV}{3\tau_c}; \quad I_t = \gamma I_d = 2I_d,$$

the values of I, a, E_d, I_d, τ_E, and τ_c are calculated for given values of T, n, E_t, A, β, $n\tau_E$, and q.

The quantity Q is calculated by the formula from [3]:

$$Q = \frac{\gamma}{1+\gamma}(f_0 + n\tau_c\langle\sigma v\rangle)\frac{E_{TN}}{E_d + \gamma E_t}.$$

Here f_0 is the probability of a DT reaction during the time of retardation of the deuterons with energy E_d in a tritium plasma with an electron temperature T; $\langle\sigma v\rangle$ is the velocity of the DT reaction in a Maxwellian plasma with an ion temperature T.

Finally, the thermal power of the reactor is calculated by the formula

$$P_t = Q\frac{E_{nu}}{E_{TN}}(I_d E_d + I_t E_t),$$

where E_{nu} is the power released in the reactor per fusion event, including the blanket; $E_{TN} = 17.6$ MeV.

Open Reactor. The plasma intensification is

$$Q = \frac{1}{4} n\tau\langle\sigma v\rangle\frac{E_{TN}}{E_i},$$

where, according to [4],

$$n\tau = 2.67 \cdot 10^{10} E_i^{3/2} \lg_{10} R.$$

The screwplug ratio in the presence of the plasma is $R = R_0/\sqrt{1-\beta}$, where R_0 is the vacuum screwplug ratio. According to [4], Q reaches a flat maximum in the vicinity of $E_i = 200$ keV. For $E_{nu} = 17.6$ MeV, the maximum intensification $Q = 1.14 \log_{10} R$. By means of the present-day niobium–titanium superconductors, it is easy to make $R_0 = 2$ ($H_m = 50$ kOe; $H_0 = 25$ kOe). In 5 to 10 years, obviously $R_0 = 4$ might be possible ($H_m = 100$ kOe; $H_0 = 25$ kOe).

In the calculation of the plasma density by β and H_0, we shall assume that the plasma pressure is $p = 1.4nE_i$.

We calculate the injection current by the formula $I_i = n^2V/n\tau$, and the volume of the plasma is taken arbitrarily as 100 m^3. The thermal power of the reactor $P_T = Q(E_{nu}/E_{TN})E_i I_i$.

According to [3], in the presence of ^{238}U in the blanket, E_{nu} can be equal to 100 MeV.

LITERATURE CITED

1. I. Dawson, H. Furth, and F. Tenney, Phys. Rev. Letters, 26, 1156 (1971).
2. V. I. Pistunovich, At. Énerg., 35, No. 1, 11 (1973).
3. I. N. Golovin, V. I. Pistunovich, and G. E. Shatalov, Report by the Working Group on the Problems of Construction of Fusion Reactors [in Russian], Harlem, Jan. 29–Feb. 15 (1974).
4. A. Futch et al., Plasma Physics, 14, 211 (1972).
5. V. Khéifele, Bulletin of the International Atomic Energy Agency, 16, No. 1/2, 3 (1974).

PLASMA MHD GENERATOR FOR MODELLING ENERGY CONVERSION IN PULSED THERMONUCLEAR REACTORS

E. P. Velikhov, Yu. M. Volkov,
V. S. Golubev, N. V. Lobanov,
F. G. Rutberg, and A. A. Yakushev

UDC 621.313.12:538.4

In pulsed thermonuclear reactors energy is given off as kinetic energy of neutrons and alpha particles, and as electromagnetic radiation during a time of order 10^{-8} sec. This energy may be released, for example, in a lithium blanket, which must then be vaporized and form a lithium plasma with a temperature of order 1-2 eV. Higher temperatures will not increase the efficiency because of enhanced radiation and convection losses in the reactor chamber. The lithium blanket surrounding a thermonuclear plasma protects the walls from radiation damage and makes it possible to recover tritium which will be needed as a fuel component in the first generation of reactors (using the D–T reaction) [1].

The lithium plasma may then be used as the working medium in an MHD generator. In principle, with a plasma MHD generator it is possible to convert 40-45% of the initial heat content into electricity in the MHD generator and to convert 30-38% of the remaining heat in a steam turbine "tail." The overall efficiency of such a combined cycle may reach 60-70%.

It is possible to begin an experimental investigation of a series of problems associated with developing an MHD generator for pulsed thermonuclear reactors right now. This kind of study is necessary since it is impossible to answer a number of physical and technical questions by computations alone.

A model MHD generator for these purposes must allow study of the energy conversion process at the maximum possible efficiencies and must be practical from the standpoints of obtaining plasmas with the necessary parameters and of our current ability to design and construct MHD channels and magnetic systems.

The following problems associated with obtaining high conversion efficiencies could already be studied on this sort of model:

1. Stability in slowing down the core of a supersonic plasma flow in a magnetic field with a relative "wearing down" of the velocity in the MHD channel by 50% or more.

2. Stability and stabilization of the boundary layers when the flow is strongly decelerated by the magnetic field.

3. Possible instabilities in an MHD channel with highly efficient conversion of thermal energy (for example, thermal constriction, production of sound, formation of shocks, etc.).

4. Effects occuring in plasma flows with magnetic Reynolds numbers $Re_M \sim 1$.

5. The possibility of obtaining high load factors (i.e., electrical efficiencies of greater than 0.8-0.9).

6. More precise determination of the thermodynamic and transport properties of lithium and other appropriate plasmas under the working conditions in an MHD channel.

7. Development of the bases for designing appropriate MHD channels and gaining experience in the technical development of similar MHD devices.

Translated from Atomnaya Énergiya, Vol. 39, No. 6, pp. 387-391, December, 1975. Original article submitted May 4, 1975.

Choice of Parameters for the Model. High energy conversion efficiencies ($\eta_N > 0.2$) are attainable in the channels of MHD generators with active flow regimes only upon transition to a supersonic flow with a mach number $M > 3$ at the channel entrance [2]. The efficiency η_N with which the enthalpy i is converted, given by $\eta_N = \Delta i_{el}/i_0$, may be written in the form

$$\eta_N = \frac{1}{t_0}\tau + \frac{t_0 - 1}{t_0}\omega, \tag{1}$$

where $\omega = 1 - (u/u_0)^2$; $\tau = 1 - T/T_0$; $t_0 = 1 + ((\gamma-1)/2)M^2 = T*/T$; T, u, and M are the temperature, velocity, and Mach numbers; and γ is the effective index for the isentropes of the expansion of the gas flow. The subscript * refers to the parameters of the retarded flow and 0 to conditions at the inlet of the MHD channel.

For $M \gg 1$ and $(\gamma - 1) \ll 1$, η_N may be written approximately as

$$\eta_N \approx \frac{\omega}{\gamma}\eta_L \frac{T_* - T}{T_*}, \tag{2}$$

where η_L is the electrical (internal) efficiency of the MHD generator.

In the supersonic region η_N depends weakly on the shape of the MHD channel (for those regimes with small temperature change along the channel), and is mainly determined by the possible velocity reduction in the channel, the local loading coefficient, and the thermodynamic conditions at the heat source (pulsed thermonuclear reactor) and at the accelerating nozzle. It is shown in [2] that for $M > 3$ and $\gamma \approx 1.2$ (typical effective isentrope indices for a high temperature lithium plasma) η_N reaches 40%.

The need to obtain high enthalpy conversion coefficients influences the choice of an operating regime for the MHD channel. In a flow regime with T = const it is possible to obtain high values of η_N in the channel due to preferential slowing down of the velocity with moderate widening of the MHD channel. In addition, when the channel area increases moderately the T = const regime permits conversion of the velocity with practically linear variation along the channel all the way to M = 1.5. This is also true with a negative gradient of the static pressure along the channel, which eliminates the problem of separation of the boundary layer on the insulating wall. In view of this we shall consider an MHD channel in the T = const regime. Other operating regimes (e.g., ρ = const) may be considered in an analogous way.

In order to obtain high values of the internal efficiency ($\eta_L = 0.8$–0.9) we shall consider a Faraday MHD channel with continuous electrodes at small values of the Hall parameter ($\beta = 10^{-2}$) and large loading coefficients (K = 0.85–0.90).

In determining the parameters at the plasma source and at the entrance to the MHD channel, we shall assume the following limitations:

the working zone of the channel has a length $L_K \leq 2$ m for convenient utilization and for reduced construction expense;

the time for the plasma to escape is more than 20–50 times the characteristic time of flight of the plasma through the channel ($\tau_0 = L_K/\bar{u}$) so as to establish a quasistationary flow regime in the core of the flow and to develop boundary layers on the channel walls;

the interaction parameter (with respect to velocity) is $S_u = 0.3$–0.4;

$M_2 > 1$ (M_2 is the Mach number at the channel outlet);

$K \leq 0.85$;

$Re_m = 4\pi\mu\sigma u L_K (1-K) \leq 1$;

the channel length to diameter ratio is $5 \leq (L_K/d_K) \leq 10$ to reduce losses due to friction and end effects;

the current density $j \leq 3 \cdot 10^5$ A/m^2 so as to lighten the load on the electrodes;

the electric field strength $E \leq 15 \cdot 10^3$ V/m to simplify construction of the insulating walls;

the flow rate of the working medium is $\dot{m} \leq 10$ kg/sec to simplify the requirements on the energy supply for the test stand as well as because of the way the plasma is produced [3] and the time the plasma has to flow in the channel in order to attain a quasistationary regime in the core and boundary layer of the flow; and

the Mach number at the channel entrance satisfied $3.5 \leq M \leq 4.2$.

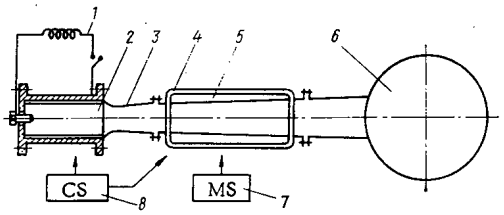

Fig. 1. A schematic of the MHD model system: 1) inductive storage unit; 2) plasma source; 3) nozzle; 4) magnetic system; 5) MHD channel; 6) exhaust reservoir; 7) measurement system; 8) control system.

From these limitations and estimates we obtain the following values of the flow parameters at the MHD channel inlet and of the plasma source parameters: P_* and $P_0 = 400$ and 1.56 bar; T_0 and $T_* = 3900$ and $12 \cdot 10^3$K; $\gamma_{eff} = 1.25$; $u_0 = 10.3$ km/sec; $\rho_0 = 0.03$ kg/m^3; $\sigma_0 = 90$ Ω/m; $Re_{m_{eff}} = 0.4$; and $B = 2$ T.

We have also examined the case in which the magnetic field decreases in time (according to a special power law) for optimal utilization of the working medium stored in the plasma source chamber. Depending on how much the chamber is emptied, the temperature and stagnation pressure of the MHD generator will fall. In order to keep the parameters of the MHD interaction constant in time (i.e., keep the conversion efficiency constant) it is most convenient to reduce the magnetic field. This makes it possible to increase the integral energy conversion efficiency.

Evaluation of Parameters and Design of the MHD Channel. To evaluate the change in the parameters in the core of the flow along the channel and the channel geometry, we have used an i–S diagram for a lithium plasma assuming adiabatic flow of the working medium from a bounded volume and its subsequent equilibrium isentropic expansion in a nozzle.* The parameters of the working medium were considered for a volume with $P_* = 300$–800 bar and $T_* = 10$–$20 \cdot 10^3$ °K.

A system of equations describing the variation in the parameters along the length of the channel [4] were used with the following additional assumptions: the voltage on the generator electrodes, the magnetic field, the load coefficient, and the mass flow rate are constant along the channel length while the longitudinal Hall electric field is equal to zero ($\beta = \omega\tau = 10^{-2}$).

The result of the calculation is that $\eta_N = 45\%$, the electric power at the load is $4 \cdot 10^8$ W, the increase in the cross-sectional area of the MHD channel is by eight times, and $M_{out} = 1.7$.

A schematic of this model is shown in Fig. 1. The variation in the parameters along the length of the channel is shown in Figs. 2–4.

The plasma source can be powered by a 10^8-J inductive storage unit [3]. A high-pressure plasma source ($P_* = 1000$ bar) is used to obtain a lithium plasma with the required parameters. It is joined to the MHD channel which is located in an uncooled magnet with a saddle-shaped copper winding. The exit portion of the MHD channel is attached to an exhaust reservoir in which the waste products from the working gas are chemically cleaned.

*The results of calculations by V. V. Breev and Yu. G. Degtev were used.

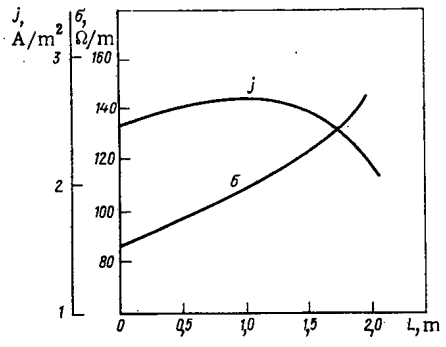

Fig. 2

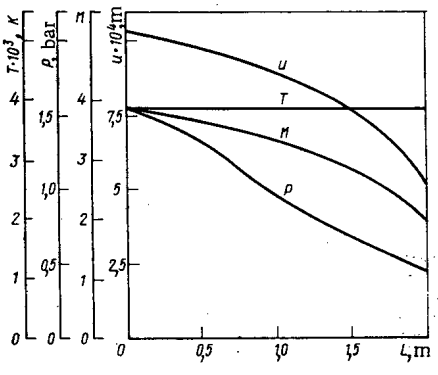

Fig. 3

Fig. 2. Change in the current density and electrical conductivity of the plasma along the MHD channel in the T = const regime.

Fig. 3. Change in the thermodynamic parameters in the core of the flow along the length of the MHD channel.

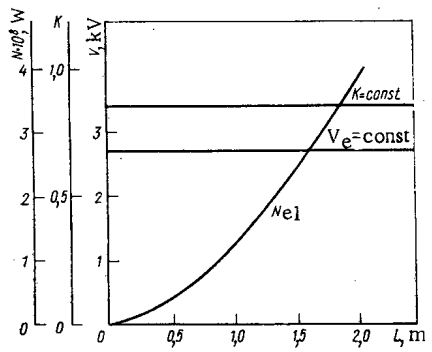

Fig. 4. Power generated along the length of the model MHD generator.

The MHD channel is of box-shaped design. The flaring of the channel from its inlet to its outlet takes place in both the insulating and electrode walls. In front of the channel there is an accelerating nozzle. The critical cross section of the nozzle is located in the circular part of the flow path which transforms to a square shape in the supersonic portion. To protect the critical cross section and walls of the nozzle from the high heat fluxes it is planned to cool the wall material by sweating out lithium. The bushings on the nozzle may be made of matrices of porous tungsten. The pores on the matrix will be permeated with lithium. As the lithium plasma passes through the nozzle the lithium in the pores will evaporate and cool the matrix due to the heat of vaporization.

The electrodes are made out of sheet molybedenum. For active control of the system by the boundary layer, the electrode surfaces must be perforated. To measure the current density distribution along the length of the channel, the electrode zone of the channel (2 m) is made up of 20 pairs of electrodes, which, after the measuring resistances, are connected to a common busbar. The insulating wall can be made in the form of ceramic modules fastened to the side covers.

The profile of the channel surface is obtained by choice of the shape of the holders. The force frame is made up of the wall support structures in the form of stringers to the electrode walls and side covers.

Peak values of energy input of 10^8 J, pressures of 1.4 kbar, and mass-average temperatures of 10^4°K are obtainable in pulsed plasma sources with nitrogen, hydrogen, and air [3].

The pulsed plasma source consists of a high pressure vessel with thermally insulating walls and an electrode system inserted into it. A diaphragm serves as a fast acting outlet valve. An electrical discharge is triggered in the filled discharge chamber. This leads to heating and increased pressure of the gas. When the desired parameters are attained the diaphragm is ruptured. Lithium hydride has been used as the working medium in preliminary experiments. After the discharge begins, the arc column expands and fills the chamber after about 200 μsec. The field strength was about 110 V/cm at a current of about 30 kA. According to [5] the field in a lithium discharge column is about 80 V/cm. Thus, we may use 100 V/cm for the expected regimes when analyzing the plasma source. This ensures a potential drop across the arc of about 10^4 V, which is optimal from the standpoint of matching to the proposed source, and inductive storage system. In this case, if the heated gas is not in the discharge chamber for more than 30-40 msec the losses should not exceed 10-20% of the applied energy. Thus, we assume the discharge time to be about $2 \cdot 10^{-2}$ sec, during which 10-20 MJ is converted to thermal energy of the working medium (plasma source efficiency 50%).

Magnet System. The proposed magnet system for this model is an iron-free pulsed magnet with a copper saddle-shaped winding with an external power source. The parameters of such a magnet system are the following: $j = 0.6 \cdot 10^3$ A/cm^2; $l = 2.5$ m; $NI = 1.4 \cdot 10^6$ A-turns; $S = 850 \times 600$ mm^2; and $\bar{B} = 1.8$ T (here S is the area of the working zone).

CONCLSUIONS

The construction of an experimental model for studying MHD energy conversion from a pulsed thermonuclear reactor is a realistic technical task at the present time. Doing this would permit development of a large scale MHD generator module for the typical parameters of the heated working medium in a pulsed thermonuclear reactor.

In principle it is possible to obtain an efficiency of at least about 40% with a linear plasma MHD generator. The efficiency of the whole plant might be increased further by utilization of the thermal energy at the outlet of the MHD channel in traditional methods.

When such an MHD generator is built difficulties with the behavior of supersonic plasma streams undergoing strong velocity reduction in a channel and the associated gasdynamic problems can clearly be solved successfully by active modification of the boundary layer and appropriate profiling of the MHD channel. Some complications may arise if a regime with time varying magnetic braking is used. Also important is the problem of the behavior of the plasma stream at large magnetic Reynolds numbers ($Re_m \sim 1$).

The basic technological problems are these: materials for the MHD channel, cooling arrangements for the channel (especially the critical cross section of the flow path), and pumping off the boundary layer at the electrodes and preventing lithium condensation on the channel walls. Because of the small magnetic field required, construction of the magnet system will clearly not present substantial technical difficulties associated with its size.

The most important physical questions as well as a number of technological questions characteristic of this problem may be investigated on a fairly simple model MHD generator with an output power level of 300-500 MW, a pulse duration of 10-20 msec, and a lithium plasma source.

The authors thank V. V. Breev, V. V. Chernukha, and V. P. Panchencko for useful discussions, Yu. G. Chernov for giving us the tables of the thermal and electrical properties of lithium plasmas used in our calculations, and V. I. Rozanov for recommending values of the cross sections for scattering of electrons by lithium atoms.

LITERATURE CITED

1. E. P. Velikhov, V. S. Golubev, and V. V. Chernukha, At. Énerg., 36, No. 4, 258 (1974).
2. J. Khat, in: Conversion of Heat and Chemical Energy into Electrical Energy in Rocket Systems [Russian translation], Izd. Inostr. Lit., Moscow (1963), p. 408.
3. B. P. Levchenko and F. G. Rutberg, Plasma Stream Generators and High Current Arcs [in Russian], Nauka, Leningrad (1973).
4. V. V. Breev, and V. P. Panchenko, Izv. Akad. Nauk SSSR, Mekhan. Zhidk. i Gaza, No. 4, 139 (1974).
5. F. A. Nikolaev, V. B. Rozanov, and Yu. P. Sviridenko, Teplofiz. Vys. Temp., 11, No. 3, 567 (1973).

KINETICS OF A SYSTEM OF COUPLED PULSED REACTORS

V. F. Kolesov, Yu. V. Petrov, and S. K. Shtarev

UDC 621.039.514

There are many papers on the kinetics of coupled reactors, mainly ones in foreign journals; reference is often made to the provision of guaranteed safety in large power reactors in conjunction with extensive breeding. Here we consider the reactor in which the fission in the core is produced only by fast neutrons, while that in the reflector (the breeding zone) is produced by fast and thermal neutrons. This is, as it were, a double system containing a fast reactor and a thermal one. It also is very favorable from the viewpoint of safety.

Avery at the Argonne National Laboratory in the USA first discussed the theory of coupled reactors [1-3]; other papers [4-11] deal with the kinetics of coupled reactors, in particular, stability. A special conference in the USA [12] also dealt with kinetics. Interest also attaches to a system of coupled pulsed reactors, in particular, a variety in which a pulsed reactor is coupled to a subcritical assembly which substantially extends the scope for reactor experiments [13].

Here we consider the kinetics of a system of two coupled pulsed reactors, in which at least one of them has a nonzero negative temperature coefficient of reactivity. We assume that the system as a whole produces high-power self-quenching pulses, i.e., when the transients are determined only by the internal coupling and the initial reactivity.

Kinetic Equations for Two Coupled Pulsed Reactors. We discuss the neutron balance for each reactor by analogy with the derivation of the usual kinetic equations, and get the following equations for these two reactors:

$$\left.\begin{aligned}
\frac{dN}{dt} &= \frac{k_{11}(1-\beta)-1}{\tau_{11}} N_1 + \frac{k_{12}(1-\beta)}{\tau_{22}} N_2 [t-(\tau_{12}-\tau_{11})] + \\
&+ \sum_{i=1}^{D} \lambda_i \{k_{11}C_{1i} + k_{12}C_{2i}\ [t-(\tau_{12}-\tau_{11})]\} + S_1(t); \\
\frac{dN_2}{dt} &= \frac{k_{22}(1-\beta)-1}{\tau_{22}} N_2 + \\
&+ \frac{k_{21}(1-\beta)}{\tau_{11}} N_1 [t-(\tau_{21}-\tau_{22})] + \sum_{i=1}^{D} \lambda_i \{k_{22}C_{2i} + k_{21}C_{1i} \times \\
&\times [t-(\tau_{21}-\tau_{22})]\} + S_2(t); \\
\frac{dC_{ji}}{dt} &= \frac{\beta_i}{\tau_{jj}} N_j - \lambda_i C_{ji}; \\
j &= 1, 2;\ i = 1, 2, \ldots, D,
\end{aligned}\right\} \quad (1)$$

where N_j and C_{ji} are the number of neutrons and delayed-neutron sources of group i in reactor j at instant t, k_{jj} and τ_{jj} are the multiplication factor (including the delayed neutrons) and the mean lifetime for the prompt neutrons in reactor j in the absence of the other reactors, k_{jk} is the neutron multiplication factor (including the delayed neutrons) for reactor j with respect to neutrons from reactor k (the reactor coupling coefficient), τ_{jk} is the mean lifetime of a prompt neutron generated in reactor k and producing fission in reactor j, λ_i, β_i, and $\beta = \sum_{i=1}^{D} \beta_i$ are the delayed-neutron parameters (assume the same for both reactors), D is the number of delayed-neutron groups, S_j is the external neutron source in reactor j (neutrons/sec),

Translated from Atomnaya Énergiya, Vol. 39, No. 6, pp. 392-396, December, 1975. Original article submitted March 3, 1975.

and the time shift $(\tau_{jk}-\tau_{jj})$ is the time from generation of a neutron in reactor k to capture in reactor j (we envisage neutrons that produce fission in reactor j).

It can be shown that system (1) is identical up to small quantities of the second order with the system of equations for coupled reactors in Avery's formulation [1]. Avery's equation system differs from (1) in two additional equations for N_{12} and N_{21}, while it lacks terms containing the delayed argument. Kinetic equations similar to those of (1) have been used by others [4-7].

Our analysis is based on (1), as being simpler in form, and also more similar to the ordinary kinetic equations for a single reactor; at the same time it provides the clearest indication of the effects of the various simplifications on the accuracy.

The coefficients k_{11} and k_{12} represent the relation of the reactivity to N_1 and N_2; for convenience in using these solutions, we replace N_1 and N_2 by quantities n_1 and n_2, which are the fission rates in the first and second reactors respectively at time t $[n_j = (N_j/\nu\tau_{jj})$, where ν is the number of neutrons arising per fission]. In that case,

$$
\begin{aligned}
k_{11}(t) &= k_{11}^0(t) - a_0^{(1)}\int_0^t n_1(t)\,dt - \sum_{m=1}^{M} a_m^{(1)} v_m^{(1)}(t);\\
k_{22}(t) &= k_{22}^0(t) - a_0^{(2)}\int_0^t n_2(t)\,dt - \sum_{m-1}^{M} a_m^{(2)} v_m^{(2)}(t);\\
\frac{1}{(\omega_m^{(1)})^2}\frac{d^2 v_m^{(1)}}{dt^2} &= \int_0^t n_1(t)\,dt - v_m^{(1)}(t);\\
\frac{1}{(\omega_m^{(2)})^2}\frac{d^2 v_m^{(2)}}{dt^2} &= \int_0^t n_2(t) - v_m^{(2)}(t);\\
m &= 1, 2, \ldots, M.
\end{aligned}
\qquad (2)
$$

The feedback in (2) is expressed in the form characteristic of fast pulsed reactors [14]. The following symbols have been introduced: $k_{jj}^0(t)$ as the value of $k_{jj}(t)$ neglecting the feedback, $a_0^{(j)}\int_0^t n_j(t)\,dt$ the contribution to $k_{jj}(t)$ from the fast temperature effect on the reactivity unrelated to thermal expansion of the core, $a_m^{(j)} v_m^{(j)}(t)$ the contribution to $k_{jj}(t)$ from component or harmonic m of the displacements in the thermal expansion of the core, which in general represents an inertial delay, and $v_m^{(j)}$ the conditional amplitude of component m of the displacements, which is defined as solution of the equation for an oscillatory system of circular frequency $\omega_m^{(j)}$. The parameters $a_m^{(j)}$ (k = 0, 1, 2, ..., M) are partial quasistatic negative-reactivity coefficients. The complete quasistatic negative-reactivity coefficient $a^{(j)}$ is defined by $a^{(j)} = a_0^{(j)} + \sum_{m=1}^{M} a_m^{(j)}$.

System (1) goes with (2) and the transfer from N_j to n_j and the initial value of n_j, C_{ji}, $v_m^{(j)}$ and $dv_m^{(j)}/dt$ to give a complete description of the transients in the two reactors within the framework of the point kinetics for each of the reactors.

The delayed neutrons can be neglected in analyzing the rapidly changing transients; in many cases also, it is not essential to incorporate the delay from thermal expansion. In that case, (1) and (2) simplify considerably to

$$
\left.
\begin{aligned}
\tau_{11}\frac{dn_1}{dt} &= (k_{11}-1)n_1 + k_{12}n_2\,[t-(\tau_{12}-\tau_{11})];\\
\tau_{22}\frac{dn_2}{dt} &= (k_{22}-1)n_2 + k_{21}n_1\,[t-(\tau_{21}-\tau_{22})];\\
k_{11} &= k_{11}^0(t) - a'^{(1)}\int_0^t n_1\,dt;\\
k_{22} &= k_{22}^0(t) - a'^{(2)}\int_0^t n_2\,dt.
\end{aligned}
\right\} \qquad (3)
$$

Here a difference from (1) and (2) is that the k_{jk} are the multiplication factors based only on the prompt neutrons.

It will be shown below that the neutron transfer delay ($\tau_{jk}-\tau_{jj}$), that is from reactor k to reactor j, plays no appreciable part in real combinations of two pulsed reactors, and it can usually be taken as zero. Here we consider the kinetics of such reactors via analytical and numerical solutions of (3) with and without the delay.

Initial Runup, Reactivity, and Mean Neutron Lifetime. Equations (1) give the reversed-clock equation similar to that in Avery's formulation [1]:

$$\left[1+\frac{\tau_{11}}{T}-k_{11}\left(1-\sum_{i=1}^{D}\frac{\beta_i}{1+\lambda_i T}\right)\right]\left[1+\frac{\tau_{22}}{T}-k_{22}\left(1-\sum_{i=1}^{D}\frac{\beta_i}{1+\lambda_i T}\right)\right]=k_{12}k_{21}\left(1-\right.$$
$$\left.-\frac{\tau_{12}-\tau_{11}}{T}\right)\left(1-\frac{\tau_{21}-\tau_{22}}{T}\right)\left(1-\sum_{i=1}^{D}\frac{\beta_i}{1+\lambda_i T}\right)^2. \tag{4}$$

It is found [1] that the effective neutron lifetime τ and multiplication factor k in such a system are defined by

$$\tau=\frac{\Delta k_2(1+\Delta k_1)}{\Delta k_1+\Delta k_2}\left[\tau_{11}+\frac{\Delta k_1(1+\Delta k_2)}{\Delta k_2(1+\Delta k_1)}\tau_{22}-\frac{\Delta k_1}{1+\Delta k_1}(\tau_{12}+\tau_{21})\right];$$
$$\Delta k=\frac{\Delta k_1+\Delta k_2}{2}\pm\sqrt{\frac{(\Delta k_1+\Delta k_2)^2}{4}+k_{12}k_{21}-\Delta k_1\Delta k_2}, \tag{5}$$

where

$$\Delta k=k-1;\ \Delta k_1=k_{11}-1;\ \Delta k_2=k_{22}-1. \tag{6}$$

If k, k_{11}, and k_{22} deviate only slightly from 1, the values of Δk, Δk_1, and Δk_2 can be considered as equal to the reactivities of the following respectively: the entire system, the first reactor, and the second reactor, which are considered in isolation one from the other. If Δk and Δk_2 (or Δk_1) are given, Δk_1 (or Δk_2) is determined by

$$\Delta k_1=\Delta k+\frac{k_{12}k_{21}}{\Delta k_2-\Delta k}\left(\Delta k_2=\Delta k+\frac{k_{12}k_{21}}{\Delta k_1-\Delta k}\right). \tag{7}$$

For calculation purposes it is also convenient to have expressions that relate Δk_1 or Δk_2 to the specified reactor period T and Δk_2(or Δk_1):

$$\Delta k_1=\sigma+\frac{k_{12}k_{21}}{\Delta k_2-\sigma}\left(\Delta k_2=\sigma+\frac{k_{12}k_{21}}{\Delta k_1-\sigma}\right);$$
$$\sigma(T)=\left(1-\sum_{i=1}^{D}\frac{\beta_i}{1+\lambda_i T}\right)^{-1}-1. \tag{8}$$

These expressions are derived from (4) in the zero-lifetime approximation for the prompt neutrons.

Solution of the Kinetic Equations. Even the simplified equations in (3) cannot be solved analytically in general form; such solutions can be found only for particular cases. Solutions to (3) can be derived for specified values of k_{11}^0, k_{22}^0 (stepwise change in the initial reactivity) and for $a^{(2)}=0$; the latter condition corresponds to the case where the second reactor either has no appreciable temperature coefficient of reactivity or is in a very much subcritical state, with the result that temperature variations in the reactivity in essence do not affect its multiplication factor. In that case (3) is used with the new variables $J_j(t)=\int_0^t n_j(t)\,dt$ $(j=1, 2)$ to give

$$\left.\begin{aligned}
\tau_{11}\frac{d^2J_1(t)}{dt^2}&=[\Delta k_1^0-a^{(1)}J_1(t)]\frac{dJ_1(t)}{dt}+\\
&+k_{12}J_2[t-(\tau_{12}-\tau_{11})];\\
\tau_{22}\frac{d^2J_2(t)}{dt^2}&=\Delta k_2^0\frac{dJ_2(t)}{dt}+\\
&+k_{21}J_1[t-(\tau_{21}-\tau_{22})];\\
\frac{dJ_j(0)}{dt}&=n_j^0;\quad J_j(0)=0\quad (j=1, 2).
\end{aligned}\right\} \tag{9}$$

We use the properties of self-quenching pulsed systems ($dJ_j/dt=n_j\to 0$; $J_j\to J_{j\infty}$ for $t\to\infty$) and integrate (9) with respect to t; algebraic steps taking n_j^0 as small give

$$J_{1\infty}=\frac{2\Delta k_1^0}{a^{(1)}}\left(1-\frac{k_{12}k_{21}}{\Delta k_1^0\Delta k_2^0}\right);\quad J_{2\infty}=\frac{-k_{21}}{\Delta k_2^0}J_{1\infty}. \tag{10}$$

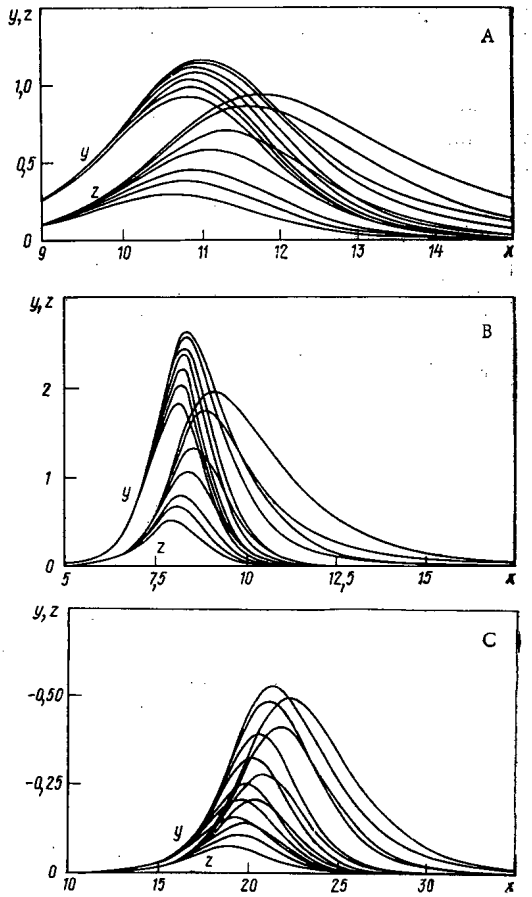

Fig. 1. Fission pulses in coupled reactors in relation to parameter c: A) a = 1; b = 1; pulses in decreasing order corresponding to: c = 0; 0.1; 0.5; 1; 2; 3; 5; B) a = 1, b = 3, pulses in decreasing order corresponding to c = 0; 0.1; 0.5; 1; 2; 3; 5; C) a = −1, b = 3, pulses in decreasing order corresponding to c = 0; −0.1; −0.5; −1; −2; −3; −5.

Expressions (10) define one of the most important characteristics of the transients in such a system, namely the total number of fissions in a pulse. An exact expression for another equally important characteristic (the pulse width at half height) cannot be obtained, though an approximate expression can. From (9) we get the pulse width at half height θ_{comb} for a combination of n_1 and n_2, namely for

$$\left[n_1 - \frac{k_{12}\tau_2 - k_{12}\Delta k_2^0(\tau_{12}-\tau_{11})}{\Delta k_2^0\tau_1 - k_{12}k_{21}(\tau_{21}-\tau_{22})} n_2\right]:$$

$$\theta_{comb} = \frac{3.5255\tau_{11}}{\Delta k_1^0} \times \frac{1 + \frac{k_{12}k_{21}}{(\Delta k_2^0)^2\tau_{11}}\{\tau_{22} - \Delta k_2^0[(\tau_{12}-\tau_{11}) + (\tau_{21}-\tau_{22})]\}}{1 - \frac{k_{12}k_{21}}{\Delta k_1^0 \Delta k_2^0}}. \quad (11)$$

Here we have expanded the components with the delayed argument as Taylor series up to terms of the first order inclusive. This approximate pulse width differs only slightly from the actual width in the reactors if these themselves in fact differ only slightly in actual width, and if there is only a small time shift between the pulses. It can be shown that in fact these conditions are usually met, so (10) and (11) give extremely full information about the characteristics. In particular, the solutions show that there is no change in the total energy release during a pulse or in the ratio of the releases in the reactor when one incorporates the delay in neutron transfer. However, the pulse width is somewhat increased.

Exact solutions to (3) without delay were obtained by computer; the dimensionless variables

$$x = -\frac{\Delta k_2^0}{\tau_{22}} t; \quad y = -\frac{a^{(1)}\tau_{22}}{\Delta k_1^0 \Delta k_2^0} n_1; \quad z = \frac{a^{(1)}\tau_{22}}{k_{21}\Delta k_1^0} n_2$$

convert (3) to the parametric form

$$\left.\begin{aligned} \frac{dy}{dx} &= a\left(1 - \int_0^x y\,dx\right) y + bz; \\ \frac{dz}{dx} &= y - \left(1 + c\int_0^x z\,dx\right) z; \\ y(0) &= y_0; \quad z(0) = 0, \end{aligned}\right\} \quad (12)$$

where

$$a = \frac{-\Delta k_1^0\tau_{22}}{\Delta k_2^0\tau_{11}}; \quad b = \frac{k_{12}k_{21}\tau_{22}}{(\Delta k_2^0)^2\tau_{11}}; \quad c = \frac{a^{(2)}\Delta k_1^0 k_{21}}{a^{(1)}(\Delta k_2^0)^2}.$$

The calculations gave the maximal values of y and z as functions of the parameters *a*, b, and c, together with the limiting values for the integrals with respect to y and z, the pulse widths in the reactors at half-height θ_y and θ_z, and the separation Δx between the peaks in y and z. As an example, Fig. 1 shows the fission pulses in the two reactors for given values of *a* and b as functions of the parameter c. The calculations show that the width θ_y and θ_z differ by not more than a factor 1.5, except when b is very large. The analytical value of θ_{comb} lies between θ_y and θ_z (roughly in the middle), and consequently the relative deviation of θ_{comb} from the true pulse width does not exceed 25% (except for very large values of b).

The displacement of the pulse in the second reactor with respect to that in the first is small: it usually does not exceed 1/3 of the pulse width. A single reactor will produce a symmetrical pulse, whereas the coupled pair produces a somewhat elongated trailing edge. This is best seen for c = 0 (no quenching in the second reactor). The pulses in the second reactor become smaller as c increases, and the same occurs in the first reactor, but not so extensively.

The ratio of the fission rates varies greatly during the transient (Fig. 1). For instance, in case B, the ratio y/z for x = 7 and c = 0 is about 3, while for x = 12 it is about 1/2. That is, the ratio of the fission rates in the two reactors increases by a factor 6. There is thus no proper basis for applying the so-called point kinetic equations (ones independent of the spatial coordinates) to a coupled-reactor system, i.e., one is not justified in replacing the coupled-reactor system by a single reactor with single values for τ, k, and $a^{(0)}$.

LITERATURE CITED

1. R. Avery, in: Proceedings of the 2nd Geneva Conference, Selected Papers by non-Russian Scientists [Russian translation], Vol. 3, Atomizdat, Moscow (1958), p. 321.
2. R. Avery et al., ibid., p. 231.
3. R. Avery, Nucl. Sci. and Engng., 3, 129 (1958).
4. G. Baldwin, ibid., 6, 320 (1959).
5. R. Danofsky and R. Uhrig, ibid., 16, 131 (1963).
6. A. Belleni-Morante, Nukleonik, 8, No. 5, 291 (1966).
7. A. Belleni-Morante, Nukleonik, 10, No. 4, 217 (1967).
8. V. V. Vatulin and V. I. Yuferev, At. Énerg. 29, No. 2, 117 (1970).
9. V. D. Goryachenko, At. Énerg., 23, No. 6, 548 (1967).
10. W. Hafele, Proceedings of the Seminar Physics on Fast and Intermediate Reactors, Vol. 3, Vienna, IAEA (1961), p. 19.
11. W. Stacey, Reactor Technology, 14, No. 2, 169 (1971).
12. C. Chezem and W. Kohler, (editors), Coupled Reactor Kinetics, Proc. National Topical Meeting American Nuclear Society, Texas (1967).
13. B. G. Dubovskii, At. Énerg., 7, No. 5, 456 (1959).
14. V. F. Kolesov, At. Énerg., 20, No. 3, 265 (1966).

OPTIMAL-CONTROL THEORY IN REACTOR FLUX CONTROL SYSTEM DESIGN

G. N. Aleksakov

UDC 621.039.562:621.039.515

The point kinetic model [1] has been used to determine the time-optimal conversion of the neutron flux n(t) from the initial level n_0 to the final level n_f subject to restriction on the reactor period $a(t) = \frac{1}{n(t)} \cdot \frac{dn}{dt} \approx \frac{1}{T(t)} \leqslant a_\uparrow$. Fig. 1a-c show log n(t), the relative rate of change, and the excess reactivity $\rho(t)$, respectively. The curve for $\rho(t)$ has been constructed for a given time-optimal n(t) via the inverse method of solving kinetic equations [2].

The $\rho(t)$ curve of Fig. 1c shows that the specified $a_\uparrow = \frac{1}{T_\uparrow}$ may be attained instantaneously in the presence of lag in the prompt-neutron processes by increasing the reactivity by the step $\rho(t_0) = a_\uparrow l = \frac{l}{T_\uparrow}$, where l is the effective neutron lifetime. It is technically extremely difficult to realize such a change in reactivity, but if a rod is displaced with the initial speed

$$\dot{\rho}(t_0^+) = a_\uparrow \beta \tag{1}$$

(β is the total proportion of delayed neutrons) that should be the speed immediately after the step (Fig. 1d), the step $\rho(t_0) = a_\uparrow l$ is performed in the time $\tau = \rho(t_0)/\dot{\rho}(t_0^+) = l/\beta$, which is about 15 msec for $l = 10^{-4}$ sec. An analogous estimate applies for the reactivity step $\rho(t_f)$ required for instantly halting the reactor runup at n_f. To halt the runup at the level n_f requires an initial rate of reactivity increase

$$\dot{\rho}(t_f^+) = \frac{1}{T_\uparrow} \sum_{i=1}^{6} \frac{\beta_i}{1+\lambda_i T} < \dot{\rho}(t_0^+), \tag{2}$$

where β_i is the proportion of group i of delayed neutrons, whose decay constant is λ_i.

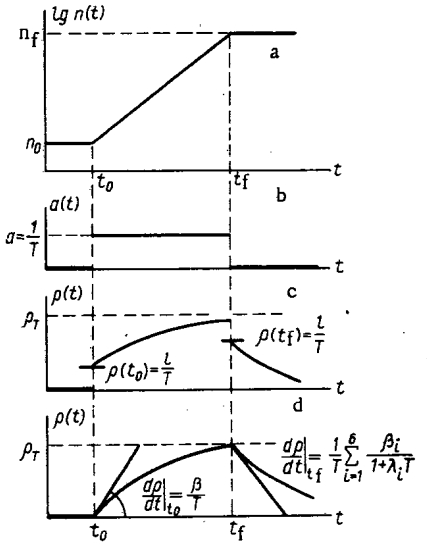

Fig. 1. Time curves for: a) logarithm of neutron flux; b) rate of charge of flux; c and d) reactivity.

The solution for time-optimal control of the flux with restriction on the period in the point model (see [1] and Fig. 1) indicates that the physical processes in the reactor allow one to control the reactivity with change at the finite initial rate $\dot{\rho}_\uparrow = \frac{1}{T_\uparrow}$ to produce practically instantaneous attainment of the period T and then stabilization of this, while one can provide a rate $\dot{\rho}_\downarrow = \frac{1}{T_\uparrow} \sum_{i=1}^{6} \frac{\beta_i}{1+\lambda_i T_\uparrow} < \frac{1}{T_\uparrow}$ to halt the neutron flux at the set level n_f and stabilize it there, the flux varying before this time with a period $T_r \geqslant T_\uparrow$. The quantity $\dot{\rho}_{max} = \frac{1}{T_\uparrow}$ enables one to provide complete control of the neutron flux for $T_r \geqslant T_\uparrow$.

Any neutron-flux control system (automatic regulation or automatic specification) may be characterized by the pair of quan-

Translated from Atomnaya Énergiya, Vol. 39, No. 6, pp. 397-399, December, 1975. Original article submitted February 18, 1974; revision submitted June 23, 1975.

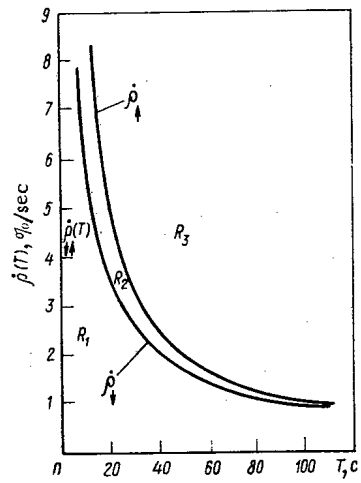

Fig. 2. Relation of reactivity to reactor period.

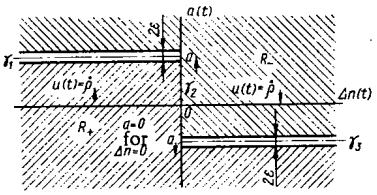

a

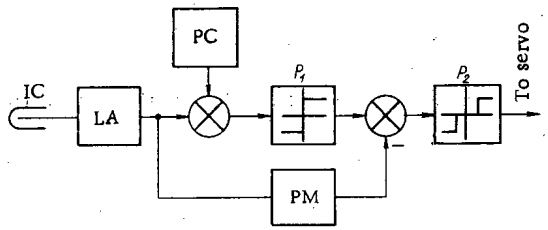

b

Fig. 3. a) Control law; b) circuit realization. IC) ionization chamber, LA) logarithmic amplifier, PC) power control, PM) period monitor.

tities $(\dot{\rho}_{max}; T_r)$: the graphs $\dot{\rho}_\uparrow(T_\uparrow)$ and $\dot{\rho}_\downarrow(T_\uparrow)$ represent optimal matching of the control system for $\dot{\rho}_{max}$ to the working reactor period T_r (Fig. 2). If the point $(\dot{\rho}_{max}; T_r) \in R_1$ (lies below the curve $\dot{\rho}_\downarrow$), the system cannot provide instant period control within the complete range of working runup periods, and so cannot meet the specifications for nuclear safety. If $(\dot{\rho}_{max}; T_r) \in R_2$, the system is safe, although it does not provide virtually instant attainment of T_r. If $(\dot{\rho}_{max}; T_r) \in \dot{\rho}_\uparrow(T_\uparrow)$, the reactivity control device is optimally matched to T_r. If $(\dot{\rho}_{max}; T_r) \in R_3$, the control system itself can be a source of hazardous situations if there is delay in the control loop as a result of excessive rate of reactivity increase, in that the runup period will be unacceptably small.

The rate of change of reactivity $\dot{\rho}_{max}$ unambiguously determines the power specification for the servodrive motor [3]. The condition $(\dot{\rho}_{max}; T_r) \in R_1$ indicates that the system is not viable on account of inadequate motor power, while the condition $(\dot{\rho}_{max}; T_r) \in R_3$ indicates that the drive power is excessive. Such a system has more hardware than necessary and is over-complicated, and therefore is less reliable than the optimal one.

The control law (Fig. 3a) or the set of rules for choosing the control $\dot{\rho}(t)$ as a function of the current state of the reactor, as represented by the pair of phase coordinates $\Delta n(t) = n(t) - n_f$ and $a(t)$, enables one to realize optimal transient response (Fig. 1) in a system with feedback. The switching line γ, which consists of the horizontal dot–dash section γ_1, the vertical section γ_2, and the further horizontal section γ_3, divides the phase plane $(\Delta n; a)$ into regions R_+ and R_-. The control $\dot{\rho}(t) = u[\Delta n(t); a(t)]$ equals $+\dot{\rho}_{max}$ if $[\Delta n(t); a(t)] \in R_+$ and $-\dot{\rho}_{max}$, if $[\Delta n(t); a(t)] \in R_-$; the control law is realized by means of two devices P_1 and P_2 with characteristics of polarized-relay type (Fig. 3b). The time response $\rho(t)$ is provided in accordance with Fig. 1d by motion of the system in a sliding mode on account of pulse-width bipolar modulation of the voltage applied to the motor. The work of the motor is eased if the horizontal parts γ_1 and γ_3 on the switching line (Fig. 3a) are replaced by bands of width 2ε within which the control is zero. The width of the bands such that the oscillations become unipolar is determined by the delay in the control loop.

We now estimate the error in control of the flux n(t) that varies with period $T_\uparrow$, before the level n_f is attained via the excursion Δn above the level n_f on account of the delay τ in the control loop, and for $\tau \ll T$ we readily obtain

$$\Delta n / n_f \approx \tau / T. \qquad (3)$$

Here

$$\tau = \tau_0 + \tau_f + \tau_c + \tau_s + \tau_d,$$

where $\tau_0 = l/\beta$ is the lag in the prompt-neutron processes in the reactor itself, while τ_f, τ_c, τ_s, and τ_d are the lags in the flux monitor, control device, servoamplifier, and drive respectively. Comparison of the last four with τ_0 shows that the main source of deviation from optimal control is not the physics of the processes in the reactor (as is often erroneously assumed in papers on reactor control), but the lag in the control system external to the reactor.

It is clear that the best choice of servomotor of least power provides simultaneously reductions in the values of τ_d and τ_s; the characteristics τ_f and τ_c are best selected on the basis of the acceptable error and the known values of τ_s and τ_d using (3).

These theoretical conclusions were confirmed by direct experiments with the IRT-2000 reactor at the Moscow Engineering-Physics Institute using a special control system based on a BIR-1 instrument.

The economic aspects of the control system based on the BIR-1 were compared with those of one based on a BAR-2M instrument; not only was there an improvement in the transient response, but also improvement in the power drawn and system size by factors 20 and 5 respectively. Here power economy was not the principal purpose, but simply a means of simplifying the system and improving the reliability.

Experiments on the IRT-2000 treated the reactor as a physical model for any reactor; we examined the optimal flux control in the presence of a negative temperature coefficient of reactivity, reactivity perturbations, and perturbations due to a neutron source. The theoretical conclusions were confirmed by the experiments on the IRT-2000, and the results (with appropriate scaling) may be transferred to give optimal flux control for reactors of other types [4].

Trends in flux-control system design indicate that the characteristics are tending to converge upwards to the values defined by $\dot{\rho}_{max} = 1/T$ and $\Delta n/n_f = \tau/T$, no matter what the design method employed. The theory of optimal control thus accelerates the design of good flux control systems, while considerably reducing the number of trials inevitable in other design methods.

The main conclusion is that time-optimal flux control subject to restrictions on the period is a mathematical formalization of considerations from a safe design for flux control systems. The mathematical design technique provides an appreciable economic advantage not only in the final result (a better control system) but also during the design stage in the form of savings in time and materials.

LITERATURE CITED

1. G. N. Aleksakov, V. N. Belousov, and A. P. Kryukov, At. Énerg., 32, No. 3, 228 (1972).
2. J. Kipin, Physical Principles of Reactor Kinetics [Russian translation], Atomizdat, Moscow (1967).
3. B. A. Dement'ev, Reactor Kinetics and Control [in Russian], Atomizdat (1973).
4. R. Mohler and S. Shen, Optimal Control of Nuclear Reactors, Academic Press, New York (1970).

ESCAPE OF GAS FROM AN UNSEALED FUEL ELEMENT AFTER REACTOR SHUTDOWN

B. V. Pshenichnikov

UDC 621.039.548:621.039.524.4-98

During the operation of nuclear reactors the fuel element cladding sometimes fails and the pipelines and equipment of the primary coolant circuit become contaminated by radioactive fission products. Thus, it is of interest to study the mechanism of the escape of fission products through the cladding of an unsealed fuel element into the coolant during reactor operation and after shutdown.

The escape of fission products from unsealed fuel elements during reactor operation has been rather thoroughly explained [1-4]. Fissions do not occur in a shutdown reactor. The low temperature of the fuel practically eliminates diffusion as a cause of the escape of fragments from the fuel. The specific conditions of the reactor cooling appreciably complicate experiments on the escape of fission products from leaking fuel elements. The greatest complication arise from temperature and pressure variations.

It is therefore appropriate to analyze a mathematical model of the escape of gaseous products from a leaking fuel element into the coolant after reactor shutdown.

Basic Assumptions. We examine gas release from a hypothetical ceramic rod fuel element in the core of a shut down water-cooled reactor. The fuel element has a length L and diameter d, the gap between the oxide fuel and the cladding is h, and the distance from the defect to the end of the fuel element is arbitrary and equal to l. We assume that $L \gg d$ and $l \gg d$. This makes the problem one-dimensional. We assume that the defect in the cladding is formed during reactor operation and that at the instant of reactor shutdown a vapor-gas mixture at the working pressure of the reactor exists inside the cladding. After shutdown the reactor pressure decreases to atmospheric. It is assumed that as the pressure decreases the temperature of the vapor-gas mixture inside the fuel element cladding remains above the saturation temperature so that water vapor does not condense.

It is of particular interest to estimate the time lag in equalizing pressures at the closed end of the fuel element and the total amount of gas remaining in the space under the cladding after the decrease in reactor pressure. We place the origin of coordinates at the defect so that the closed end of the fuel element is a distance l from the origin.

Differential Equation of Gas Release. Henceforth, we treat the vapor-gas mixture as a gas. Under the above assumptions the motion of the gas inside the fuel element cladding can be treated as the motion of a compressible fluid in a capillary-porous body; such motion is rather slow and therefore the temperature of the gas is always practically equal to the temperature of the capillary walls and the process is isothermal.

According to Darcy's law, the flow through a capillary porous body is related to the pressure gradient by the expression

$$J = -\frac{K}{\mu} \operatorname{grad} P, \tag{1}$$

where K is the permeability, μ is the dynamic viscosity, and P is the pressure inside the fuel element cladding.

For gases the rate of change of density is described by the expression [5]

$$\frac{\partial}{\partial \tau}(\rho \Pi) = -\operatorname{div}[\rho J], \tag{2}$$

Translated from Atomnaya Énergiya, Vol. 39, No. 6, pp. 400-402, December, 1975. Original article submitted October 28, 1974.

where ρ is the density of the gas under pressure, Π is the porosity, and τ is the time.

Using Eq. (1) and the equation of state of an ideal gas for an isothermal process we obtain

$$\frac{\partial P}{\partial \tau} = \frac{K}{\mu \Pi} \operatorname{div} [P \operatorname{grad} P] \tag{3}$$

or for the one-dimensional case

$$\frac{\partial P}{\partial \tau} = \frac{K}{\mu \Pi} \frac{\partial}{\partial x} \left[P \frac{\partial P}{\partial x} \right]. \tag{4}$$

After transformation and changing to the function P^2 we find the equation for the flow of gas inside the fuel element cladding

$$\frac{\partial}{\partial \tau} (P^2) = \frac{KP}{\mu \Pi} \frac{\partial^2}{\partial x^2} (P^2). \tag{5}$$

The equation obtained is nonlinear and cannot be solved in the general form. The nonlinearity is related to the change in the pressure difference between the outside and inside of the fuel element as the gas escapes through the cladding. The extra resistance of the defect is not taken into account in the derivation of the equation since it is assumed that the area of the defect is larger than or equal to the straight through cross section of the empty space inside the fuel element cladding.

Solution of the Equation. It is clear that the greater the pressure inside the fuel element cladding the higher the rate of efflux of gas and the shorter the time lag for equalizing the pressure at the far end of the fuel element with the external pressure in the reactor. If the value of P in the coefficient on the right-hand side of the equation is assumed equal to the pressure P_c in the reactor, the time lag turns out to be longer than the actual time. For a constant value of P_c Eq. (5) is linear in P^2 and can be solved in general form by taking the Laplace transform. In this case the boundary conditions must indicate the constant external pressure at the site of the defect and the absence of gas sources at the closed end of the fuel element; i.e.,

$$P^2(0, \tau) = P_c \text{ and } \frac{\partial}{\partial x} P^2(l, \tau) = 0. \tag{6}$$

The initial condition indicates the equality of the pressure P inside the cladding and P_0 in the reactor

$$P^2(x, 0) = P_0^2. \tag{7}$$

If we understand by P_c the final pressure in the reactor, i.e., atmospheric, the problem will reflect the conditions of an instantaneous pressure drop in the reactor from the working pressure P_0 to atmospheric.

In this case the solution of Eq. (5) for boundary conditions (6) and (7) at the closed end of the fuel element will have the form

$$P^2(l, \tau) = P_c^2 + \frac{4}{\pi} (P_0^2 - P_c^2) \sum_{n=1}^{\infty} \frac{(-1)^{n+1}}{(2n-1)} \exp \left\{ - \frac{(2n-1)^2 \pi^2 P_c K \tau}{4 \Pi \mu l^2} \right\}. \tag{8}$$

For values of the Fourier number F_0 in the exponent larger than or equal to 0.5 only the first term of the infinite series need be retained [6]. Then Eq. (8) simplifies to

$$P^2(l, \tau) = P_c^2 + \frac{4}{\pi} (P_0^2 - P_c^2) \cdot \exp \left(- \frac{\pi}{4} F_0 \right) \quad \text{for } F_0 \geqslant 0.5, \tag{9}$$

where the Fourier number has the form

$$F_0 = \frac{P_c K \tau}{l^2 \Pi \mu}. \tag{10}$$

The solution found leads to the following expression for the time lag in equalizing the pressures:

$$\tau_{lag} = \frac{\pi^2 l^2 \Pi \mu}{4 K P_c} \ln \left[\frac{4 (P_0^2 - P_c^2)}{\pi (P^2 - P_c^2)} \right]. \tag{11}$$

Estimate of the Time Lag. To estimate τ_{lag} we neglect the volume of the pores communicating with free space and take the porosity equal to unity.

By using the solutions of the classical hydrodynamics equations for slow steady flow it is shown in [7] that the permeability in darcys of a system of capillary tubes can be written in the form

$$K = \frac{c \cdot \Pi^3}{\Omega^2} 10^8, \tag{12}$$

where the Kozeny constant c for a rectangular cross section is 0.56 and Ω is the specific surface of the porous material.

$$\Omega = \frac{2\pi\, dl}{\pi\, dhl} = \frac{2}{h}. \tag{13}$$

In this case the permeability is $0.14 \cdot 10^8 h^2$.

We take the dynamic viscosity of the gas equal to $2.5 \cdot 10^{-2}$ cP, which is the average of the viscosities of water vapor, Xe, and Kr. Taking $P_0 = 71$ atm, $P_c = 1$ atm, and $l = 100$ cm we find that the pressure at the closed end of the fuel element reaches the value 1.1Pc in 4.6 sec.

If the defect is 200 cm from the end the time lag is ~20 sec.

The estimates obtained are valid for $F_0 \geq 0.5$. Substituting the assumed values into Eq. (10) we find that τ_{lag} must be longer than 0.1 sec, and our assumption is valid.

From the estimate of the time lag we conclude that the pressure inside the cladding of a leaking fuel element follows the pressure change in the reactor with only a short delay as the reactor cools down.

Estimate of the Amount of Gas inside the Cladding. Analysis of a simplified model of the release of gas from a leaking fuel element as the reactor pressure decreases shows that at the instant the pressure in the reactor vessel reaches atmospheric only part of the gas which was inside the fuel element cladding is still there. The amount of gas which escapes can be estimated by using the gas laws. For the values of P_c and P_0 assumed above and T_0 ~1200°K we find that 4.3% of the gas which was inside the cladding of a leaking fuel element remains there. Thus as the working pressure in a shutdown reactor decreases to atmospheric more than 95% of the gaseous fission products originally present inside the cladding of a leaking fuel element escape into the coolant. This occurs practically instantaneously following the pressure change in the reactor vessel.

LITERATURE CITED

1. V. I. Polikarpov et al., Control of Hermeticity of Fuel Elements [in Russian], Gosatomizdat, Moscow (1962).
2. B. Lastman, Radiation Phenomena in Uranium Dioxide [in Russian], Atomizdat, Moscow (1964).
3. B. V. Samsonov and A. K. Frei, "The role of gas bubbles in the release of gaseous fission products of UO_2," Atomnaya Tekhnika za Rubezhom, No. 8 (1970).
4. K. Kummerer, "The behavior of fuel elements at high burnup," Atomnaya Tekhnika za Rubezhom, No. 9 (1972).
5. A. V. Lykov and Yu. A. Mikhailov, The Theory of Heat and Mass Transfer [in Russian], Gosenérgoizdat, Moscow (1963).
6. A. V. Lykov, The Theory of Heat Conduction [in Russian], Vysshaya Shkola, Moscow (1967).
7. R. Collins, Flow of Fluids through Porous Materials, Reinhold, New York (1961).

DISTRIBUTION OF THE PARAMETERS OF TWO-PHASE FLOW OVER THE CROSS SECTION OF A CHANNEL WITH A FUEL ROD BUNDLE

Yu. V. Mironov and S. V. Shpanskii

UDC 621.039.5:532.5

We describe the PUChOK-2 program designed for the thermal-hydraulic calculation of a channel with a bundle of smooth fuel rods taking account of the nonuniformity of the distribution of flow parameters over the cross section of the channel. The results of the calculations are compared with experiment.

The essence of the method consists in dividing the "useful" cross section of a channel of complex shape into elementary cells within each of which the variation of the flow parameters (mass velocity, heat and steam content) can be neglected. The bundle is considered as a system of parallel communicating channels, and the hydraulic equations are written for each of them, taking account of their interaction. This procedure has been used in a number of algorithms [1-5]. At the same time the hydrodynamics and the laws of interaction of the flow in the cells are being studied intensively [6-10].

Suppose the cross section of a channel is divided into N cells. We denote the useful cross section of the k-th cell by F_k, and the perimeters of the rods entering this cell by Π_k^j, where j corresponds to the numbering of the walls in the cell. A steam–water mixture flows through the cell under consideration with a flow rate G_k, a heat content i_k, and a steam content x_k. We denote friction at the j-th wall by τ_k^j, and the heat flux by q_k^j. Cell k borders on cell n whose parameters are given the subscript n. The length of an arbitrary line separating the cells is Π_{kn}.

We denote by G_{kn} the mass flow rate from the n-th cell into the k-th. We call this quantity positive if the flow is from the n-th to the k-th cell, and negative if it is in the opposite direction. We denote the Reynolds stress and the turbulent transfer of heat at the cell boundary by variables with two subscripts: τ_{kn} and q_{kn}. Clearly

$$G_{nk} = -G_{kn}. \tag{1}$$

By using (1) we see that the maximum number of possible intercurrents M_{max} between cells is

$$M_{\max} = \frac{N(N-1)}{2}. \tag{2}$$

By taking account of the outflow from all cells connected with the k-th we write the mass balance equation for the k-th cell in the form

$$\frac{dG_k}{dz} = \sum_n G_{kn}, \tag{3}$$

where z is the coordinate along the axis of the channel.

Summing (3) over all k and using (1) we obtain the mass balance for the whole channel

$$\sum_{k=1}^{N} G_k = G = \text{const}. \tag{4}$$

We introduce the relative quantities

$$y_k = G_k/G \quad \text{and} \quad g_{kn} = G_{kn}/G; \tag{5}$$

then Eqs. (3) and (4) take the form

Translated from Atomnaya Énergiya, Vol. 39, No. 6, pp. 403-408, December, 1975. Original article submitted February 10, 1975.

A system of three cells can have a maximum of three connections and one cycle; i.e., the difference between the number of connections and the number of cycles is two. If it has only two connections there are no cycles and this difference is again two. Let us add a fourth cell. This can add one, two, or three connections with the formation of one or two cycles leaving the difference between the increase in the number of connections and the number of cycles equal to one. A similar situation obtains in the general case also when the initial system has an arbitrary number of cells. Thus for N cells the difference between the number of connections and the number of cycles is

$$(N-3)+2=N-1.$$

This means that after using the equations of the cycles N − 1 intercurrents remain undetermined. To this number must be added the N quantities y_k and p; i.e., the total number of unknowns is

$$N-1+N+1=2N.$$

But the mass and momentum balance equations for the cells give us just this number of equations. These results enable us to eliminate the intercurrents g_{kn} explicitly from the system of equations to be integrated. This procedure permits the representation of the convective intercurrents g_{kn} by linear functions with constant coefficients of the rates of change of flow rates in the cells (dy_k/dz) and thus to eliminate the necessity of iterations to equalize the pressures over the cells.

Dissipation and the kinetic energy of the flow can be neglected in setting up the energy balance for the flow in the k-th cell. For the heat content i_k in the cell we have

$$\frac{d}{dz}(G_k i_k)=\sum_j q_k^j \Pi_k^j+\sum_n G_{kn} i_{kn}+\sum_n q_{kn}\Pi_{kn}. \tag{11}$$

Here the first term on the right-hand side is equal to the heat supplied to the walls entering the cell; the second term corresponds to the energy entering the cell with the convective mass intercurrents, and the third term is the influx of heat as a result of turbulent heat conduction at the cell boundary. The heat content brought by convective intercurrents is equal to the heat content in the donor cell. The enthalpies of the flow in Eq. (11) are defined as the average discharge enthalpies. One can assume that in boiling the state of the steam corresponds to equilibrium: $i_s = i''$ and $v_s = v''$. It is known, however, that the parameters of the liquid phase can differ from the equilibrium values because of the surface boiling of an underheated liquid. In this case further relations are required to describe the state of the liquid phase.

The mass balance for the liquid phase in a cell has the form

$$\frac{dG_{wk}}{dz}=-G_k^{evap}+\sum_n G_{wkn}, \tag{12}$$

where $G_{wk}=(1-x_k)y_k G$ is the flow rate of the liquid phase in the cell, G_k^{evap} is the rate of evaporation of the liquid phase, x_k is the steam content of the flow in the cell, and the sum on the right-hand side corresponds to the inflow of the liquid phase from the neighboring cells. Assuming as before that the structure of the interflow is similar to that of the main flow in the cell we have

$$G_{wkn}=(1-x_{kn})\,g_{kn}G, \tag{13}$$

where x_{kn} is the steam content in the donor cell. Then the equation of energy flow in the cell has the form

$$\frac{d}{dz}(G_{wk}i_{wk})=\sum_j q_k^j\Pi_k^j\varepsilon_k^j-i_{wk}G_k^{evap}+\sum_n G_{wkn}i_{wkn}+\sum_n q_{wkn}\Pi_{wkn}. \tag{14}$$

In this expression the coefficients ε_k^j give the fraction of the entering heat flux going into heating the liquid phase. Consequently $(1-\varepsilon_k^j)q_k^j$ goes into the formation of steam. As before i_{wkn} is the heat content of the liquid phase in the donor cell, and q_{wkn} is the turbulent heat flux at the boundary of adjacent cells. Expressing G_k^{evap} from (12) by using (5) and (13) we obtain

$$(1-x_k)\,y_k\frac{di_{wk}}{dz}=\frac{1}{G}\sum_j q_k^j\Pi_k^j\varepsilon_k^j+\sum_n g_{kn}i_{wkn}-\frac{1}{G}\sum_n q_{wkn}\Pi_{kn}. \tag{15}$$

Thus Eqs. (7), (8), (11), and (15) together with (6) and (10) for determining the intercurrents g_{kn} comprise a system of 3N+1 first-order equations containing the 3N+1 unknowns p, y_k, i_k, and i_{wk} (k = 1, 2, ..., N) which suffice for the calculation of the flow of the steam–water mixture in a system of interconnected elementary channels.

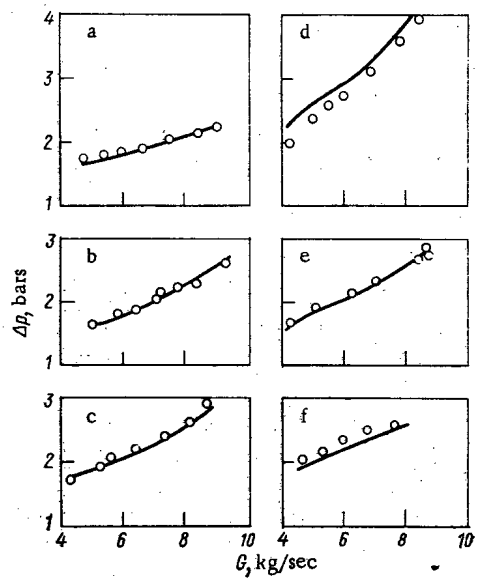

Fig. 1

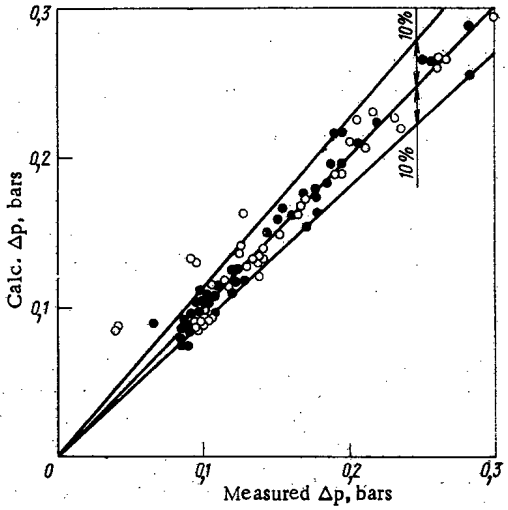

Fig. 2

Fig. 1. Comparison of calculated and experimental values of the pressure drop (channel No. 1 [6]). Heat flux 0.434 MW/m^2, inlet temperature: a) 210-215; b) 221-228; c) 238-240, d) 257-262, e) 244-250, f) 219-222°C for a heat flux of 0.540 MW/m^2.

Fig. 2. Comparison of calculated pressure drop with experimental data of [7]. ○) channel A; ●) channel B.

If it is assumed, as usual, that the specific volume v_{ik} in Eq. (8) is a function of the local flow parameters in the cell (p, x_k, G_k), i.e.,

$$\frac{dv_{ik}}{dz}=\frac{\partial v_{ik}}{\partial p}\frac{dp}{dz}+\frac{\partial v_{ik}}{\partial y_k}\frac{dy_k}{dz}+\frac{\partial v_{ik}}{\partial i_k}\frac{di_k}{dz}+\frac{\partial v_{ik}}{\partial i_{wk}}\frac{di_{wk}}{dz}, \tag{16}$$

the system obtained is almost linear in the derivatives with respect to z because a number of the quantities (J_{kn}, i_{kn}, i_{wkn}) depend on the signs of the interflows which in turn are determined by the derivatives of the flow rates over the cells. However, there is a rather long section of the channel where the interflows retain their directions; i.e., the signs change rather rarely. This is important for the numerical integration of the system. The system obtained is integrated lengthwise by Euler's method with a scaling which gives adequate accuracy for a small expenditure of machine time.

Placing spacing grids in a channel not only produces additional resistance but also causes a redistribution of the flow rates between cells. The analysis of the fluid flow through a grid can be conveniently separated into two stages. In the first stage there is a redistribution of flow rates between the cells of the channel, and in the second there is observed a trend toward a constant flow rate in each cell through the local resistance accompanied by pressure losses which can be characterized by the coefficient of resistance of the grid in the cell. Taking account of the equality of the pressure drops in all the cells this model leads to a system of nonlinear algebraic equations which is solved by the method of successive approximations in the PUChOK-2 program.

The terms characterizing turbulent exchange by momentum and energy in Eqs. (8), (11), and (15) are proportional to the difference in velocities or heat contents in the cells and can be written in the form

$$\tau_{kn}=\varepsilon^{T}_{kn}\frac{G}{L_{kn}}\left(\frac{y_n v_{\varphi n}}{F_n}-\frac{y_k v_{\varphi k}}{F_k}\right);$$
$$q_{kn}=\frac{\varepsilon^{T}_{kn}}{L_{kn}}(i_{\varphi n}-i_{\varphi k}), \tag{17}$$

where ε^{T}_{kn} is the coefficient of turbulent exchange between cells depending on the system flow parameters, L_{kn} is the characteristic mixing length, and φ denotes averaging over the cross section of the cell. In the PUChOK-2 program the ε^{T}_{kn} are extrapolated from the equations given in [1] for single-phase flows, which is equivalent to assuming a homogeneous structure of the two-phase flow at the cell boundary.

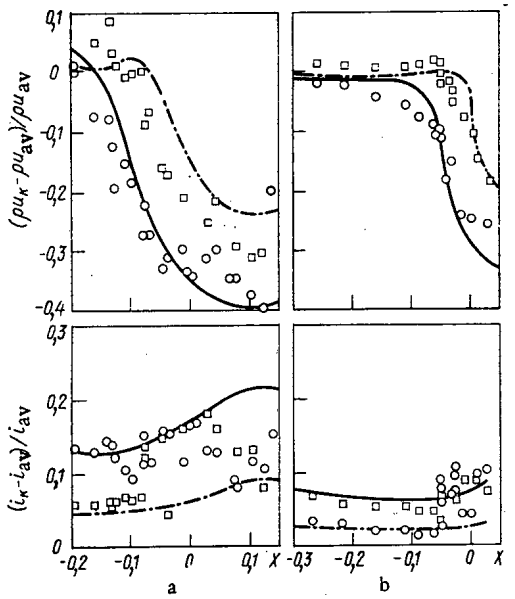

Fig. 3

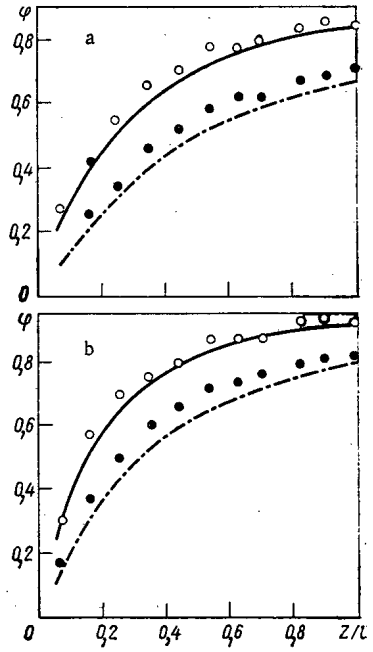

Fig. 4

Fig. 3. Distribution of mass velocity and heat content in cells of a 16 rod bundle (data from [8]). Pressure 82.6 bars, power 1.5 MW. Mass velocity: a) 1350; b) 2700 kg/m^2 sec; ○, □) experiment; ——, –. –. – –) calculation for hot and cold cells respectively.

Fig. 4. Longitudinal distribution of volumetric steam content in cells of a channel with six rods [9]. a) Experiment No. 13037; b) experiment No. 13042. ○, ●) experiment; ——, –. –. – –) calculation for central and peripheral cells, respectively.

Relations obtained in experiments with pipes [11, 12] were used to complete the above system of equations and to characterize friction, the origin of surface boiling, and the slipping of phases in the cells. In this case the hydraulic diameter of a cell is taken as the controlling dimension.

The pressure, heat content, and coolant flow rate are generally known at the channel entrance. However, in order to solve the equations obtained it is necessary to specify the initial distribution of flow rates over the cells. As a rule there is an unheated portion of the channel before the heated part, and this permits taking the stabilized distribution of mass velocities in the cells as the initial condition. The system has a large attenuation and therefore, as calculations show, small variations of the initial distributions do not affect the results of the calculation at a large distance.

Thus, with the PUChOK-2 program one can investigate the distribution of thermal-hydraulic parameters of two-phase flow over the height and cross section of the rod assembly.

Figures 1 and 2 compare the pressure drop calculated by the PUChOK-2 program with experimental data from [6, 7]. The experiments in [6] were performed at the Kurchatov Institute of Atomic Energy on bundles of 19 rods 13.5 mm in diameter and 7 m long. The rods were packed in a triangular and square arrangement in a circular drum. Two types of spacers were placed 350 mm apart. The data from [7] were obtained on a bundle of nine rods 1 m long and 10.2 mm in diameter. The rods were arranged in a square lattice with five spacers along their length. The calculated results generally agree with experiment to within 10-15%. This accuracy is satisfactory for such complex hydraulic calculations.

Although the calculated hydraulic losses do not agree with experiment, such agreement is, strictly speaking, a sufficient condition for the reliability of theoretical data on the internal structure of flow in a channel, but it is necessarily also an indirect confirmation of the correctness of the theoretical model for a large number of experiments analyzed. The most useful test of the procedure is, of course, a comparison with directly measured distributions of flow parameters over the useful cross section of the channel. Not many such studies have been made. In addition the technical complexity of such measurements significantly affects the accuracy of the results obtained.

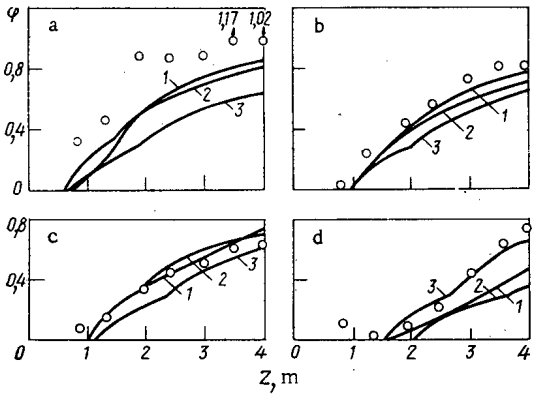

Fig. 5. Longitudinal distribution of volumetric steam content in cells of a channel with 36 rods [10]. Experiment No. 313020: a) cell 1 (central); b) cell 2; c) cell 3; d) cell 4 (peripheral); ○) experiment. Calculation: 1) by PUChOK-2 program; 2, 3) by HAMBO program; mixing coefficients 2) 0; 3) 5.

Figure 3 compares calculations by the PUChOK-2 program with experimental data from [8]. The experiments were performed on a bundle of 10.72-mm-diameter rods in a square lattice with a pitch s/d = 1.32. The nonuniformity of heat release over the cross section of a channel was simulated in the experiments, and at the exit from the section there were different flow rates from two geometrically identical cells with different heating ("hot" and "cold" cells; the whole useful cross section of the channel was divided into 16 cells in the calculations). The calculation gives a good description of the decrease of mass velocity in cells with initial surface boiling. For steam contents of ~10% there is a considerable spread of the experimental results, so that the heat content in a "cold" cell sometimes exceeds that of a "hot" cell. The calculations do not give such effects. It should be kept in mind that arranging for separate discharges from the cells causes perturbations in the flow of a magnitude which is difficult to estimate theoretically and to control experimentally.

Investigation of the distribution of the volumetric steam content of cells by the transmission of narrow beams of gamma rays gives less information than separate discharges, but it does not distort the structure of the flow in a bundle. This method was used in [9] to investigate a bundle of six rods in a circular cylinder. Figure 4 compares calculations with experiments in which the steam content in cells was measured over the whole channel length. The calculation is in good agreement with experiment for the central "hot" cell, but for a peripheral cell the experimental points lie somewhat above the calculated curve. The relations for volumetric steam content based on data for circular pipes may require a certain refinement in transforming to cells of complex shape.

Figure 5 compares calculations with one of the experiments of [10] on the volumetric steam content in cells for a bundle of 36 rods. The useful cross section of the channel was divided into four concentric cells for the calculations. The channel was gamma rayed in 12 directions. The figure also shows curves calculated with the HAMBO program [2]. The second and third cells show the best agreement of calculation and experiment. The experimental data for the first cell have a very large spread; in the fourth cell, as for the data of [9], the calculated values lie below the experimental data.

Further improvement of the calculational methods required refining our knowledge of the hydraulics of two-phase flow in an elementary cell of a channel, exchange at the cell boundaries, and the flow around the spacers in the channels.

LITERATURE CITED

1. D. Rowe, COBRA-II: A Computer Digital Programme for Thermal-Hydraulic Subchannel Analysis of Rod Bundle Nuclear Fuel Elements, BNWL-1229 (1970).
2. R. Bowring, HAMBO: A Computer Program for the Subchannel Analysis of the Hydraulic and Burnout Characteristics of Rod Clusters, Part I, AEEW-R524 (1967); Part II, AEEW-R582 (1968).
3. V. Osmachkin and D. Borisov, Intern. Heat-Trans. Conf., Vol. 5, Paris-Versailles (1970), p. 273.
4. N. Kattchee and W. Reynolds, HECTIC-II: An IBM 7090 FORTRAN Computer Programme for Heat-Transfer Analysis of Gas or Liquid Cooled Reactor Passage, IDO-28595 (1962).
5. St. Pierre and C. Carl, SASS Code-1, Subchannel Analysis for the Steady State, APPE-41 (1966).
6. V. S. Osmachkin, Preprint IAE-2343, Moscow (1974).
7. A. Campanile et al., Forced Convection Burnout and Hydrodynamic Instability Experiments for Water at High Pressure, Part VI, EURATOM, EUR 4468e (1970).
8. J. Castellana and J. Casterline, Nucl. Engng. and Design, 22, No. 1, 3 (1972).
9. A. Bhattacharya, S. Sallary, and S. Haga, in: Proc. EURATOM Symp. on Two-Phase Flow Dynamics, Sept. 22-27 (1967).

10. O. Nylund et al., Hydrodynamic and Heat Transfer Measurements on a Full Scale Simulated 36-Rod MARVIKEN Fuel Element with Uniform Heat Flux Distribution, FRIGG-2, R4-447/RTL-1007, Sweden (1968).
11. N. Zuber, F. Staub, and G. Baiuord, in: Advances in Heat Transfer, Academic Press, New York (1970).
12. J. Thom, Intern. J. Heat and Mass Transfer, 7, No. 7, 709 (1964).

QUANTITATIVE ESTIMATION OF THE CORROSION OF ALUMINUM ALLOYS UNDER CONDITIONS OF HEAT TRANSFER

V. V. Gerasimov, A. I. Gromova, and V. G. Denisov

UDC 621.039.54

Experience in reactor building shows that aluminum alloys may be successfully used as material for the cans of water-cooled-reactor fuel elements [1].

It is accordingly very important to study the corrosion resistance of these alloys under conditions of heat transfer. Authors studying the effect of thermal flux on the corrosion resistance of various materials [2-5] earlier came to the conclusion that corrosion took place more rapidly under these conditions as a result of the rise in temperature at the metal/oxide boundary. For aluminum alloys the situation is exacerbated by the low thermal conductivity of the corrosion products.

The rise in temperature at the metal–oxide interface may be very considerable for high values of the thermal flux. If we consider that a temperature of 300°C is close to the maximum value at which (from considerations of corrosion) the use of aluminum alloys is permissible, the presence of a thermal flux may exert a considerable influence on the corrosion resistance of the alloy in high-temperature water. A number of methodical difficulties impede the study of corrosion at high temperatures, pressures, and thermal fluxes; it is therefore very important to correlate existing results and develop methods of predicting the corrosion resistance of an alloy quantitatively.

In this paper we shall make use of existing data relating to corrosion tests on the aluminum alloy M388 (Kh8001) containing ~0.5% Fe and ~1% Ni, and shall estimate the corrosion resistance of this alloy theoretically under heat-transfer conditions corresponding to the movement of the cooling water.

The results of an earlier study of the corrosion resistance of aluminum alloy M388 under autoclave conditions at various temperatures [6] show that up to 350°C the corrosion process obeys a parabolic law, i.e., it is controlled by diffusion. The loss of weight by the metal may be expressed as a function of the testing time for any specified temperature (Fig. 1) by using the equation

$$W = a\tau^{\frac{1}{2}}, \tag{1}$$

where W is the loss of weight by the metal in mg/cm^2, a is a temperature-dependent coefficient, τ is the testing time in h. Between the coefficient a and the corrosion velocity constant we have the relation

$$K = \frac{a^2}{2}, \tag{2}$$

where K is the corrosion velocity constant in (mg/cm^2)^2/h, which is a function of temperature under specified conditions and is related to the latter by the Arrhenius equation

$$K = A\,e^{-\frac{Q}{RT}}. \tag{3}$$

The activation energy of the corrosion process Q may be found from the equation log K = f(1/T), illustrated in Fig. 2.

In order to calculate the corrosion in the presence of a thermal flux, the value of the temperature in Eq. (3) must be found from the heat-conduction equation. Remembering that the film thickness of the

Translated from Atomnaya Énergiya, Vol. 39, No. 6, pp. 409-411, December, 1975. Original article submitted May 16, 1975.

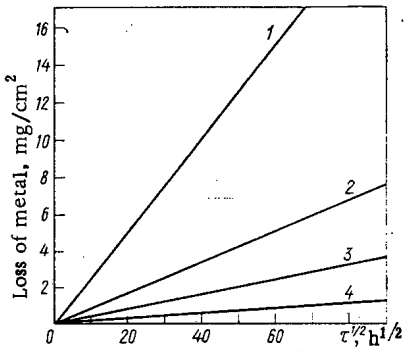

Fig. 1. Corrosion of alloy M388 in distilled water [6] at various temperatures, °C: 1) 350; 2) 250; 3) 200; 4) 100.

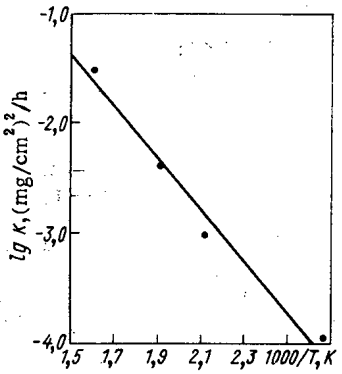

Fig. 2. Logarithm of K as a function of temperature.

corrosion products is much smaller than the diameter of the fuel-element can, we may use the heat-conduction equation for a plane wall

$$T = T_0 + \frac{q\delta}{\lambda 2}, \tag{4}$$

where T is the average temperature of the corrosion products in °K, T_0 is the temperature of the oxide–water interface in °K, δ is the thickness of the corrosion film, m, q is the specific thermal flux, kcal/(m²·h), λ is the thermal conductivity of the corrosion products, kcal/(m·h·°C).

Equation (4) contains a term equal to half the thickness of the corrosion film, since it is used to determine the mean temperature of the corrosion products. It is this temperature which should be substituted into Eq. (3), since the limiting stage of the corrosion process is the diffusion of the oxygen anions through the protective films of corrosion products [6, 7].

In view of the fact that the corrosion of aluminum alloys in water is controlled by diffusion, the rate of the oxidation process may be expressed by the equation

$$\frac{dW}{d\tau} = \frac{K}{W_f} \tag{5}$$

where W_f is the amount of aluminum entering into the protective oxide film in mg/cm².

For static test conditions in an autoclave it may be considered that all the metal corrosion products occur in the form of a film, until the instant at which they peel off. Taking account of this, we may express Eq. (5) in the following form for corrosion under heat-transfer conditions:

$$\frac{dW}{d\tau} = \frac{A\exp(-Q/RT)}{W}. \tag{6}$$

In order to reduce Eq. (6) to a single variable we make use of Eq. (4), in which the film thickness of the corrosion products is replaced by the quantity W (linearly related to the film thickness), and obtain

$$\frac{dW}{d\tau} = \frac{A\exp(-Q/R(T_0+cW)}{W}, \tag{7}$$

where c is a quantity equal to $2.9 \cdot 10^{-6} q/\lambda$ for aluminum alloys.

On solving the differential equation (7) by the Runge–Kutta method in an electronic computer, we may thus obtain the $W = f(\tau)$ relationship under static conditions in the presence of heat transfer.

Under dynamic test conditions, in the presence of heat transfer, we must allow for the increase in the coefficient K in Eq. (2) and also for the intensive transfer of the corrosion products into the water as a result of dissolution and the mechanical abrasion of the oxide from the metal surface. The rate of transition of the oxide into the water is approximately constant for steady-state hydrodynamic conditions, and is determined by the temperature at the oxide–water interface [8]. Since the corrosion rate falls as the film of corrosion products grows, while the rate of their transfer to the water remains constant, a dynamic equilibrium should be established, after which the thickness of the film on the metal surface will remain constant. This explains the linear time dependence of the corrosion products in long experiments. Since the corrosion rate on the linear part of the corrosion-time curve equals the rate of dissolution, we may determine the latter from the equation $S = \Delta W/\Delta\tau$, where S is the rate at which the oxide passes into the water (referred to the amount of aluminum), in mg/(cm²·h); ΔW is the mass loss of metal corresponding to the linear part of the curve, in mg/cm²; and Δt is the time during which mass loss occurs, in h.

It has already been mentioned that for the system in which the tests are being conducted the rate of transition of the oxide into the water is a function of the temperature at the oxide–water interface only.

TABLE 1. Corrosion of Alloy 8001 in Desalinated Water at T = 250°C

Time, h	Calc. for Al, mg/cm²			Expt. for Al, mg/cm²		
	in the oxide film	in H_2O	total corrosion	in the oxide film	in H_2O	total corrosion
1000	8,08	12,40	20,48	6,50	11,30	17,80
2013	9,51	24,90	34,41	8,26	25,13	33,39

Note. Thermal flux q = 40 W/cm², water flow velocity 5 m/sec.

Thus S may be determined from the results of tests carried out on the alloy without heat transfer, but at the temperature corresponding to T_0 in the case of tests in a thermal flux. From the material balance we have

$$W = W_f + S\tau. \tag{8}$$

Substituting Eq. (8) into (5) we obtain

$$\frac{dW}{d\tau} = \frac{K}{W - S\tau}. \tag{9}$$

As already indicated, under dynamic conditions the corrosion velocity constant is higher than under static conditions; for subsequent calculations we shall need to determine its value. For a dynamic system in which the formation of the protective corrosion film is accompanied by its dissolution in the water, we have the following equation:

$$\tau = \frac{W}{S} - \frac{K}{S^2}(1 - \exp(-WS/K)), \tag{10}$$

where W is the loss of metal as a result of corrosion in mg/cm², S is the rate of transition of the oxide into the water in mg/(cm²·h), K is the corrosion velocity constant in (mg/cm²)²/h, τ is the test period in h.

Equation (10) may be derived, as in [9], by allowing for the parabolic process of film formation and the linear dissolution of the corrosion products. The constant K may be found from Eq. (10) by simple calculation for large values of W, when the exponential term may be neglected:

$$K = S(W - S\tau). \tag{11}$$

Using Eq. (11) to determine the corrosion velocity constant at any temperature, and also the equation

$$\ln\frac{K_2}{K_1} = \frac{Q}{R}\frac{T_2 - T_1}{T_1 T_2}, \tag{12}$$

we may find K for the conditions under which the corrosion was calculated in the presence of heat transfer. If we assume that this value is K_2, from Eq. (12) we obtain

$$K_2 = K_1 \exp[Q(T_2 - T_1)/RT_1T_2], \tag{13}$$

and correspondingly, on allowing for (4), (7), and (8), we shall have the following equation for T_2:

$$T_2 = T_0 + c(W - S\tau), \tag{14}$$

where c is equal to $2.9 \cdot 10^{-6} q/\lambda$ for aluminum alloys.

Under dynamic conditions the corrosion in the presence of heat transfer may be expressed in the following way after using (5), (9), (13), and (14):

$$\frac{dW}{d\tau} = \frac{\exp\frac{Q}{R}[T_0 + c(W - S\tau) - T_1]/[T_0 + c(W - S\tau)T_1]}{W - S\tau}. \tag{15}$$

This equation may be solved, as in the case of Eq. (7), by the Runge–Kutta method, or in some other way, using an electronic computer.

If computer calculation is for any reason difficult, the variables in Eq. (15) may be separated by making the substitution

$$W_f = W - S\tau.$$

In this case the solution may be reduced to the integrated form

$$\tau = \int_0^{W_f} \frac{W_f \, dW_f}{K_1 \exp\left\{\frac{Q}{R}\left[\frac{(T_0 + cW_f) - T_1}{(T_0 + cW_f) T_1}\right]\right\} - S\tau}. \quad (16)$$

The latter expression may be calculated by the Simpson method, estimated graphically, or again submitted to the computer.

Thus, we may neglect the amounts of the deposits formed on the heat-transferring surfaces. This is because the oxide film consisting of aluminum corrosion products is extremely susceptible to dissolution. Under such conditions we can hardly expect the deposits to be firmly attached to the heat-emitting surface [10]. The method here proposed was verified for the case of corrosion on the aluminum alloy Kh8001, which has been the subject of a great deal of research. The results of the calculation are shown in Table 1, together with experimental data published in [8].

LITERATURE CITED

1. A. S. Zaimovskii et al., Fuel Elements of Nuclear Reactors [in Russian], Atomizdat, Moscow (1972).
2. A. Fisher et al., Corrosion, 15, No. 5, 53 (1959).
3. I. Draley, in: Proc. 2nd Intern. Conf., Vol. 5, Geneva (1958), p. 113.
4. I. Ayres, ibid., p. 153.
5. N. G. Rassokhin et al., in: Water Conditions and Processes in the Steam Generators of Power Stations [in Russian], No. 83, Izd. MÉI, Moscow (1971), p. 98.
6. R. Dillon, Corrosion, 15, No. 1, 21 (1959).
7. V. Troutner, ibid., p. 17.
8. D. Dickinson, Corrosion, 21, No. 1, 19 (1965).
9. R. Dillon, in: Proc. Intern. Conf. on Aqueous Corrosion of Reactor Materials, Brussels (1959), p. 134.
10. J. Griess, H. Savage, and J. English, ORNL-3541 (1954).

CONTINUOUS RADIOCHEMICAL ANALYSIS OF THE FISSION PRODUCTS IN AN AQUEOUS COOLANT OF A NUCLEAR REACTOR

L. N. Moskvin, L. K. Zakharov,
G. G. Leont'ev, V. A. Mel'nikov,
I. S. Orlenkov, and G. K. Slutskii

UDC 543.544.621.039.5

Continually supplied information on the concentrations (activities) of the fission products in a coolant can be used to monitor the state of fuel-element jackets in a reactor. Methods of continuously monitoring the activity of some krypton and xenon isotopes and of some fission products which are sources of delayed neutrons are investigated in [1]. The goal of the present work is to develop a continuous radiochemical analysis method for I, Cs, Ba, Sr, and Ce isotopes in an aqueous coolant of a reactor. A continuous two-dimensional chromatographic separation of the elements is employed to separate cesium from salt solution of complex composition and to separate rubidium from cesium [2].

The conventional two-dimensional chromatographic separation of substances takes place in a rotating sorbent layer of homogeneous composition. The simultaneous separation of I, Cs, Ce, Ba, and Sr isotopes by virtue of their sharply differing chemical properties is conveniently made with various sorbents [3]. A possible scheme of this process involving several sorbent layers arranged in series is shown in Fig. 1.

The mixture to be analyzed is continuously fed to the sorbent layers which are arranged in series and rotated at a constant rate. Depending upon their chemical properties, the components of the mixture are selectively absorbed by the various sorbent layers and, after arriving at the zone with eluting solvents, are washed from the sorbents. A practically continuous process can be obtained with uniformly rotating sorbent layers which are separated by fixed intermediate collectors. A component which was not absorbed in the preceding sorbent layers arrives at the lower layer, is absorbed by it, and, having entered the elution zone, is washed from the sorbent layer. The position of the intermediate collector chamber must account for the shift of a particular component during its passage through the upper rotating sorbent layer; the shift takes place over the angle

$$\psi = \omega \frac{h}{v}, \qquad (1)$$

where ω denotes the rate of rotation of the sorbent layers; h denotes the height of the upper sorbent layer; and v denotes the velocity with which a component moves.

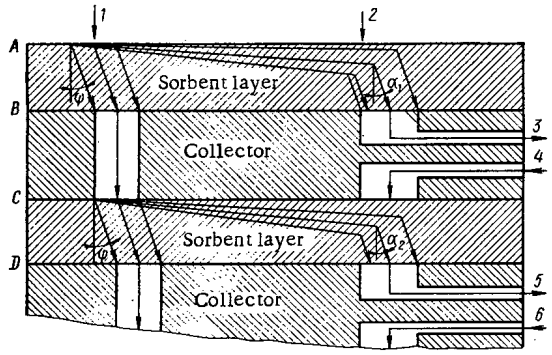

Fig. 1. Scheme of the two-dimensional chromatographic separation of a multicomponent mixture: 1) mixture to be analyzed; 2, 4, 6) eluents for the first, second, and third component, respectively; 3, 5) first and second component.

The exit points of the zone containing the component to be separated from a sorbent layer can be determined from the function which describes the shift of the zone during the two-dimensional chromatographic process:

$$\alpha = \frac{360}{T}\left(\frac{1+K_d\frac{V_1}{V_2}}{v}\right)h, \qquad (2)$$

where α (degrees) denotes the angle by which the maximum of the zone deviates from the direction of eluent

Translated from Atomnaya Énergiya, Vol. 39, No. 6, pp. 412-415, December, 1975. Original article submitted February 10, 1975; revision submitted May 12, 1975.

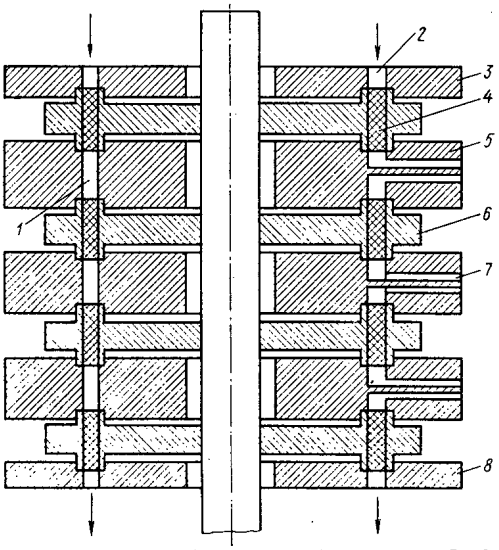

Fig. 2. Scheme of the two-dimensional chromatographic apparatus for the continuous separation of the I, Cs, Ce, Ba, and Sr isotopes: 1) transverse slot through the intermediate collector; 2) chamber of the upper collector; 3) upper collector; 4) porous sorbent; 5) intermediate collector; 6) sorbent ring; 7) chamber of the intermediate collector; 8) lower collector.

TABLE 1. Distribution Coefficients of I, Ce, Cs, Sr, and Ba in the Sorbent-Eluting Solution System

Sorbent	Element separated	Eluting solution	K_d
TOA	Iodine	1 M NH_4NO_3	0,3
D2EHPhA	Cerium	0,01 M Trilon B, pH = 5,5	0,1
APM	Cesium	5 M NH_4NO_3	3,0
KU-2	Strontium and barium	0,01 M Trilon B, pH = 10	1,5 (strontium) 2,6 (barium)

flow; T denotes the period (min) of rotation of the sorbent layers; v (cm/min) denotes the linear velocity of the solvent flow; h (cm) denotes the height of the sorbent layer; K_d denotes the distribution coefficient of an element in the sorbent–eluent system; and V_1/V_2 denotes the volume ratio of the fixed and moving phases in the mass of the sorbent.

Two-dimensional chromatography must satisfy additional requirements when several sorbent layers are used in the separation of various substances. When the mixture to be analyzed is simultaneously fed to the rotating layers, the eluents must be added separately to each sorbent layer and the fractions must be separately removed from each sorbent layer. Figure 2 shows a two-dimensional chromatographic apparatus with several sorbent layers for separating multicomponent mixtures. The sorbent layers have the same shape and consist of fluoroplastic (Teflon) rings with cylindrical openings filled with porous sorbent modules which were cut from a single porous block with a diameter tolerance of ±1-2%; the modules were pressed into the ring opening. When this preparation of the two-dimensional columns is employed, the difficulties are avoided which otherwise arise when porous material is simultaneously fritted with the surrounding walls of a monolithic fluoroplast; therefore our method is more convenient than the previously described method of [2]. Each sorbent layer is composed of 36 cylindrical columns with a height of 20 mm and a diameter of 8 mm. It was established that these dimensions guarantee quantitative sorption of the elements to be separated at flow rates of 1-10 cm/min of the sample to be analyzed. Sorbent layers are arranged between fixed upper and lower collectors and separated by the fixed intermediate collectors. The upper collector comprises four insulated chambers having a length of 1/4 of the length of the circumference of the sorbent layer; the lower collector comprises 12 chambers. The intermediate collectors are rings of monolithic Teflon provided with a transverse vertical slot having half the length of the circumference of the sorbent ring and a radius equal to the radius of the porous part of the sorbent layer; the intermediate collectors also comprise chambers which are insulated from each other. Four chambers in the upper and lower parts are provided in each intermediate collector; the chambers have a length of 1/8 of the length of the circumference. The chambers in the upper part serve to collect the eluents from the upper sorbent layer; the chambers in the lower part are used to supply eluents to the lower sorbent layer. The transverse slot in the fixed intermediate collectors facilitates the passage of the sample material through the layers.

Four sorbent layers are inserted in the chromatographic apparatus for the continuous separation of I, Cs, Ce, Ba, and Sr isotopes. These sorbent layers are arranged in the following sequence: trioctyl amine (TOA) for separating iodine; di-2-ethylhexyl phosphoric acid (D2EHPhA) for separating cerium; ammonium phosphoromolybdate (APM) for separating cesium; and KU-2 cationite for separating barium and strontium.

The sorbents were prepared in the form of blocks by uniformly distributing the extractants and solid ion-exchange resins in the bulk of a compact inert carrier material according to the known method of [3]. The conditions for the continuous separation of I, Cs, Ce, Ba, and Sr isotopes were calculated according to [2]. In order to avoid a smearing of the zones at increasing α, the initial parameters (K_d, V, T) were selected so that the α values were minimal. The eluting solutions and their concentrations were selected on the basis of data obtained under static conditions for the distribution coefficients of the elements to be separated in the sorbent-eluting solution system (Table 1). The period of rotation of the sorbent layers

TABLE 2. Sequence of Feeding the Solutions into the Chromatographic Apparatus

Solution	No. of collector and channel
Mix to be analyzed	1, 1
1 *M* NH_4NO_3	1, 3
Trilon B, pH = 5,5	2, 2; 2, 3
5 *M* NH_4NO_3	3, 2; 3, 3
Trilon B, pH = 10	4, 2; 4, 3
0,1 *M* HCOOH	1, 2; 1, 4; 2, 1; 2, 4; 3, 1; 3, 4; 4, 1: 4, 4

Remark. Collector 1 is the upper collector; the first, second, and third intermediate collectors correspond to collectors 2, 3, 4, respectively (see Fig 2).

TABLE 3. Activity of the Isotopes which were Separated from the Various Sorbents (% of the initial isotope quantities)

No. of channel and collector	TOA	D2EHPhA	APM	KU-2
1	—	—	1,0 ^{137}Cs	—
2	98,0±2,0 ^{131}I	91±3 ^{144}Ce	92±3 ^{137}Cs	97±2 ^{133}Ba
3	—	1,0 ^{144}Ce	5,0±1 ^{137}Cs	2,0 ^{133}Ba
4	—	—	—	—

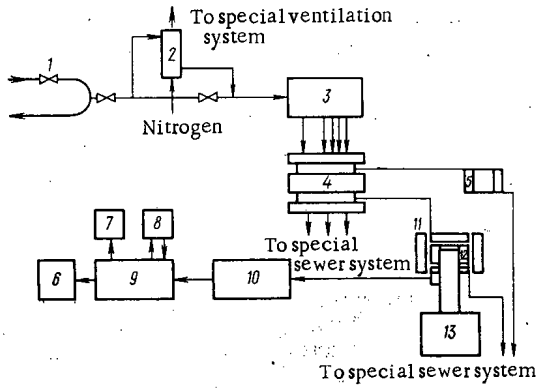

Fig. 3. Block scheme of the apparatus for the continuous monitoring of the iodine and cesium activities: 1) sampling line No. 5; 2) sparger; 3) sample preparation unit; 4) apparatus for the two-dimensional chromatographic separation; 5) measuring chamber for the cesium fraction; 6) digital printer; 7) recorder; 8) tape recorder; 9) LP-4840 analyzer; 10) UMShA-2 amplifier; 11) shielding; 12) measuring chamber for the iodine fraction; 13) DGΔ(K)-25 sensor.

was 30 min, and the feed rate of the solution 2.8 cm/min, which corresponded to a sample consumption of 0.5 liter/h when the sample was fed in through the channel of the upper collector. Under these conditions the α values calculated with Eq. (2) did not exceed 15° and, hence, the output of the zones of substances to be separated by the two-dimensional apparatus could be predicted for the chambers situated directly under the feed chambers of the eluting solutions. The deviation of the flow of components which were not absorbed was determined with Eq. (1) and brought into account by successive 3° shifting of the fixed intermediate collectors relative to the upper collector and relative to each other. Before the separation, certain amounts of formic acid (for stabilizing the isotope ions) and ammonium chloride (for suppressing the absorption of alkali-earth elements on APM) were introduced until the concentration of the substances in the sample to be tested reached 0.1 M. The sequence in which the mixture to be analyzed, the eluents, and the washing solution (0.1 M HCOOH) were fed into the chromatographic apparatus is indicated in Table 2.

The I, Ce, and Cs fractions were collected through the (upper) receiving channels of the first, second, and third intermediate collectors; the fractions of the rare-earth elements were collected through the channels of the lower collector. The analysis of the continuously separated fractions began after 30 min (time required for a single rotation of the sorbent layers; after this time, a stationary front of the components separated had been established).

The two-dimensional multisorbent chromatograph was tested with a model solution containing radioactive ^{131}I, ^{144}Ce, ^{137}Cs, and ^{133}Ba isotopes. The results of γ spectrometric measurements on the fractions separated from each sorbent layer is listed in Table 3. More than 90% of each isotope had been separated practically in a single channel which was situated under the feed channel for the eluent of the corresponding collector.

The apparatus was tested in practice with samples of the coolant taken from the main circuit of the Power Reactor in the I. V. Kurchatov Institute of Atomic Energy, where the two-dimensional chromatographic apparatus with two sorbent layers (TOA and APM; Fig. 3) was used.

We indicate below the specific activities of the various isotopes at the time at which the coolant sample was taken (activity expressed in Ci/liter):

^{138}Cs	$9.6 \cdot 10^{-5}$	^{131}I	$9.0 \cdot 10^{-7}$
^{139}Ba	$8.9 \cdot 10^{-5}$	^{132}I	$8.0 \cdot 10^{-6}$
^{140}Ba	$1.2 \cdot 10^{-6}$	^{133}I	$1.0 \cdot 10^{-5}$
^{91}Sr	$2.4 \cdot 10^{-5}$	^{134}I	$2.3 \cdot 10^{-5}$
^{92}Sr	$3.5 \cdot 10^{-5}$	^{135}I	$1.3 \cdot 10^{-5}$

The rate at which the solutions of the separated fractions flow through the measuring chamber is equal to the flow of both the coolant and the eluents and amounts to 0.5 liter/h. The time required for transferring the sample from the core to the point of measurement was 15 min in this case. Spectrometric measurements of the iodine and cesium fractions were made with an 80-ml measuring chamber and a Ge(Li) detector with a volume of 25 cm^3, which were used in conjunction with a UMShA-2 amplifier and an LP-4840 800-channel amplitude analyzer.

The resolution of the spectrometer was 7.5 keV for investigations at the energy 1332 keV; the accuracy of the calibration was ±6 keV in the range 0-2200 keV and ±4 keV in the range 0-1400 keV. For shielding the detector from the background radiation, the detector was inserted into a lead casing with a wall thickness of 10 cm. Two cycles of continuous 7-h operation of the chromatographic apparatus were run under constant conditions of reactor operation. Evaluation of the γ radiation spectra has shown that the activity of the iodine fraction originates from the $^{131-135}I$ isotopes, whereas the activity of the cesium fraction stems from the $^{134, 138}Cs$ isotopes. The spread of the measured activity values did not exceed 25% when the power level of the reactor was constant. The results obtained in testing the method lead us to the conclusion that two-dimensional chromatography with several sorbent layers arranged in series can be used in systems for the continuous monitoring of the composition of multicomponent mixtures.

LITERATURE CITED

1. Methods and Apparatus for Checking the Core and the System of Nuclear KGO Reactors [in Russian], Vol. 2, Izd. SNIIP, Moscow (1969).
2. L. N. Moskvin and V. A. Mel'nikov, At. Énerg., 36, No. 5, 367 (1974).
3. L. N. Moskvin et al., At. Énerg., 35, No. 2, 83 (1973).

PHYSICOCHEMICAL BASES AND CALCULATION OF VAPORIZATION PROCESSES FOR HIGHLY ACTIVE NITRIC ACID SOLUTIONS

A. N. Efimov, M. I. Zhikharev, and Yu. P. Zhirnov

UDC 541.123:546.791.6

Highly active, aqueous nitric acid discharge solutions formed during the extractive treatment of irradiated nuclear fuel are stored in special containers made of stainless steel; they are usually vaporized in order to reduce their storage cost [1].

The solutions subject to vaporization represent multisalt systems of the type: $HNO_3-H_2O-Me(NO_3)_n$, where Me is Na^+, K^+, Ca^{2+}, Be^{2+}, Al^{3+}, Fe^{3+}, and other ions of their mixtures.

The physicochemical bases of the vaporization processes for such solutions constitute the data concerning liquid–vapor equilibrium in the systems under consideration. Knowing the distribution of HNO_3 between the liquid and the vapor, one can calculate and choose the optimal schemes for vaporization processes guaranteeing a high degree of concentration. Up to the present, however, an empirical approach: reproduction of the process in an experimental apparatus [2], which solves individual problems, has been seen in papers on the investigation of vaporization processes.

In this paper, results of the investigation of liquid–vapor equilibrium in systems simulating highly active nitric acid solutions are cited and a method for calculating the distribution of HNO_3 in vaporization processes is proposed. Data concerning equilibrium in some of these systems [3, 4] are obtained at atmospheric pressure, whereas one carries out the vaporization of highly active aqueous solutions, as a rule, under a vacuum and in evaporating apparatus with a cleaning column intended for the radioactive decontamination of the secondary vapor. The presence of a cleaning column affects the distribution of HNO_3 between the vat residue and the condensate. Consequently, determination of the distribution of acid during vaporization and in an evaporating apparatus with a cleaning column is a new problem for which a method of solution is proposed in the present paper.

Liquid–Vapor Equilibrium in $HNO_3-H_2O-Me(NO_3)_n$ Systems. This equilibrium has been investigated by a circulation method in a modified Otmer apparatus [5]. The data obtained are given in Tables 1-3, where x and c are the concentrations of HNO_3 (neglecting the salt) and the salt in the liquid phase, respectively; P is the pressure; y is the concentration of HNO_3 in the equilibrium vapors, mole %.

Analysis and mathematical processing of the data showed that the liquid–vapor equilibrium in the systems under consideration is characterized by the following: as a rule, the metallic nitrates salt out the HNO_3 in the vapor phase; the salting-out action of the nitrates, expressed in terms of the separation coefficient I, is satisfactorily described by the equation [6]

$$\lg I = Ac, \tag{1}$$

where A and c are constants.

The value of the logarithm of the separation coefficient for systems containing a mixture of nitrates is approximately additive:

$$\lg I_\Sigma = \frac{c_1}{c_\Sigma}\lg I_1 + \frac{c_2}{c_\Sigma}\lg I_2 + \ldots + \frac{c_i}{c_\Sigma}\lg I_i, \tag{2}$$

Translated from Atomnaya Énergiya, Vol. 39, No. 6, pp. 416-419, December, 1975. Original article submitted January 22, 1975.

TABLE 1. Concentration of HNO_3 in Equilibrium Vapors (y) in Systems Containing Be, Cu, La, and Ni Nitrates

Systems	P, mm Hg	x, mole %	c, mole %			
			3,0	6,0	9,0	12,0
$HNO_3-H_2O-Be(NO_3)_2$	130	3,0	0,17	0,51	2,33	9,38
		6,0	0,61	1,96	5,94	16,43
		9,0	1,31	4,09	11,55	24,60
		15,0	5,99	13,72	27,21	42,06
		21,0	14,85	27,11	41,71	—
		24,0	21,09	32,86	—	—
	400	3,0	0,33	0,63	2,89	9,81
		6,0	0,77	2,42	7,12	17,47
		9,0	1,74	5,13	12,07	24,42
		15,0	6,47	14,42	27,21	39,76
		21,0	15,79	25,89	42,0	—
		24,0	20,95	32,87	—	—
$HNO_3-H_2O-Cu(NO_3)_2$	130	3,0	0,15	0,70	2,14	7,60
		9,0	0,90	3,94	10,99	24,93
		15,0	4,80	12,18	25,78	42,72
		21,0	14,45	26,03	43,32	—
		27,0	26,43	41,53	—	—
	400	3,0	0,28	0,96	2,38	8,10
		9,0	1,49	4,52	12,28	25,30
		15,0	5,98	13,13	25,78	40,87
		21,0	15,34	25,46	39,05	—
		27,0	26,43	39,44	—	—
$HNO_3-H_2O-La(NO_3)_3$	400	6,0	0,91	2,59	6,80	—
		9,0	1,65	5,03	13,36	—
		15,0	6,28	15,25	32,70	—
		24,0	21,57	40,83	—	—
$HNO_3-H_2O-Ni(NO_3)_2$	130	6,0	0,45	2,52	—	—
		15,0	2,97	15,61	—	—
		24,0	23,0	38,7	—	—
	400	6,0	0,84	3,50	—	—
		15,0	5,14	16,11	—	—
		24,0	22,4	35,3	—	—

TABLE 2. Concentration of HNO_3 in Equilibrium Vapors (y) in a $HNO_3-H_2O-Cr(NO_3)_3$ System

P, mm Hg	x, mole %	c, mole %	
		2,0	5,0
130	6,0	0,38	3,44
	15,0	4,86	22,16
	24,0	22,16	45,6
400	6,0	0,79	4,66
	15,0	5,85	21,30
	24,0	21,13	40,9

where the indexes Σ refer to a system which includes a mixture of nitrates, while 1, 2, . . . , i refer to systems containing a single salt with $c_\Sigma = c_1 + c_2 + \ldots + c_i$.

The dependence of the composition of the vapor on the pressure (for a constant liquid phase composition) is described by the equation

$$\lg y = a \lg P + b, \qquad (3)$$

where a and b are constants, with an accuracy which is satisfactory for technical purposes.

The ability of nitrates to salt out HNO_3 allows one to distill off the acid, to obtain a minimum concentration of it in the vat residue and (provided that the solubility of the nitrates increases with a decrease in the acid content) thereby to ensure in practice a minimum degree of concentration of the solutions. For this purpose, it is advisable to carry out the vaporization up to a concentration of the salts near saturation at elevated temperatures (for example, at the boiling temperature), and then to dilute the vat residue with water.

Calculation of the Vaporization Process. A schematic diagram of a continuous vaporization process is shown in Fig. 1. The raw solution F is vaporized in an evaporization apparatus. The vapors pass through a cleaning column sprayed with reflux L and condensed. The reflux passing through the column is returned to the evaporation apparatus. The final products of the process are the vat residue Q and the condensate D. The number of plates and the ratio of the reflux and vapor flows in the column are given in terms of the requirements for the decontamination of the vapors.

The distribution of HNO_3 between the vapor y_D and the vat residue x_a must satisfy the conditions for material balance and an equilibrium distribution. Consequently, a calculation of the process reduces to the simultaneous solution of the equations for material balance and an equilibrium distribution.* The equation for an equilibrium distribution is unknown in analytic form; therefore, it is necessary to perform the calculation graphically.

Let us consider three basic variants of the process.

1. The special case of the vaporization scheme discussed above: an evaporation apparatus without cleaning columns. In this variant the curve for the equilibrium distribution agrees with the equilibrium curve which is plotted from the experimental data on liquid–vapor equilibrium since the NTS (number of theoretical steps) of the vat in the evaporation apparatus equals one.

2. A salt-free solution, the HNO_3-H_2O system, is vaporized. Here, the curve for the equilibrium distribution will be shifted relative to the curve for the equilibrium. The magnitude of this shift is deter-

*The equation (curve) for an equilibrium distribution expresses the connection between the concentrations of acid in the distillate and the vat under static conditions for NTS > 1.

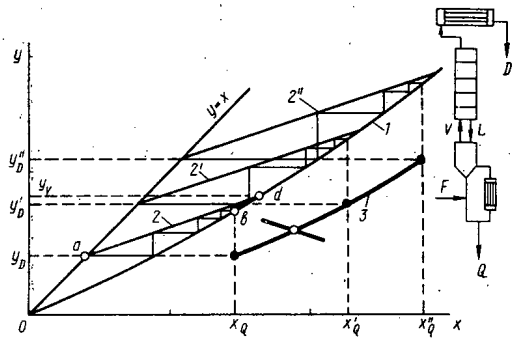

Fig. 1

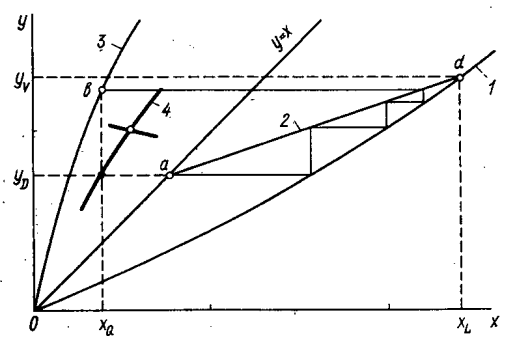

Fig. 2

Fig. 1. Plot of the curve of an equilibrium distribution for calculating the vaporization process for a salt-free solution (HNO_3-H_2O system).

Fig. 2. Construction of equilibrium distribution curve for calculating the vaporization of a salt solution (HNO_3-H_2O–nitrate system).

TABLE 3. Concentration of Nitric Acid in Equilibrium Vapors (y) in Systems Containing Fe and Al Nitrates

Systems	P, mm Hg	x, mole %	c, mass %				
			10	20	30	40	50
$HNO_3-H_2O-Fe(NO_3)_3$	130	3,08	0,06	0,14	0,49	1,64	5,01
		6,67	0,26	0,64	1,56	4,42	12,75
		10,91	1,18	2,40	4,54	10,38	25,13
		16,00	3,98	7,89	13,95	25,93	—
		22,23	10,70	18,42	29,68	—	—
	400	3,08	0,13	0,28	0,76	2,31	5,73
		6,67	0,51	1,05	2,48	5,60	13,18
		10,91	1,66	3,53	6,10	12,05	22,31
		16,00	5,26	9,33	16,17	23,98	—
		22,23	12,12	18,66	27,56	—	—
$HNO_3-H_2O-Al(NO_3)_3$	130	3,08	0,11	0,20	0,61	2,48	9,47
		6,67	0,40	0,91	2,60	8,30	24,84
		10,91	1,13	3,39	8,84	23,12	—
		16,0	4,57	11,24	20,45	—	—
		22,23	14,19	27,13	—	—	—
	400	3,08	0,19	0,35	0,99	3,13	10,02
		6,67	0,66	1,29	3,45	9,73	25,57
		10,91	1,67	4,40	9,20	23,70	—
		16,0	5,11	11,72	20,81	45,8	—
		22,23	13,52	25,03	47,1	—	—

mined by the given value of the NTS for the column and the ratio of the reflux and vapor flows. In practice, the respective values for x_Q and y_D, which determine the position of the equilibrium distribution curve, are found in the following manner. An equilibrium curve 1 for the binary system HNO_3-H_2O is plotted in y–x coordinates (see Fig. 1). A straight line 2 is arbitrarily drawn at an angle whose tangent equals the given ratio of the reflux and vapor flows in the column. Between this line and the equilibrium curve, the given NTS for the cleaning column (for example, three) and the vat of the evaporation apparatus are constructed beginning at point *a*, the intersection of 2 with the diagonal y = x.

The unknown quantities y_D and x_Q are determined by the ordinate of point *a* and the abscissa of point b, characterizing the compositions of the equilibrium vapor and liquid phases, respectively, in the first and last (i.e., in the vat of the evaporation apparatus) theoretical steps. Several of these constructions (curves 2' and 2") are carried out and the equilibrium distribution curve 3 is constructed in terms of the appropriate values found for x_Q, y_D; x'_Q, y'_D; x''_Q, y''_D, etc.

The reflux is usually small in the cleaning columns and L/V = 0.10–0.15. With this flow ratio and a value of NTS > 3, the values of x_Q are virtually independent of the number of steps and are determined by the abscissa of the point of intersection d of line 2 with the equilibrium curve 1. In addition, the calculation of the equilibrium distribution curve is simplified. The appropriate values of x_Q and y_D are determined from the relationship

$$y_D = \frac{y_V - L/V x_Q}{1 - L/V}, \quad (4)$$

which follows from the geometrical constructions (see Fig. 1). In the calculation, x_Q is arbitrarily given and y_V is determined from the equilibrium curve 1 for given values of x_Q.

3. A solution containing the salt-system $HNO_3-H_2O-Me(NO_3)_n$ is vaporized. In this case, the volatile components in the vat of the evaporation apparatus are distributed consistent with the equilibrium curve for a system containing a salt. The calculation of the values of x_Q and y_D satisfying the equilibrium distribution curve is performed in the following manner. Construction of theoretical steps for the cleaning column is carried out between the equilibrium curve 1 for a binary system and line 2 in the y–x diagram (Fig. 2) the same as in the preceding variant. The construction of the theoretical step for the vat of the evaporation

apparatus is carried out between line 2 and the equilibrium curve 3 for a ternary system. The unknown quantities x_Q and y_D are determined by the abscissa of point b and the ordinate of point *a* etc., respectively, as in the second variant.

If the NTS of the cleaning column is greater than three, we obtain an expression similar to Eq. (4),

$$y_D = \frac{y_V - L/V x_L}{1 - L/V}, \quad (5)$$

where x_L is the composition of the reflux leaving the column. In using Eq. (5), the x_Q are specified arbitrarily and we determine the y_V from the equilibrium curve 3 (see Fig. 2). Then we determine x_L from the equilibrium curve 1 for the value of y_V found, substitute y_V and x_L into Eq. (5), and obtain y_D. The corresponding values of x_Q and y_D are the coordinates of points lying on the equilibrium distribution curve 4.

The material balance equation for all of the variants considered has the form

$$y_D = \frac{x_F n - x_Q}{n - 1}, \quad (6)$$

where x_F is the concentration of acid in the raw solution and n is the given step of the vaporization.

The coordinates of the point of intersection of the material balance curve and the equilibrium distribution curve (see Figs. 1 and 2) characterize the concentration of acid in the vat residue and in the vapors leaving the cleaning column.

LITERATURE CITED

1. Management of Radioactive Wastes from Fuel Reprocessing, OECD, Paris (1972).
2. D. Clelland, in: Proceedings of the IAEA Symposium, Treatment and Storage of High-Level Radioactive Wastes, Vienna (1963), p. 63.
3. I. N. Tsiparis, in: Effect of a Salt on the Phase Equilibrium between a Liquid and a Vapor [in Russian], Kaunas (1966).
4. S. Wolf and K. Schier, Chem. Eng. Techn., 19, No. 6, 339 (1967).
5. A. N. Efimov, M. I. Zhikharev, and Yu. P. Zhirnov, Radiokhimiya, 12, No. 5, 766 (1970).
6. A. M. Rosen, Dokl. Akad. Nauk SSR, 81, No. 5, 863 (1951).

DETERMINING THE PERCENTAGE COMPOSITION OF A MIXTURE OF ^{235}U AND ^{239}Pu BY MEANS OF DELAYED NEUTRONS

B. P. Maksyutenko, Yu. F. Balakshev, V. I. Bulanenko, G. I. Zhdanova, and A. A. Shimanskii

UDC 539.125.5:539.163.1

The difference in the relative yields of delayed neutrons by various fissionable materials makes possible their identification or the determination of their percentage content in a mixture. ^{235}U and ^{239}Pu are the most difficult to distinguish on the basis of this characteristic. It has been shown in [1] that the distributions of the delayed neutron yields for these two materials as a function of the half-life differ only in the 8–35 second range, i.e., where the main contributors are ^{137}I and ^{88}Br. Therefore, the best method for distinguishing these two fissionable materials in a mixture consists of determining the ratios of the yield of the second group (a mixture of the yields from ^{137}I and ^{88}Br) to that of the first group (^{87}Br), using an expansion of the activity decline curve by the method of least squares (m. l. s.) or dividing the yield of the second group into the yields from ^{137}I and ^{87}Br and using once more these materials' differing ratios of the yields from ^{137}I and ^{87}Br. In this paper the percentage content of the isotopes ^{235}U and ^{239}Pu in a mixture of them is determined by means of the relative yields of delayed neutrons, taking into account the non-negligible statistical scatter in the results of the measurements.

We calculate the ratio of the yields of the two groups of delayed neutrons for a mixture of the two fissionable materials as a function of concentration, if the ratio

$$Y=\frac{\Phi n_a\sigma_{fa}Y_{2a}+\Phi n_b\sigma_{fb}Y_{2b}}{\Phi n_a\sigma_{fa}Y_{1a}+\Phi n_b\sigma_{fb}Y_{1b}}. \tag{1}$$

is known for each of them, where the indices a and b refer to ^{235}U and ^{239}Pu, the indices 1 and 2 refer to the yields of delayed neutrons from the first and second groups, n is the number of atoms of fissionable material, and σ_f is the fission cross section; Y with indices refers to a specific group and material; Y without indices refers to a mixture of fissionable materials; Φ is the neutron flux.

We introduce the following notation to simplify the writing of Eq. (1):

$$\eta_a=n_a/n_a+n_b;\ Y_a=Y_{2a}/Y_{1a};\ Y_b=Y_{2b}/_{1b};$$
$$C=Y_{1b}/Y_{1a};\ C_1=\sigma_{fb}/\sigma_{fa}.$$

Then Eq. (1) is rewritten as follows:

$$Y=\frac{Y_a\eta_a+CC_1(1-\eta_a)Y_b}{\eta_a+CC_1(1-\eta_a)}. \tag{2}$$

Thus, the dependence of the ratio of the yields of the two groups on the concentration is hyperbolic. Equation (2) acquires a more compact form after a reduction to asymptotic axes:

$$Y'\eta_a'=\frac{CC_1}{(1-CC_1)^2}(Y_b-Y_a). \tag{3}$$

The coordinates of the asymptotic axes (in the old system) are:

$$\left.\begin{aligned}\eta_{asy}&=CC_1/(CC_1-1);\\ Y_{asy}&=\eta_{asy}(Y_b-Y_a/CC_1).\end{aligned}\right\} \tag{4}$$

Translated from Atomnaya Énergiya, Vol. 39, No. 6, pp. 420–422, December, 1975. Original article submitted April 9, 1975.

TABLE 1. Ratio of the Yields of the Groups of Delayed Neutrons

Sample No.	No. of series	η_a	Expansion by m.l.s. y	Yield ratio, $^{137}I/^{87}Br$ y
12	6	0	8.51±0.16	8.40±0.27
11	1	0.206	7.69±0.08	7.01±0.20
10	3	0.415	7.307±0.060	5.76±0.16
9	2	0.628	6.91±0.16	5.04±0.16
8	2	0.812	6.452±0.092	4.35±0.01
7	7	1	6.209±0.055	3.91±0.14

TABLE 2. Ratio of the Yields Reduced to Asymptotic Axes

Sample No.	η'	Expansion by m.l.s. y'	Expansion by m.l.s. $y'\eta'_a$	Yield ratio, $^{137}I/^{87}Br$ y'	Yield ratio, $^{137}I/^{87}Br$ $y'\eta'_a$
12	1.040	4.700	4.888	9.160	9.526
11	1.246	3.880	4.834	7.770	9.681
10	1.455	3.497	5.088	5.520	9.487
9	1.668	3.100	5.171	5.800	9.674
8	1.852	2.642	4.893	5.109	9.462
7	2.040	2.399	4.894	4.670	9.527
		Av 4.961±0.055		Av 9.560±0.03	

It is obvious from the equations presented that it is necessary to know the ratio of the fission cross sections and the ratio of the yields (per fission event) of delayed neutrons from the first group in addition to the ratio of the yields of the two groups of delayed neutrons for the pure fissionable materials in order to calculate the desired dependence. The value of CC_1 (it is in the form of a product everywhere) can be determined from published data and from our experimental determination of the y (ηa) relation. If the ratios of the yields of delayed neutrons from the two groups are found for several mixtures of these materials (we denote them by the indices i, k, j) with a known concentration, then one can set up a system of equations for any combination of the three mixtures:

$$(Y_i - Y_{asy})(\eta_i - \eta_{asy}) = (Y_k - Y_{asy})(\eta_k - \eta_{asy}) = \\ = (Y_j - Y_{asy})(\eta_j - \eta_{asy}). \quad (5)$$

y_{asy} and η_{asy} are immediately determined from this array, and the value of CC_1 in Eq. (4) is found from the last of them.

Thus another problem can be solved: the ratio of the yields of the first group of delayed neutrons for two fissionable materials has been determined. This method has a clear advantage over direct measurements, since in the present case a two-stage calibration of the flux has not been applied, but the desired quantity has been determined simultaneously from a few points.

The percentage composition of two mixtures of fissionable materials can be distinguished if the difference between the values of Y exceeds the sum of the absolute errors, i.e.,

$$Y_i - Y_k \geqslant \Delta Y_i + \Delta Y_k. \quad (6)$$

Assuming that the relative error δ_y at comparable points is the same, we find in the system of coordinates (asymptotic axes of a hyperbola)

$$\delta Y' \leqslant \frac{1}{2}(\Delta\eta'/\eta'_i), \quad (7)$$

where $\Delta\eta' = \eta'_k - \eta'_i$. Thus, a step along the η' axis exceeds the relative error in Y by a factor of two. In order to distinguish between two mixtures having a concentration differing by 5%, it is necessary to know the ratio of the yields of the two groups with an accuracy of 2.5%. It also follows from Eq. (7) that as the concentrations η'_i increase, the requirements for accuracy become more stringent. Therefore, it is necessary to know the relative yield with high accuracy in order to determine a large concentration of ^{235}U.

Experimental Results. Six samples of a mixture ~1 g in mass, each differing from one another by approximately a 20% content of one of the fissionable materials, were successively irradiated with thermal neutrons, and then the decline in the activity of the delayed neutrons was recorded. A mixture of powders of UO_2 (90% enrichment) and PuO_2 was placed in a container 30 mm in diameter. Thermal neutrons were obtained by moderation of the rapid neutrons from the T(p, n)^{3}He reaction in a block of polyethylene surrounding the target and the irradiated sample (after the irradiation it was dropped into a counter unit at a distance of 2.5 m). The experiments were carried out on the KG-2.5 accelerator at a proton energy of 1.7 MeV. Several series of the neutron activity decline were recorded for each of the samples after a five-minute irradiation in order that the integrated count be ~700,000 pulses per series during the recording time (1024 sec.).

It is possible to extract from one and the same set of experimental results the two types of ratios necessary for an analysis of the percentage composition of the mixture. The first type is the ratio of the yield of the second group of delayed neutrons to the first group in the case of the traditional six-group description of the activity decline by the least squares method of analysis. The second type is the ratio

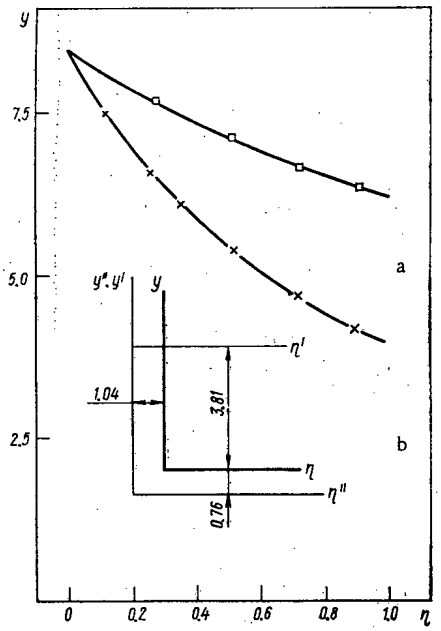

Fig. 1. Dependence of the yield ratio of the groups of delayed neutrons on the concentration of ^{235}U (a): □) denotes the ratio of the yields of the 2/1 groups (m.l.s), and × denotes $^{137}I/^{87}Br$. Schematic diagram of the arrangement of the natural (η, Y) and asymptotic (b) axes in the case of expansion by the m.l.s. (η', Y') and for the yield ratio $^{137}I/^{87}Br$ (η'', Y'').

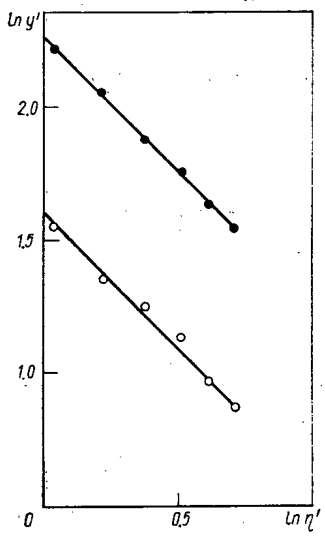

Fig. 2. Dependence of the yield ratio of the groups of delayed neutrons on the ^{235}U concentration in the system of asymptotic coordinate axes: ●) $^{137}I/^{87}Br$; ○) the yield ratio of the 2/1 groups by the m.l.s.

of the yield of delayed neutrons from ^{137}I to ^{87}Br. The latter ratio for ^{239}Pu in comparison with ^{235}U exceeds by approximately a factor of two the ratio of the yield of the combined second group to the first, and thus better resolution can be obtained at the same accuracy.

It should be stipulated that in the analysis by the method of least squares the expansion was carried out in terms of four exponential functions and not six, since the analysis of the activity decline began at the 6th second after the cessation of irradiation, when the contribution of the two short-lived groups (with periods of ~0.2 and ~0.5 sec) was already negligibly small. The expansion was made at specified half-lives, and the half-lives for ^{239}Pu [2] were used as the latter. The following half-lives were assigned in determining the yield ratios of delayed neutrons from ^{137}I and ^{88}Br: 55.6, 24.7, 16.3, 6.1, 4.45, 2.5, 2.0, 1.5, 1.0, and 0.5 sec. The errors in the expansion by the method of least squares and in separating the ratios of the yields of delayed neutrons from ^{137}I and ^{88}Br were determined as the mean squares with respect to the corresponding number of series (Tables 1, 2).

The first problem lay in determining the position of the asymptotic axes from Eqs. (5) and finding C from Eq. (4) (C is the ratio of the absolute yields of delayed neutrons per nuclear fission from ^{87}Br for the two materials). Three points (the values of Y at three concentrations) are required to find each pair of values η_{asy} and Y_{asy}. Since there are six of them in all, one can come up with 20 such combinations, i.e., obtain 20 pairs of values. However, not all of these are of equal value. Sometimes physically meaningless results can be obtained (for example, negative values of C). This circumstance is associated with the fact that the matrix of such a system is not well-conditioned. The solutions for the most separated points – the boundary values ($\eta_a = 0$ and 1) and one adjacent point – are reliable. The high accuracy is associated with the fact that the boundary values are obtained as a result of averaging 6-7 series of measurements while all the intermediate values are based on 1-3 series, i.e., they are statistically better determined. The results given are calculated from the values of η and Y for samples 7, 8, 12 and 7, 11, and 12. A comparison of the derived and published data confirms that the accuracy achieved in the values of C (12%) is significantly better [2] than that of the direct measurements (42%): $C = 0.397 \pm 0.047$ (present work); $C = 0.41 \pm 0.17$ [2]. The value obtained for C is calculated on the assumption that σ_f $^{235}U = 577.1 \pm 0.9$ barns and σ_f $^{239}Pu = 740 \pm 3.5$ barns [3].

The second problem and final goal of this paper is to find the accuracy attainable in determining the relative concentration of a mixture of the two fissionable materials ^{235}U and ^{239}Pu as the most difficult to distinguish on the basis of the relative yields of delayed neutrons. After the position of the asymptotic axes is found, the scatter in the values of the quantity $Y'\eta' = \text{const}$ is the criterion of accuracy. If we consider the value of η to be exact, then $Y'\eta'$ characterizes the slope Y'. The values of η' and Y' and their products are given in Tables 1 and 2. The error in the mean value amounts to 1% in the case of the least squares analysis; therefore one can guarantee a resolution (i.e., determination of the percentage content of ^{235}U) no worse than 5%, and no worse than 3% for analysis according to the new method (Fig. 1a).

As is evident from Eqs. (4), the position of the asymptote Y' does not depend on the type of analysis of the results, but the position of η' is different for analysis by the m.l.s. than for the determination of the delayed neutron yield ratio from ^{137}I and ^{87}Br (Fig. 1b; Fig. 2). In the case of analysis by the m.l.s., $Y_{asy} \sim +4$ and in the second case $Y_{asy} \sim -1$. If the experimental value of ΔY is identical in both types of analysis, the relative error is smaller in the second case and the attainable accuracy is higher.

LITERATURE CITED

1. B. P. Maksyutenko and M. Z. Tarasko, Preprint FÉI-370 (1972).
2. J. Kipin, Physical Principles of Reactor Kinetics [in Russian], Atomizdat, Moscow (1967).
3. BNL-325, USA (1965).

SAMPLES SIMULATING THE TRACE-ELEMENT COMPOSITION IN ROCK STANDARDS FOR THE NEUTRON-ACTIVATION ANALYSIS WITH INSTRUMENT OBSERVATION

D. I. Leipunskaya, V. I. Drynkin,
M. A. Kolomiitsev, B. V. Belen'kii,
V. Yu. Dundua, and N. V. Pachuliya

UDC 550.82:553.411

Owing to high-resolution γ spectrometry, it is now possible to simultaneously determine the concentration of numerous elements (more than 20) in rock samples with the aid of neutron-activation analysis performed with instruments. In order to guarantee the required accuracy and the correctness of multielement analyses, an appropriate calibrating system must be selected. Rock standards are usually employed in analyses of this type. Rock standards with multielement specifications have been produced in the USSR: these are ST-1 traprock, albitized SG-1 granite, SGD-1 gabbro–diorite, etc. But these rock standards are hard to use in mass analyses. Furthermore, when the concentrations of trace elements are determined, the activation of the macroelements in the base material of the standard has a disturbing influence. We therefore propose in the present work a method of producing complex reference samples imitating the trace element composition of the rock standards. The samples are made from purified phenol formaldehyde resin and are solid solutions of compounds of elements whose concentrations are calculated so that they are as close as possible to the concentration of the corresponding elements in the standards. The reference samples have the form of tablets with a diameter of 6 mm and a thickness of 2 mm.

Measurements have shown that within the errors of the analysis, the concentration of Ce, Co, Cr, Cs, Hf, La, Rb, Sc, Sm, Ta, Th, and U is the same as in the ST-1, SGD-1, and SG-1 rock standards.

Thus, in order to guarantee correct, accurate analyses, the imitating reference samples can be used in the multielement mass analyses of rocks by neutron activation. The shape of the imitating references does not change; the references have high mechanical strength and are not affected by radiation.

The simple preparation of these imitating samples makes it possible to supply them in the desired quantities.

Translated from Atomnaya Énergiya, Vol. 39, No. 6, p. 423, December, 1975. Original article submitted October 24, 1974.

POLARIZATION DYNAMICS DURING THE MOTION OF AN ELECTRON IN A SYNCHROTRON ALONG A PERTURBED EQUILIBRIUM ORBIT

A. N. Didenko, Z. N. Esina, and V. M. Kuznetsov

UDC 539.121.85

The motion of the spin of an electron in a weakly focusing synchrotron in the presence of magnetic-field perturbations in an equilibrium orbit is considered. The solution of the equation of motion of the spin of an electron with an anomalous magnetic moment in an external field is obtained by the Shtokalo method in matrix form for resonance and nonresonance conditions. For particles in motion along an equilibrium orbit, spin resonances $\Omega = n$ (n is an integer 1, 2, 3, ...) are possible if there is a harmonic with number n in the perturbation spectrum of the radial or longitudinal components of the magnetic field. Expressions for the resonance widths, defined as the interval over which the projection of the spin vector in the direction of the driving magnetic field varies from 1 to -1, are given. Conditions for the existence of a periodic solution for motion far from resonances are obtained. The effect of the perturbation of the magnetic field at the edges of the quadrants on the motion of the spin vector is considered.

Translated from Atomnaya Énergiya, Vol. 39, No. 6, p. 423, December, 1975. Original article submitted March 27, 1975.

SOME PROBLEMS INVOLVED IN THE PRODUCTION AND QUENCHING OF URANIUM – FLUORINE PLASMA

Yu. N. Tumanov

UDC 621.039.616

An electrical discharge in uranium hexafluoride leads to the breakdown of the U–F bond and the formation of U–F plasma. In a flowing system we obtain in the discharge zone a mixture of fragments of UF_6 molecules, in which intensive recombination reactions take place as the fragments leave the discharge. Under certain conditions the composition of the mixture downstream from the discharge zone relaxes to what it was initially, but if the mixture is subjected to forced cooling, a heterogeneous system consisting of lower fluorides of uranium is formed in it. In the present study we consider the production of U–F plasma and the ratio of rates of recombination and condensation of the UF_6 fragments.

At p = 1 atm UF_6 is atomized in the $T \geq 6000°K$ range (Fig. 1). In order to maintain a self-sustaining discharge in the UF_6 at $p \approx 1$ atm, we must have $T \approx 7000$–$8000°K$.

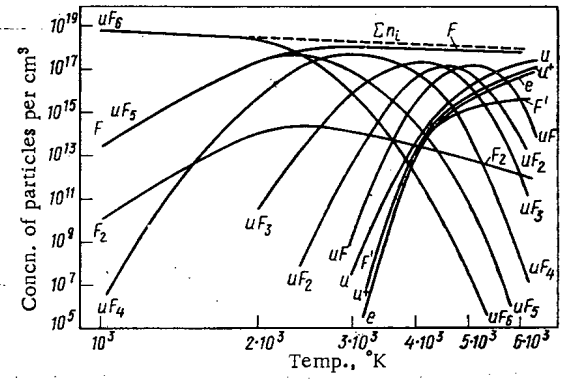

Fig. 1

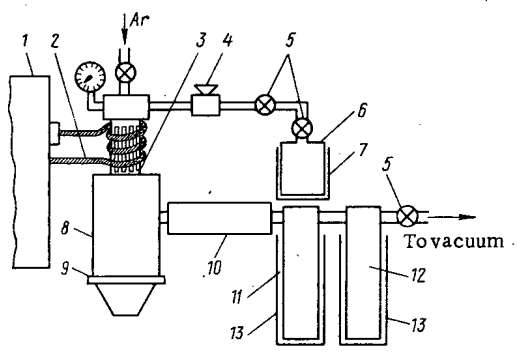

Fig. 2

Fig. 1. Composition of U–F plasma at p = 1 atm.

Fig. 2. Scheme for obtaining U–F plasma: 1) high-frequency generator; 2) inductor; 3) metal-dielectric reactor; 4) doser; 5) valves; 6) container; 7) thermostat; 8) quenching device; 9) collecting vessel; 10) filter; 11) condenser; 12) iodine-fluorine converter; 13) thermostat.

TABLE 1. Value of Condensation Time of UF_4 Nucleation Centers (τ_c) and Gaseous-Phase Recombination Time of UF_5 (t_r) at p = 1 atm

T, K	Residual press. of UF_4, atm					
	$3.32 \cdot 10^{-2}$		$3.33 \cdot 10^{-4}$		$3.33 \cdot 10^{-6}$	
	τ_c	τ_r	τ_c	τ_r	τ_c	τ_r
300	$4.56 \cdot 10^{-8}$	$6.66 \cdot 10^{-6}$	$1.37 \cdot 10^{-8}$	$2.41 \cdot 10^{-5}$	$2.28 \cdot 10^{-7}$	$4{,}2 \cdot 10^{-5}$
500	$2.84 \cdot 10^{-8}$	$9.96 \cdot 10^{-6}$	$8.54 \cdot 10^{-8}$	$3{,}63 \cdot 10^{-5}$	$1.42 \cdot 10^{-7}$	$6{,}33 \cdot 10^{-5}$
800	$3.87 \cdot 10^{-8}$	$1.47 \cdot 10^{-5}$	$1.16 \cdot 10^{-7}$	$5.37 \cdot 10^{-5}$	$1.93 \cdot 10^{-7}$	$9{,}35 \cdot 10^{-5}$
1000	$2.56 \cdot 10^{-8}$	$1.7 \cdot 10^{-5}$	$7.68 \cdot 10^{-7}$	$6.2 \cdot 10^{-5}$	$1.28 \cdot 10^{-7}$	$1{,}08 \cdot 10^{-4}$
1300	$7.54 \cdot 10^{-8}$	$2.13 \cdot 10^{-5}$	$2.26 \cdot 10^{-6}$	$7{,}79 \cdot 10^{-5}$	$3{,}77 \cdot 10^{-7}$	$1{,}36 \cdot 10^{-4}$
1500	$3.21 \cdot 10^{-2}$	$2.39 \cdot 10^{-5}$	$9.64 \cdot 10^{-2}$	$8{,}73 \cdot 10^{-5}$	$1.61 \cdot 10^{-1}$	$1{,}52 \cdot 10^{-4}$

Translated from Atomnaya Énergiya, Vol. 39, No. 6, pp. 424–425, December, 1975. Original article submitted April 2, 1975.

In order to obtain a U−F plasma, we may use radio-frequency or microwave discharges in uranium hexafluoride. One of the schemes for obtaining the U−F plasma is shown in Fig. 2. The discharge is initially excited in argon, after which the argon is replaced with uranium hexafluoride. The stability of the discharge is determined by the pressure of the gas and the frequency of the generator. At frequencies of approximately 10, 17, and 2450 MHz, respectively, the electrodeless discharge in the UF_6 glows steadily at pressures of $\leq$ 10-15, $\sim$30, and $\sim$ 1 atm.

At the exit from the discharge the U−F plasma is cooled, the nonvolatile fluorides are collected in a collecting vessel, and the fluorine is trapped in an iodine−fluorine converter.

For UF_4 the condensation time is shorter by two or three orders of magnitude than the time of gaseous-phase recombination up to temperatures of $\sim$1300°K (Table 1).

Estimates indicate that in order to quench the UF_4 from the U−F plasma it is sufficient to have a cooling rate of $1.3 \cdot 10^8$ °K/sec, and for quenching the uranium it is sufficient to have $\sim 10^{10}$ °K/sec.

The rate of heterophase recombination is slower by seven or eight orders of magnitude than the rate of homophase recombination, so that it is possible to separate the condensed and gaseous phases even by mechanical methods. Existing methods of quenching make it possible to separate the UF_4 and the F from the U−F plasma, but the rates of cooling necessary for quenching the uranium ($\sim 10^{10}$ °K/sec) are not yet technically feasible.

B. S. Petukhov, L. G. Genin,

and S. A. Kovalev

HEAT EXCHANGE IN NUCLEAR REACTORS*

Reviewed by I. S. Kochenov

The development of nuclear energy has been the subject of great attention in recent years in both the Soviet Union and abroad. Problems of heat technology occupy a central position. For it is the extraction of heat from the core of the reactor that essentially determines the maximal power, the reliability, and other important characteristics of nuclear reactors. However, there have been few books that deal with the heat technology of nuclear reactors. The publication of this book is therefore important and timely. It has immediately attracted the attention of large circles of high-temperature physicists.

The book is divided into fourteen chapters, and at the end of each of these there is a bibliography. The questions considered in the book are very extensive. Here are some of them: distribution of heat release in the core of the reactor, equation of heat conduction and calculation of temperature fields, equations of convective heat exchange, heat exchange and hydraulic resistance in the case of laminar flow in ducts, fundamentals of the semiempirical theory of turbulence, heat exchange and hydraulic resistance in the case of turbulent flow in ducts, including cases of the initial section, ducts of noncircular cross section, variable properties of the fluid, the presence of internal heat sources in the heat carrier, heat exchange in finned gas-cooled systems, in deposits and a pseudoliquefied layer, heat exchange in the case of boiling (including conditions of occurrence of a heat transfer crisis) in a large volume, tubes and pencils of rods, elements of the hydrodynamics of two-phase flow, including critical flow.

The book is based on material from investigations of the authors and the results of many other authors.

Parts of the extensive material are presented less well than others. These include the first chapter, with a brief description of nuclear reactors, the density distribution of the neutron flux, and the elements of the thermal and hydraulic design of cores.

Interesting conclusions are drawn in the eighth chapter that for drop liquids the heat transfer coefficient (the number Nu) increases with increasing density of the heat flux, whereas the coefficient of hydraulic resistance decreases, and interesting conclusions are also drawn about the contradiction between the results of theoretical and experimental investigations into the influence of the "temperature factor" on the coefficients of heat transfer and hydraulic resistance in the case of cooling of gases.

Some of the conclusions of the authors are questionable, for example (§4.3 and §8.4), the incorrectness of using previously unknown quantities to construct dimensionless numbers (variables). Nor is it clear why in the case of heat exchange with gases in tubes the Nu number can depend on the length (through the "temperature factor") up to 100 x/d and the coefficient of friction up to 80 x/d (§8.4) if the stabilization section does not exceed 30x/d.

A shortcoming of the book is the fact that some of the compilative material is presented without sufficient analysis and criticism, and sometimes with excessive generality. One can also make a number of other particular comments, but they do not detract from the positive opinion about the book as a whole.

The book is intended for students at universities as a textbook, though it will also be valuable for many research students, engineers, and scientific assistants working in the field of atomic energy.

*Atomizdat, Moscow (1974).

Translated from Atomnaya Énergiya, Vol. 39, No. 6, p. 425, December, 1975.

K. N. Mukhin

EXPERIMENTAL NUCLEAR PHYSICS, VOL. II. PHYSICS OF ELEMENTARY PARTICLES*

Reviewed by V. G. Vaks and L. A. Mikaélyan

This book occupies a particular position among Soviet textbooks on nuclear physics.

The first editions were published in 1962-1963 when a particular need was felt for a textbook on the physics of the atomic nucleus. The book was widely used, both at universities and physics institutes in the country.

The third edition, which is reviewed here, has been published in two volumes.†

The second volume is devoted to the physics of elementary particles and their interactions. It consists of two main parts. In the first, nucleon–nucleon interactions at different energies and the properties of nuclear forces are considered. The theory of the deuteron is given and pp, nn, and np scattering is analyzed in the light of the conjecture of isotopic invariance; scattering theory is considered as well as experiments on nucleon–nucleon scattering at high energies (with the elements of phase-shift analysis); Feynman diagrams are discussed and the mathematical apparatus of isospin; elementary meson theory is considered. In the second part, the properties of all the known elementary particles and resonances and also the properties of antiparticles and antinuclei are described. As in the first volume, the treatment is based on the conservation laws, to which are added the laws of conservation of the lepton charge, strangeness, and combined parity. Great attention is devoted to the fine details of interactions: strong (isospin and strangeness systematization, unitary symmetry), electromagnetic (radiative corrections to the magnetic moments of electrons and muons, nucleon form factors, and mesoatoms) and weak (violation of the laws of conservation of spatial and combined parity, conjecture of universal weak interaction, the two forms of the neutrino, double β decay).

The book is written in a good physical language, covers all the basic questions of the physics of the nucleus and particles, is theoretical to an extent, and completely modern. The results of some investigations of the author are reflected in the book.

The book is dedicated to the memory of Igor Vasil'evich Kurchatov, whose name is inseparably linked to the establishment and development of Soviet nuclear physics. Kurchatov values popularization of science highly.

Finally, we should like to say a few words about the work of the publishing house Atomizdat. The book is printed on beautiful paper, contains a large number of original and well drawn figures, has attractive binding, and is richly endowed with ancillary and reference material (tables of particles and elements on the fly leaves, subject index, column headings, appendices, brief conclusions at the ends of chapters, etc). All this makes the book very attractive as a textbook.

The first editions of the book enjoyed great popularity among readers and were well reviewed. There is no doubt that the third edition will be read with interest and approval.

*Atomizdat, Moscow (1974).

†The first volume was reviewed in At. Énerg., 39, No. 5 (1975).

Translated from Atomnaya Énergiya, Vol. 39, No. 6, pp. 425-426, December, 1975.

EXPERIMENTAL INVESTIGATION OF OPTIMUM PROCESSES FOR THE CONTROL OF A NUCLEAR REACTOR BY THE NEUTRON FLUX

G. N. Aleksakov, V. P. Alferov, and V. I. Belousov

UDC 621.039.562

The application of optimum control theory in the planning of a system of control by the neutron flux in a nuclear reactor permits the limiting possibilities of the reactor itself to be recognized as a control object and the technical requirements on equipment, which will ensure a sufficiently good approximation of the actual system to the optimum system, to be formulated. Theoretical analysis shows that the period of the reactor can be controlled almost instantaneously by the introduction of excess reactivity at a finite rate [1]. The times during which the period is reached, corresponding to a chosen rate of injection of reactivity, to an order of magnitude is close to $\tau = l/\beta$, where l is the lifetime of the prompt neutrons and β is the relative fraction of delayed neutrons. The time of establishment of the reactor period, for various types of reactors amounts to 0.15 sec for $l = 10^{-3}$ sec and to $1.5 \cdot 10^{-6}$ sec for $l = 10^{-8}$ sec. These possibilities for controlling the period of the reactor simultaneously with increase of the static and dynamic accuracy of the control system, permit the system to be simplified due to the use of a logical law of control, which can be written in the following way:

$$u[x_1(t),\ x_2(t)] = \begin{cases} U_m \operatorname{sign}[x_2(t) - x_{2\uparrow}] & \text{for } x_1(t) \leqslant x_{10} - \delta \text{ and } |x_2(t) - x_{2\uparrow}| \geqslant \varepsilon; \\ -U_m \operatorname{sign}[x_2(t) - x_{2\downarrow}] & \text{for } x_1(t) \geqslant x_{10} + \delta \text{ and } |x_2(t) - x_{2\downarrow}| \geqslant \varepsilon; \\ & \text{for } x_1(t) < x_{10} - \varepsilon \text{ and } |x_2(t) - x_{2\downarrow}| < \varepsilon \\ 0 & \text{for } x_1(t) > x_{10} + \varepsilon \text{ and } |x_2(t) - x_{2\downarrow}| < \varepsilon, \\ & \text{for } |x_1(t) - x_{10}| < \delta \text{ and } x_{2\downarrow} - \varepsilon < x_2(t) < x_{2\uparrow} + \varepsilon, \end{cases} \tag{1}$$

where $\bar{u}[x_1(t); x_2(t)]$ is the control (voltage on the servomotor) as a function of the running values of the phase coordinates $x_1(t)$ and $\bar{x}_2(t)$; $x_1(t) = n(t)$ is the running value of the neutron flux density; x_{10} is the desired (specified) value of the neutron flux density; 2δ is the permissible error on the neutron flux density; $x_2(t) = \frac{1}{n(t)} \cdot \frac{dn(t)}{dt}$ is the relative rate of change of the neutron flux (inverse period); $x_{2\uparrow}$ is the desired (specified) relative rate of rise of power; $x_{2\downarrow}$ is the desired (specified) relative rate of reduction of power and 2ε is the permissible error on the relative rate.

For the experimental verification of the possibility of improving the control and safety equipment on the basis of optimum control theory, a display unit has been operated in the Moscow Institute of Physics Research for the state and optimum control of the power of the BIR-1 nuclear reactor. The specific properties of the instrument, in comparison with the conventional two-channel system of control of the power and the period, consists in the amalgamation of these channels into one instrument, forming the logical law of control (1), in the development of a meter both for positive and negative periods, in the significant increase of the speed of response of both the period meter (by a factor 10) and the scram-rod actuator (factor

Translated from Atomnaya Énergiya, Vol. 39, No. 6, pp. 427-430, December, 1975. Original article submitted December 17, 1974; revision submitted March 25, 1975.

TABLE 1. Comparable Characteristics of the Automatic Control System Based on BIR-1 and BAR-2M

Technical Characteristics	BAR-2M	BIR-1
No. and type of ionization chambers	Two KNK-56 chambers	Single KNK-56 chamber
Range of measured power levels, A	10^{-11}-10^{-4}	10^{-9}-$2 \cdot 10^{-4}$
Chamber current, corresponding to the setting "inaccuracy of logarithmic amplifier," A*	Absent	10^{-10}
Range of power control levels, %	0.4-200	0.01-100
Chamber currents, A	$0.8 \cdot 10^{-6}$-$4 \cdot 10^{-4}$	$2 \cdot 10^{-8}$-$2 \cdot 10^{-4}$
Accuracy of control	Not specified in description	Less than 0.5%
Constant of differentiation of period meter	6	0.6
Range of measured periods, sec	+10- +150	−10-∞ - +10
Meas. accuracy, %	±20	±5
Range of period settings with positive (increase of power) and negative (decrease of power)	Stepwise setting (30; 60)	Smooth setting (15-60)
	Absent	15-80
Accuracy of control of period	Not specified in description	Not worse than 10%
Indication of state of reactor	Built-in separate pointer-type instruments	Built-in state indicator on CRT and external pointer-type instruments
Operating devices	Power amplifier or amplidyne and motor	RD-09 motor
Corrections of functional part of system	Tachometric bridge	Absent
Instrument power supply	220V ±10%; 50 Hz	220V ±10%; 50 Hz
Required power, VA	100	35
Power required by auxiliary amplifiers, VA	200-500	0
Total power of automatic control channel power supply (without chamber), VA	300-600	35
Dimensions of facility, mm	400 × 240 × 250 plus dimensions of auxiliary power amplifier or amplidyne	250 × 120 × 200

*With a chamber current of 10^{-10} A the time constant of the input circuit of the triode logarithmic amplifier is 2-10 sec, and with a current of 10^{-11} A it is equal to 20-100 sec; therefore, the delay of signal of the power and period logarithm is unacceptably large.

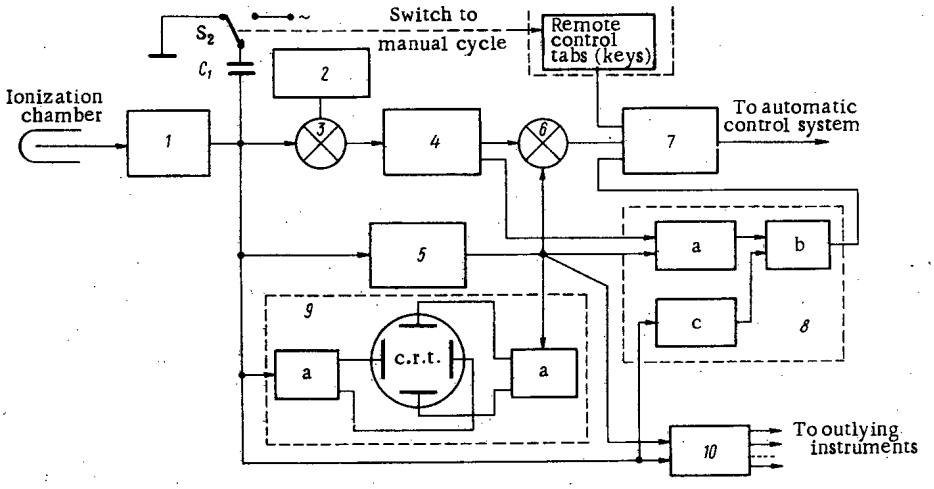

Fig. 1. Block diagram of the BIR-1 instrument.

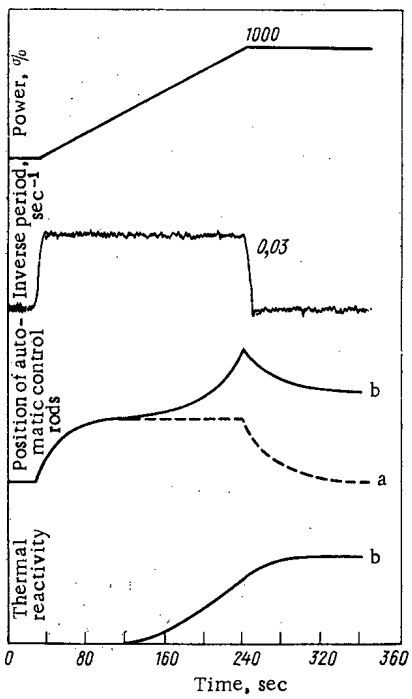

Fig. 2. Transient processes in an optimum control system by the neutron flux [a) at zero power; b) at working power levels].

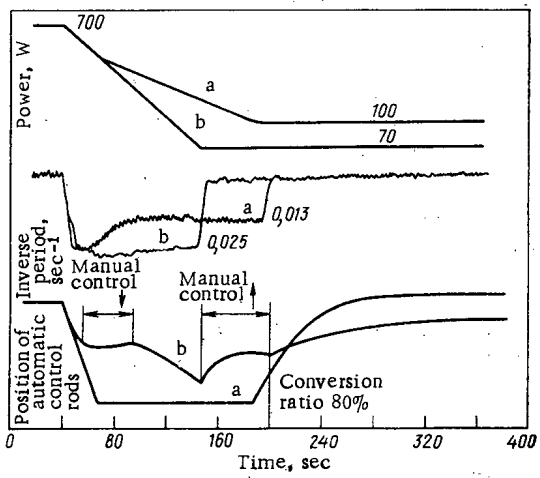

Fig. 3. Controlled power reduction processes of the IRT-2000 reactor.

3-5), in the production of more flexible possibilities for specifying the law of control and for extending the ranges of control over the power and the period. The new unit of the instrument is an indicator of the state of a nuclear reactor [2], which will allow not only information on the running values of the two variables on the screen of a single indicator to be displayed, but also by means of this same indicator will allow the operation of the entire control system to be controlled.

The block diagram of the BIR-1 is shown in Fig. 1.

The current from an ionization chamber is fed to the input of the logarithmic amplifier 1. Its output voltage, proportional to the logarithm of the ionization chamber current, is compared with the reference voltage of the master power logarithm 2 in the comparator unit 3. The definition on the period is formed in the period assignment unit 4 as a function of the sign and magnitude of the imbalance voltage. The period is measured by means of a differentiating amplifier with feedback 5, to the input of which is fed the signal from the output of the logarithmic amplifier 1. The voltage corresponding to the measured period is compared with the reference voltage of the period controller 4 in the comparator unit 6, from the output of which the imbalance signal is fed to the control relay unit by the motor 7 of the automatic control servodrive. This same voltage is fed to the input of the screening unit 8 [a) period control circuit; b) trigger; c) servicability control circuit]. Signals proportional to the logarithm of the chamber current and to the measured inverse period are fed to the reactor state indicator 9 [a) amplifier]. In the instrument there is a comparator unit 10 to which are connected the outlying power and period control instruments. The design of the instrument provides for its installation on the control desk instead of the power control.

The principal technical characteristics of an automatic control system based on the BIR-1 instrument and their comparison with the characteristics of a similar system based on the series-produced BAR-2M instrument are shown in Table 1.

The BIR-1 was tested and operated during one year as a part of the control and safety rods of the IRT-2000 reactor of the Moscow Institute of Physics Research. The following experimental investigations were carried out by the means of this instrument:

1. Direct measurements of the rate of injection of excess reactivity [1], necessary for the almost instantaneous achievement of a specified period T (control constraint $u_\uparrow$)

$$u_\uparrow = \frac{1}{T} \text{ dollar/sec}, \tag{2}$$

and for stabilization at a specified level of the flux, having varied for a fairly long time before this with a period T (control constraint $u_\downarrow$),

$$u_\downarrow = \sum_{i=1}^{6} \frac{\lambda_i (\beta_i^*/\beta^*)}{1+\lambda_i T}, \text{ dollar/sec}. \tag{3}$$

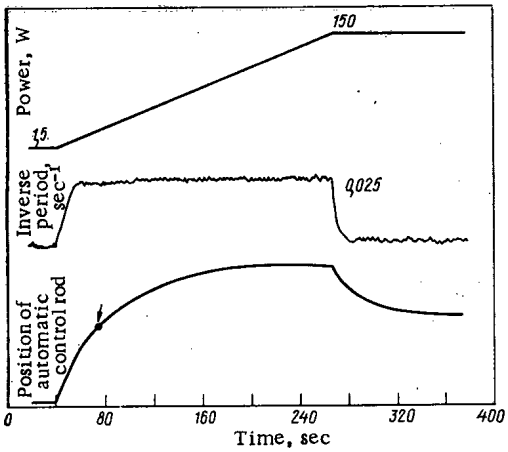

Fig. 4. Emergence of the IRT-2000 reactor from the subcritical state with a specified period.

Deviations of the experimental data from the calculated data over the range of periods 15-60 sec did not exceed the values corresponding to the BIR-1 instrument errors.

2. Good application in the BIR-1 instrument of the law of control (1) allowed transient programs of reactivity changes to be produced experimentally and recorded in the system with feedback, ensuring almost instantaneous achievement and stabilization of a specified period T, and also almost instantaneous stabilization of the neutron flux at a specified level. The results of a theoretical calculation of these programs, are given in a number of papers (see, for example, [3, 4]; relations (6) and (8) of [1], etc.). Experimental graphs are shown in Fig. 2, where the curves *a* correspond to a low power (P = 0.1-10 kW and there is no temperature feedback) and curves b correspond to high power (P = 20-2000 kW, and the temperature feedback appears quite noticably).

3. Controlled power reduction processes with a given period and subsequent flux stabilization at an attained level were investigated experimentally. These experiments not only give a direct practical result from the point of view of designing safety systems for nuclear power installations, but also are of definite theoretical interest. Control processes of point reactors in the presence of a very high "external" neutron source are simulated in them. These conditions correspond, on the one hand to the control of a deeply subcritical reactor and, on the other hand, to the local control of a zone of a large reactor [5]. In Fig. 3, graph *a* shows the possibilities for power reduction by means of only a single automatic control rod; graph b corresponds to a single rod with a weight equal to the weight of a manual control rod, and with a rate of reactivity injection necessary for optimum control of an increase of power with a period of 15 sec. In drawing this graph, the operator controlled the manual control rod, having withdrawn the automatic control rod to the middle of the operating range.

4. Theoretical analysis of the controlled power reduction allowed the assumption that during reactor startup, the achievement and stabilization of a specified period is possible in the subcritical state, with further stabilization of this period on reaching and exceeding the critical state. The oscillograms shown in Fig. 4 were recorded during startup of the IRT reactor from the subcritical state with a given period. The point of the graph marked by the arrow corresponds to the critical state.

5. It has been shown experimentally that a 20-fold reduction of the motor power in the automatic control device did not reduce the quality of control, due to the decrease of the speed of travel of the automatic control rods, increased the accuracy of the period and power control because of the increase of the speed of response of the servodrive and its control circuit, simplified the system and facilitated the operating cycle of the units, which enabled the reliability of the system as a whole to be increased, with simultaneous reduction of cost and power requirements.

In conclusion, the following inferences can be drawn:

1. The theoretically shown possibilities of reactor control, based on optimum control theory, correspond to actual physical processes in the reactor itself and therefore could be set as the basis for designing control and safety rods.

2. The technical requirements on the components of the control and safety rods, and the system as a whole stipulated by analysis of the system with the attitude of optimum control theory, are effected by quite simple technical means and the periodic processes in the system approximate to optimum in speed of response.

3. The conventional separation of systems into automatic and manual (or semi-automatic) compensation channels limit the possibilities of automatic control by the neutron flux. These possibilities might be accomplished more completely with a system, identical with the rod, the weight of which corresponds to the weight of a manual control rod, and the velocity is defined by the minimum operating period.

The authors express their sincere appreciation to the control and safety rod servicing personnel of the IRT-2000 reactor of the Moscow Institute of Physics Research and A. P. Krykov, without whose enthu-

siasm and active participation in the preparations and carrying out of the experiments, the work could not have been undertaken.

LITERATURE CITED

1. G. N. Aleksakov, V. I. Belousov, and A. P. Kryukov, Atomnaya Énergiya, 32, No. 3, 228 (1972).
2. G. N. Aleksakov and V. I. Belousov, Indicator for the State of a Nuclear Reactor [in Russian], Author's Patent No. 400234, Byulleten' Izobretenii, No. 27 (1974).
3. Dzh. R. Kipin, Physical Principles of Nuclear Reactor Kinetics, [Russian translation], Atomizdat, Moscow (1967).
4. R. Mohler and S. Shen, Optimal Control of Nuclear Reactors, Academic Press, New York (1970).
5. E. V. Filipchuk, P. T. Potapenko, and A. N. Kosilov, Atomnaya Énergiya, 35, No. 5, 317 (1973).

RADIATION HARDENING OF GRAPHITE PARTS WITH STRESS RAISERS

Yu. S. Virgil'ev, V. G. Makarchenko, V. N. Barabanov, and A. N. Sazhin*

UDC 621.039:532.21

Stress raisers of various types cause nonuniformities in the stress field, and this in the final analysis, reduces the reliability of parts.

Along with stress raisers which are due to design (abrupt changes in the cross sections of parts, holes, recesses, slots, etc.), there are always stress raisers of technological origin in synthetic graphite, such as scratches, micropores, cavities, and cracks, which are harmful, since they intensify brittleness.

It is known that neutron irradiation intensifies the brittleness of structural graphite. The effect of hyperbolic recesses and through holes in parts and in specimens of high-density VPP graphite on their strength in uniaxial extension and compression was investigated earlier [1]. It has been shown that the strength variation in laboratory specimens and full-scale parts is influenced only by those artificial stress raisers which produce stresses higher than those caused by the structural nonuniformities characteristic for a certain type of graphite. Therefore, specimens with holes 1 and 2 mm in diameter, i.e., holes commensurable with the size of coke grains in the investigated material, have virtually the same ultimate strength in uniaxial tensile and compressive tests.

TABLE 1. Dependence of the Ultimate Bending Strength on the Rounding-Off Radius at the Bottom of the Notch

R, mm	σ, kg/cm²
00*	170
2,85	120
1,4	110
0,8	100
0,2	95
0,05	95

*Without notch.

We estimated the effect of stress raisers in bending tests. We first estimated the effect of the notch radius on the strength of fine-grained MG-1 graphite (Table 1).

The obtained data indicate that reduction in the rounding-off radius intensifies the weakening, which reaches a virtual limit for rounding-off radii smaller than 0.2 mm.

TABLE 2. Dependence of the Ultimate Strength on the Notch Depth

MG-1		VPP		MPG	
C*, mm	σ, kg/cm²	C†, mm	σ, kg/cm²	C*, mm	σ, kg/cm²
0**	170	0	290/335‡	0	354
2	105	2	205/225	2,25	127
3	92	5	198/202	4,1	121
6	93	8	200/205	10,3	109
8	99	10	218/209	14,6	124
11	104	12	238/229		
		14	276/234		

*Rounding-off radius at notch bottom, 0.1 mm.
†Rounding-off radius, 1 mm.
‡ Data from two series of tests for specimens cut from two billets.
**Without notch.

The effect of the notch depth was investigated on prismatic specimens of three types of material: fine-grained MG-1 and MPG and high-density, medium-grained VPP graphite (Table 2). The dimensions of the specimens were 20 × 10 × 100 mm. The data indicate that the ultimate bending strength decreases with an increase in the notch depth, especially for the high-strength, fine-grained MPG material. The maximum weakening occurs for ratios of the notch depth to the specimen thickness in the range from 0.1 to 0.4. With a further increase in this ratio, the ultimate strength calculated by means of the commonly used equations increases. The latter can be explained by a considerable shift of the specimens's neutral axis into the extension zone.

*In collaboration with A. I. Plavskii.

Translated from Atomnaya Énergiya, No. 6, pp. 430-432, December, 1975. Original article submitted January 15, 1975.

TABLE 3. Radiation Hardening of MPG-6 Graphite Specimens with and without Stress Raisers

Integral flux, neutrons/cm²	T, °C	σ_{com}, kg/cm²	$\frac{\Delta\sigma_{com}}{\sigma_{com}}$	$\Delta E/E$	σ, kg/cm²		σ/σ_{con}	$\Delta\sigma/\sigma$	
					A	B		A	B
0	20	900±45	0	0	485±40	160±20	3,05	0	0
$3\cdot10^{18}$	70	1640±70	0,82	0,30	800±35	330±10	2,40	0,65	1,05
$4,8\cdot10^{18}$	70	1680±90	0,87	0,39	850±80	360±15	2,35	0,75	1,25
$2,4\cdot10^{20}$	70	2300±290	1,55	1,48	900±40	380±10	2,35	0,85	1,36
$3,0\cdot10^{20}$	70	2210±190	1,45	1,51	730±100	385±15	1,90	0,50	1,40
$3,7\cdot10^{20}$	70	2460±300	1,70	1,59	730±90	395±30	1,85	0,50	1,45
$6,5\cdot10^{18}$	70	1580±60	0,75	0,25	760±40	320±30	2,40	0,60	1,00
$8,4\cdot10^{18}$	110	1430±120	0,59	0,19	760±70	315±15	2,40	0,60	0,97
$1,0\cdot10^{19}$	130	1340±30	0,49	0,27	750±55	290±15	2,60	0,54	0,81
$1,2\cdot10^{19}$	140	1290±50	0,43	0,25	715±50	260±25	2,45	0,47	0,62

Remark: A) without stress raisers; B) with stress raisers.

Taking into account the above results, we chose specimens of high-strength, fine-grained, equal-density MPG-6 graphite. The rounding-off radius at the bottom of the notch R was equal to 0.1 mm, while the ratio of the notch depth to the thickness of the specimen (C) was equal to 0.2, which ensured the maximum weakening effect.

In order to secure a sufficient number of parallel measurements and also because of the limited size of the irradiation device, the tests were performed on 5 × 5 × 40 mm prismatic specimens. The specimens were cut from the same billet and were selected with respect to specific weight; they had the same degree of crystal structure perfection, which was estimated by measuring the electric resistance. The strength was estimated first by using the nondestructive test method and determining the dynamic elasticity modulus with respect to bending vibrations [2]. Calibrated notches with a depth of 1 mm and a rounding-off radius of 0.1 mm at the bottom were made in the specimens by means of a special machine.

Equal numbers (4-13) of specimens with and without notches were irradiated at a temperature of 70-140°C until a integral flux from $3\cdot10^{18}$ to $3.7\cdot10^{20}$ neutrons/cm² was reached. The integral flux was determined with respect to the operating time of the reactor by taking into account the power level and the known fast neutron flux (E > 0.18 MeV) in the channel in question, while the temperature was measured by means of diamond indicators. For control, the elasticity modulus of irradiated specimens was measured again before performing the bending tests.

The uniformity of the tested specimens can be characterized by the arithmetic-mean errors in measuring the electric resistance (±8%) and the elasticity modulus (±14%). The arithmetic-mean error in determining the ultimate bending strength of the control specimens was equal to 13%.

The bending tests were performed in a laboratory device with a maximum load of 30 kg and a load recording accuracy not worse than 0.1 kg. The span between the supports was equal to 30 mm. Unirradiated control specimens were tested simultaneously with the irradiated specimens. The ultimate bending strength for prismatic specimens was calculated by means of the expression $\sigma = 3pl/2bh^2$, where b is the width of the specimen (cm), h is the height of the specimen, equal to 0.5 and 0.4 cm for specimens with and without stress raisers, respectively, p is the breaking stress (kg/cm²), and l is the distance between supports, which is equal to 3 cm.

The prisms broken in tests were used to prepare 5 × 5 × 6 mm specimens for determining the ultimate compressive strength in an MR-0.5 machine. Verification showed that the breaking of specimens in previous bending tests did not affect the results obtained in compressive tests.

The averaged results obtained in determining the ultimate bending strength of specimens with and without notches depend on the cumulative dose at 70°C and on the temperature for a constant integral flux of $(0.65\text{-}1.2)\cdot10^{19}$ neutrons/cm²; the variation of the ultimate compressive strength is also given for comparison.

It is known that the strength of irradiated graphite increases rapidly with the dose until "saturation" sets in. The level reached decreases exponentially with an increase in the irradiation temperature [3]. Our data indicate that irradiation at 70°C with a neutron flux of up to $3.7\cdot10^{20}$ neutrons/cm² does not produce stable values of the ultimate compressive strength and the elasticity modulus. The ultimate bending strength, however, reached its maximum value of 900 ± 40 kg/cm² with an integral flux as low as $\sim2.4\cdot10^{20}$

neutrons/cm^2. This quantity even had a tendency to decrease with additional irradiation. The presence of stress raisers produced a more significant strengthening of graphite. For this reason, the ratio of the ultimate bending strength values for specimens without notches and notched specimens decreased with continued irradiation from 3.0 (unirradiated specimens) to 1.85 (after absorption of a dose of $3.7 \cdot 10^{20}$ neutrons/cm^2). This ratio did not change with an increase in the irradiation temperature from 70 to 140°C in the absorbed dose range $(0.65-1.2) \cdot 10^{19}$ neutrons/cm^2. Consequently, for the irradiation levels reached, the presence of various defects, such as cracks, pores, etc., does not impair the stability of structural graphite as a result of irradiation.

In the weaker, medium-grained GMZ materials, the weakening effect of stress raisers should manifest itself to a lesser extent than in the tested high-strength, fine-grained MPG-6 graphite.

LITERATURE CITED

1. V. N. Barabanov et al., in: Structural Materials Based on Graphite [in Russian], Vol. 6, Metallurgiya, Moscow (1971), p. 160.
2. G. A. Lushnikov, in: Investigations in Metal Physics and Nondestructive Testing Methods [in Russian], Nauka i Tekhnika, Minsk (1968), p. 35.
3. Yu. S. Virgil'ev, At. Énerg., 36, No. 6, 479 (1974).

DETECTION OF WATER LEAKAGE INTO SODIUM WITH RESPECT TO ACOUSTIC NOISE

F. A. Kozlov, G. P. Sergeev, and V. S. Yugai

UDC 621.039.564

The noise produced by water leakage into sodium has been studied in order to explore the potentialities of the acoustic method as a means of detecting leakages in sodium–water steam generators. The interest in these investigations is stimulated by the search for efficient methods more than the presently used methods for detecting small leakages in steam generators.

The basic disadvantage of the existing leakage detection methods is the relatively long signal delay for steam generators with a large volume and large sodium discharge. Moreover, with the coolant purification systems now in operation, these methods do not permit, even in an unlimited length of time, detecting leakages of a magnitude smaller than a certain given value, which is determined by the parameters of the device (the volume and discharge of sodium and the purification rate) as well as the characteristics of the detection instruments [1]. Any leakage in a steam generator is considered as potentially hazardous, and, therefore, information on its development must be obtained as quickly as possible.

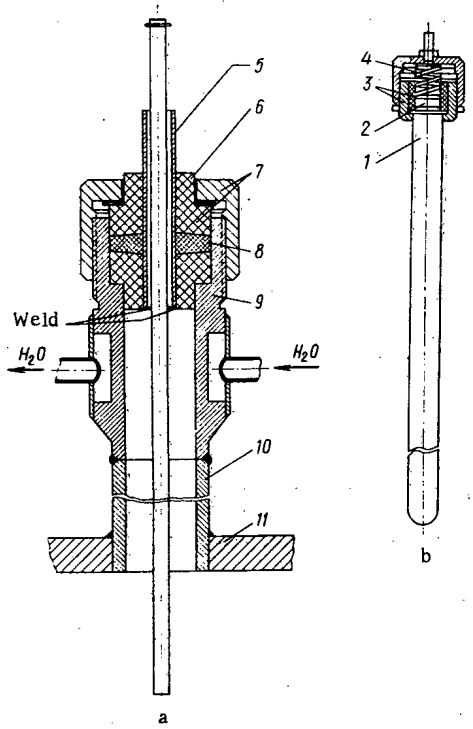

Fig. 1. Mounting unit for the waveguide of sound receiver (a) and design of sound receiver (b). 1) Waveguide; 2) piezoelectric transducer; 3) insulating bushings; 4) spring; 5) centering tube; 6) nut; 7) and 8) tightening bushings and washer; 9) cooled fitting; 10) reducing pipe; 11) tank lid.

With modern technology acoustic noise in liquid metals can be detected almost instantaneously. However, the practical realization of this in an industrial device, in the case of small leakages in the steam generator, is complicated by many serious difficulties (the high level of background noise in the device, the complexity of choice of the best methods and locations for mounting the acoustic receivers, etc.). The success in using the acoustic method for detecting water leakages into sodium depends on the signal-to-noise ratio for small leakages that can be secured for an actual system.

Determination of the optimum acoustic system for leakage detection is at present complicated by a lack of understanding of the processes whereby sound is generated when water enters sodium. We can cite the following factors which apparently affect the characteristic acoustic spectrum pertaining to the reaction between sodium and water: generation, vibration, and disappearance of vapor and hydrogen bubbles; the dynamics of sodium and of the jet issuing from the leakage location; the geometry of the reaction zone; formation of standing waves between the location of water leakage into sodium, the neighboring pipes, and the reaction vessel; the resonance characteristics of the vessel and the acoustic transducer; the mounting location of the transducer, etc.

Translated from Atomnaya Énergiya, Vol. 39, No. 6, pp. 432-434, December, 1975. Original article submitted November 27, 1974.

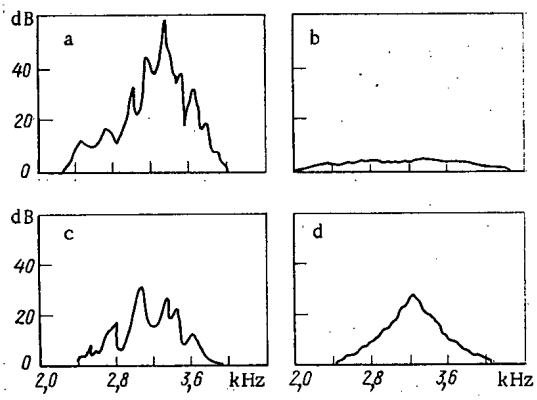

Fig. 2. Signal spectra from sound receiver *a* for different intensities of water leakage into sodium. a) $G_{H_2O} = 10$; b) 0; c) 4.5; d) 2.8 g/h.

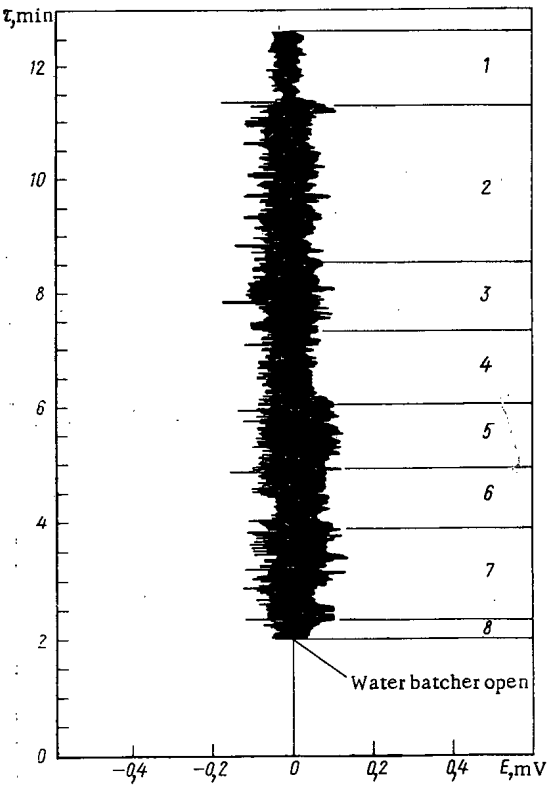

Fig. 3. Recording of the signal from the acoustic transducer after analysis by the S5-2 instrument.

In order to obtain undistorted information on acoustic noise in as wide a frequency range as possible, it is desirable to have the sound receiver directly within the zone of the supposed noise source. For a steam generator, the noise source caused by water leakage into sodium must be inside the steam generator, i.e., in moving sodium, which is at a high temperature (300-500°C). Development of an acoustic receiver sufficiently sensitive in a wide frequency band and capable of operating for a long time under these conditions constitutes a complex problem. Therefore, although development of sound receivers for operation in liquid metals at high temperatures is in progress (papers have been published on acoustic receivers operating at temperatures of up to 900°C), acoustic receivers with metal rods (waveguides) are widely used for acoustic signal reception from high-temperature regions [2]. In such waveguides, the acoustic vibration converter (usually a piezoelectric transducer) is fastened at the low-temperature end of the waveguide (250°C or less), while the other end of the waveguide is placed in the zone of the sound source.

The obvious advantages of acoustic receiver systems with waveguides are the possibility of using low-temperature piezoelectric ceramics, which are manufactured industrially in a large number of varieties, and the convenience in calibration. However, such systems have considerable disadvantages: loss of sound energy in the passage of signals through the waveguide, signal distortion due to reflections and resonances, etc. In order to determine the potentialities of acoustic noise monitoring as a possible method for detecting sodium–water leakages in steam generators, it is first necessary to investigate noise in experimental devices in the presence and in the absence of water leakage into sodium. This makes it possible to determine the spectral characteristics of the noise generated by water leakage into sodium as functions of the leakage parameters (outflow velocity, defect dimensions, sodium discharge and flow geometry, etc.,) and estimate the possible effect of scale and structural factors of the devices on the above parameters. It is very important to obtain information on noise characteristics in industrial devices.

Acoustic data units with transducers consisting of TsTS-19 piezoelectric ceramic and stainless-steel waveguides were used in our acoustic noise experiments on experimental sodium stands in the presence and in the absence of water leakage into sodium. The sound receiver design is shown in Fig. 1. The waveguide of sound receiver (a) is introduced into sodium through the cavity of the experimental section; the sodium discharge was equal to ~2 m^3/h. The water inlet device is located at the entrance of sodium into the section. The waveguide of another sound receiver (b) is fitted into a pipe section of the main circuit at a distance of ~100 mm from this device. The height and the diameter of the piezoelectric transducer based on TsTS-19 are equal to 5 and 9 mm, respectively. The diameter and the length of the Kh18N10T steel waveguides are equal to 10 and 500 mm, respectively. The measuring equipment consists of an S4-12 spectrum analyzer, an S5-2 harmonic analyzer, a UIS-2M amplifier, and an ÉPP-09 self-recorder.

Figure 2 shows the amplitude–frequency characteristics of noise obtained on the experimental stand with and without water leakage into sodium. In these experiments, the water discharge through the inlet unit of the section with a gas cavity varied from 2.8-10 g/h. The largest signal amplitudes are observed

in the frequency range 1-4 kHz, while the maximum corresponds to approximately 3 kHz. There was practically no signal at frequencies above 20 kHz. Some dependence of the noise amplitude on the leakage intensity (water discharge) is observed in Fig. 2 at frequencies from 1 to 4 kHz. For a water discharge of ~100 g/h, along with considerable signal amplitudes in the frequency range 1-4 kHz, intensive noise was recorded in the frequency range 30-32 kHz.

The data in Fig. 2 were obtained while using sound receiver *a* (Fig. 1), located at a distance of ~2 m from the leakage site. The signal spectrum was recorded by means of an S4-12 spectrum analyzer without preamplification. Figure 3 shows a typical recording of the signal from an acoustic data unit with a waveguide, mounted on the basic circuit of the stand, after analysis by means of the S5-2 instrument in the frequency range 60-200 kHz with a 3-kHz passband. The time intervals marked by the figures 1-8 correspond to analysis at frequencies of 180, 160, 140, 120, 100, 80, 60, and 200 kHz. It is evident from the figure that the frequency dependence of the signal amplitude is weak in the investigated range. In the absence of leakage, the signal practically vanishes. With the acoustic data unit mounted on the main pipe, it was also possible to record water leakages into sodium < 1 g/h, for which the upper limit of the signal frequency range was equal to approximately 80 kHz.

Consequently, small water leakages into sodium can be detected almost instantaneously by means of the acoustic method. The noise spectrum recorded as a result of water leakage into sodium is a broadband spectrum, which depends on the location where the sound receiver is mounted. The highest noise intensity is observed in the frequency range 1-4 kHz with a maximum at approximately 3 kHz.

The intensity of noise generated by water flow into sodium is considerable in comparison with the background in the ultrasonic frequency range. Noise monitoring in this range for purposes of leakage detection is probably the most promising possibility, since the background noise of devices in this frequency range is usually lower than in the low-frequency range.

LITERATURE CITED

1. V. I. Subbotin et al., in: Proc. IAEA Symp. Sodium-Cooled Fast Reactor Engineering, Vienna (1970), p. 471.
2. M. Gross et al., Atomkernenergie, 17, No. 4, 255 (1971).

MEASUREMENT OF ABSOLUTE POWER OF A NUCLEAR REACTOR

V. V. Dmitrienko, A. I. Efanov,
V. I. Zakharov, A. I. Karyakin,
and L. V. Konstantinov

UDC 621.039.564.2

Statistical methods of determining the absolute power of a nuclear reactor have a number of advantages over "classical" methods and are more and more widely used [1]. One such method – the frequency method [2] – permits prompt measurements. In this method an ionization chamber is placed in the reactor and the spectral noise density of the chamber current is measured at two frequencies. From these measurements the absolute power of the subcritical or critical reactor is found from the expression

$$N = \frac{2}{(\rho+\beta_{eff})^2}\frac{\nu(\overline{\nu-1})}{\bar{\nu}^2}\frac{I^2}{S_L - S_H}, \quad (1)$$

where ρ is the reactivity of the reactor, $\beta_{eff} = (1 - K_{eff})/K_{eff}$ is the effective fraction of delayed neutrons, ν_{eff} is the number of secondary neutrons per fission, I is the steady component of the chamber current, and S_L and S_H are the spectral noise densities of the chamber current at low and high frequencies, respectively. It is assumed that the frequency characteristic of the chamber is flat for the frequencies measured.

We describe a device for automatically determining the difference in spectral noise densities of the ionization chamber current and present results of the measurements.

A block diagram of the apparatus and a simplified functional diagram of the absolute power meter are shown in Fig. 1.

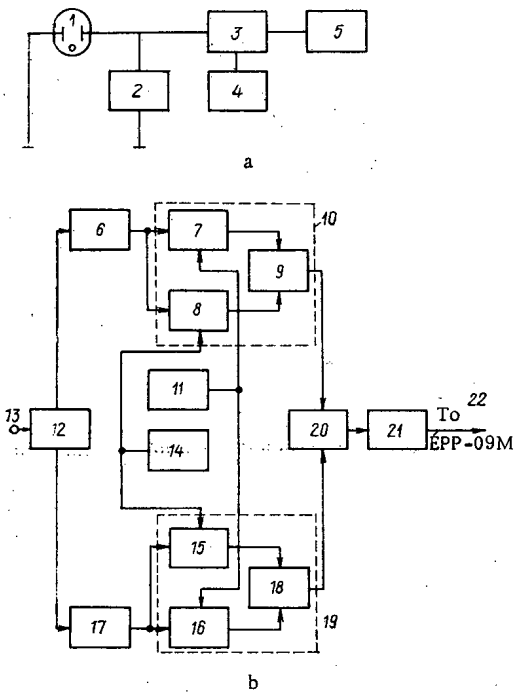

Fig. 1. a) Block diagram; b) simplified functional diagram of absolute power meter. a: 1) Ionization chamber; 2) power supply; 3) absolute power meter; 4) digital voltmeter; 5) ÉPP-09M. b: 6) Filter 1; 7) null element 1'; 8) null element 1"; 9) coincidence circuit; 10) power meter 1; 11) supplementary signal generator 1; 12) operational amplifier; 13) input; 14) supplementary signal generator 2; 15) null element 2"; 16) null element 2'; 17) filter 2; 18) coincidence circuit; 19) power meter 2; 20) substracting system; 21) output system; 22) to ÉPP-09M.

The determination of the spectral density is based on the well-known principle of narrow-band filtering [3], according to which it is sufficient to measure the output signal from a filter with a known passband. The ratio of the filter output power to its passband width is proportional to the spectral density at the central frequency of the filter. The device contains two similar power measuring channels. The central frequency of the low-frequency (channel I) filter is 5.75 Hz and that of the high-frequency (channel II) filter is 420 Hz. The amplification factors of these filters are chosen so that their unequal passband widths do not affect the final result. A direct power measurement is made in each of the channels in digital form and based on the method of the sign quantization of the sum of the input

Translated from Atomnaya Énergiya, Vol. 39, No. 6, pp. 434-436, December, 1975. Original article submitted March 10, 1975.

TABLE 1. Measured Values of Absolute Reactor Power

Chamber current, μA	Power meas. by regular apparatus, W	Power meas. by device described, W
1,98	2	1,85±0,13
1.1	50	47,4±3,3
51	51,6	48,5±3,4
97,5	99,8	101,8±7
2,3	103,2	100,3±4,1
9,2	378	395±27
200	500	519±36
485	500	546±38

and supplementary signals of special form [3]. This considerably simplifies the construction of an instrument of sufficient accuracy for a wide variation of output signal. The substracting system is a reversible counter, and a coincidence circuit serves as a squarer. The active filters used in the device have incomparably better characteristics at low frequencies than passive filters. The output system averages the signal and transforms it to a form suitable for delivery to an ÉPP-09M recording potentiometer. If the reading of this instrument is A, the absolute reactor power is given by the expression

$$N = K\frac{U^2}{A}, \tag{2}$$

where U is the output signal voltage of the operational amplifier

$$K = \frac{2}{(\rho+\beta_{eff})^2}\frac{\overline{\nu(\nu-1)}}{\bar{\nu}^2}\frac{1}{K_0},$$

where K_0 is a calibration factor.

The device is calibrated with a specially developed 1-1000 Hz white noise generator having an output signal with a known spectral density. The device is constructed in a portable bench form. The range of the input signal is 1.2 mV to 1.8 V with respect to the alternating component.

The relative error δ in measuring the difference of the spectral densities resulting from the statistical nature of the input signal is given by the expression

$$\delta = \frac{S_L}{S_L - S_H}\frac{1}{\sqrt{BT}}, \tag{3}$$

where B is the energy passband width of the low frequency filter and T is the integration time.

To ensure a relative error of the measurment of no more than 5% the integration time is chosen equal to 133 sec in accord with Eq. (3). The theoretical error of the measurement of the absolute power calculated from the relation

$$\delta N = \sqrt{4\delta^2 u + \delta^2 A + \delta^2 K} \tag{4}$$

is 6.5%. Neglecting the fall off of the frequency characteristic of the KNK-56 chamber for a supply voltage of 500 V at a frequency of 420 Hz [4] for $S_L \geq 10\,S_H$, a condition which is satisfied in the experiment described, leads to an additional error of ~0.4-0.5%.

The absolute power meter was tested on the IRT-1000 reactor. KNK-56 and KNK-53M ionization chambers were placed in an experimental channel on the reactor behind the reflector and connected to the instrument by 25 m of Mark RK-50 cable. The measurements were performed with the detector at various distances from the core. The maximum distance from the center of the chamber to the center of the core was 255 cm. Results were obtained for various positions of the chamber and therefore the steady current and the power are not proportional (Table 1).

Experiments showed that prompt measurements of the absolute power of a nuclear reactor can be made with this device with a relative error of no more than 7%.

LITERATURE CITED

1. A. I. Mogil'ner and D. M. Shvetsov, At. Énerg., 20, No. 2, 117 (1966).
2. R. Schröder, Nukleonik, No. 4, 227 (1962).
3. G. Ya. Mirskii, Apparatus Determination of the Characteristics of Random Processes [in Russian], Énergiya (1972).
4. L. Gasiorowski and L. Labno, Nukleonika, No. 3, 11 (1966).

SEMICONDUCTOR DETECTORS FOR X-RAY RADIATION USED IN WELL INVESTIGATIONS

S. A. Baldin, S. F. Gubin,
B. G. Egiazarov, and M. D. Kholomov

UDC 539.1.074.55

In the last few years the methods and instruments of nuclear physics have been increasingly used in various stages of the prospecting, winning, and processing of minerals. The speedy implementation of these techniques is caused by the better technological and economical parameters which these techniques have in comparison with conventional techniques used in investigations made in boreholes and blastholes underground or on the surface, and in the assaying of ore masses in tubs, on conveyor bands, etc.

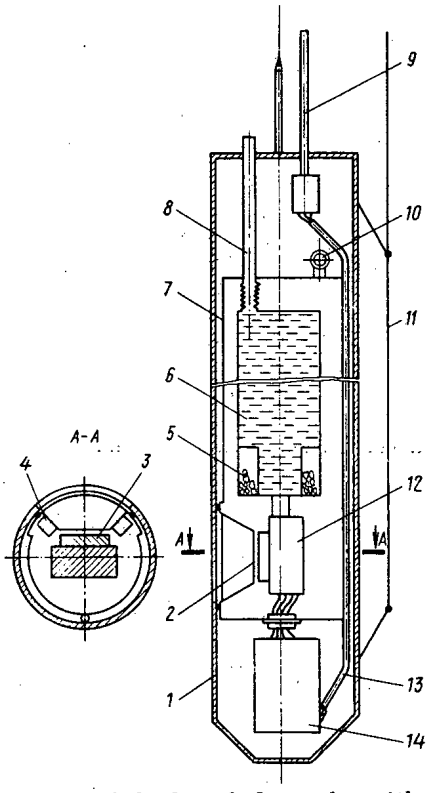

Fig. 1. Scheme of the borehole probe with semiconductor detectors for x-ray radiation: 1) outer housing; 2) beryllium foil; 3) semiconductor detector; 4) sources of primary radiation; 5) zeolite; 6) dewar vessel with liquid nitrogen; 7) vacuum vessel; 8) tube for filling the dewar with liquid nitrogen; 9) external cable; 10) vacuum valve; 11) device for pressing the probe to the borehole wall; 12) heatsink with the cooled first stage; 13) internal cable; 14) preamplifier.

Operational assay work in boreholes and blastholes is the most important, but routine work of this kind is laborious (hundreds of thousands of boreholes and blastholes per year). The rigorous specific production-dependent conditions for measurements in boreholes impose the greatest difficulties upon the development of the corresponding instruments and methods. This also applies to the instruments which are used for investigations made in wells with the aid of characteristic x-ray radiation.

Characteristic x-ray radiation which is excited in the walls of boreholes is now recorded either with proportional counters or with scintillation detectors [1, 2]. Proportional counters are designed for the analysis of elements having low or medium atomic number; scintillation detectors are usually employed for the determination of elements having medium or high atomic number. The insufficient energy resolution of detectors, particularly of scintillation detectors, and the intense scattering of the primary radiation do not allow analyses with the required sensitivity and selectivity. The number of elements which can be analyzed and which differ only by 3 or 4 from Z is at most two or three. The sensitivity threshold amounts at best to a few hundredths of a percent. However, the development of composite deposits requires logging for a larger number of elements, commonly arranged side by side in the

Translated from Atomnaya Énergiya, Vol. 39, No. 6, pp. 436-438, December, 1975. Original article submitted March 17, 1975.

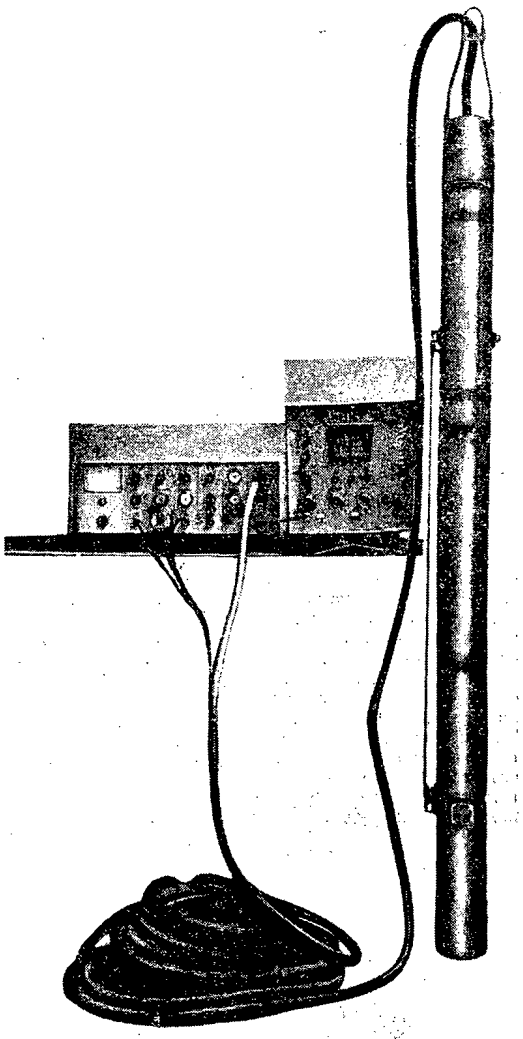

Fig. 2. Borehole equipment with semiconductor detector, "Feb-1" panel, and AI-256-5 analyzer.

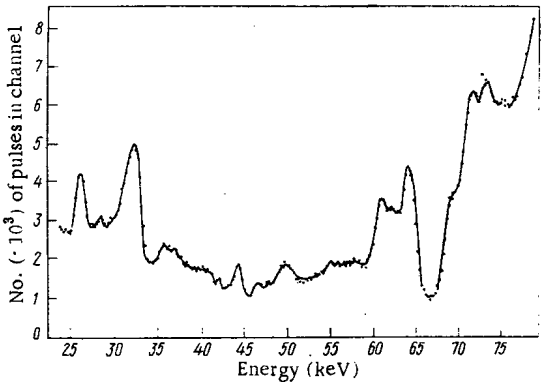

Fig. 3. Amplitude spectrum measured at a depth of 14 m with a ^{57}Co source in the energy range 25-75 keV.

periodic chart, and the marginal content for many elements is considerably lower.

The presently available laboratory spectrometers with semiconductor detectors for x-ray radiation are characterized by excellent performance parameters and allow the rapid, simultaneous multielement analyses of samples with a sensitivity threshold of the order of 10^{-3}%; most of the elements from carbon up to higher elements can be analyzed [3]. However, the transition from analytic measurements with semiconductor detectors in the laboratory to measurements under field conditions, in boreholes, and in geophysical team work requires special apparatus which is hermetically sealed, has an independent power supply and low power consumption, and can be used under severe mechanical and climatic conditions. Yet the instruments must not lower the excellent characteristics of semiconductor detectors for measurements.

Equipment of this type (the "Feb-1" instrument) was developed in the last few years specifically for use under difficult conditions encountered by geological prospecting parties in exploration work in which laboratory-type equipment or instruments with semiconductor detectors hardly function. The circuits of the "Feb-1" instrument shape a "pseudo-Gaussian" pulse with a peak duration of 2-16 μsec and comprise a stage restoring the constant component so that operation at input pulse rates of up to $2 \cdot 10^4$ pulses/sec is possible without substantial deterioration of the resolution. A threshold amplifier provides for fourfold broadening of the energy scale. The energy resolution at 5.9 keV is better than 400 eV in the selected detectors. The instrument is hermetically sealed and sustains mechanical load applications in accordance with the III group specification for instruments (GOST 9763-67); the instrument needs less than 10 W from a ±12-V source. The set of sensors with silicon or germanium semiconductor detectors is designated for the analyses of either specimens or ore bodies in their natural bedding.

The development of this instrument was the prerequisite for the solution of problems encountered in borehole investigations in which semiconductor detectors for x-ray radiation are employed. A borehole instrument with a DGRZ-1 germanium semiconductor detector was designed and produced for this purpose. The sensitive area of the detector is 150 mm^2 at a thickness of 3 mm. The total energy resolution of the instrument equipped with this semiconductor detector was 700, 1000, and 1300 eV at the energies 5.9, 60, and 122 keV, respectively, at a pulse shaping time of 4 μsec. The sensitivity threshold of the analysis of powder samples having elements with medium Z amounted to $(2\text{-}4) \cdot 10^{-3}$% at measurement times of 1-2 min. The detector can be stored at room temperature.

Figure 1 schematically shows the instrument. A hermetically sealed vessel which consists of a tube and upper and lower lids and which can be evacuated through a valve contains a stainless-steel container for liquid nitrogen which through a little tube connects with the atmosphere. The liquid nitrogen volume is 1 liter. A heatsink which is joined with the bottom of the vessel carries the semiconductor detector (its

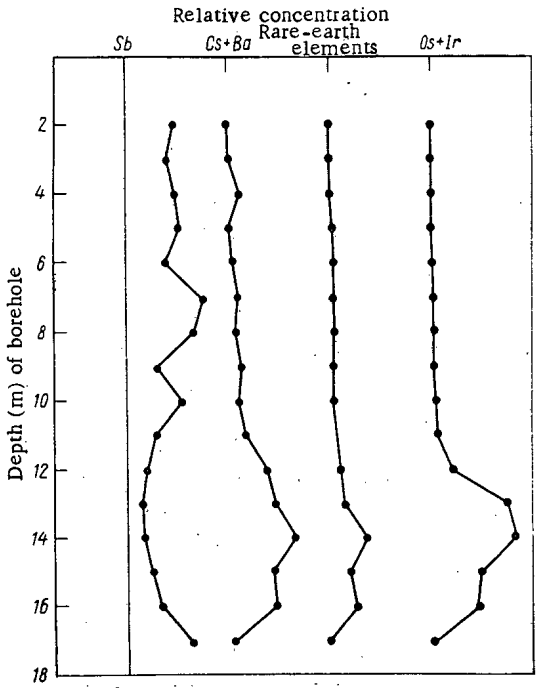

Fig. 4. Distribution of Sb, Cs +Ba, the total of rare-earth elements, and Os +Ir over the borehole profile.

sensitive surface is parallel to the axis of the probe) and all electronic components of the first preamplifier stage. The first preamplifier stage is connected to the rest of the preamplifier circuitry by a connector. The preamplifier, in turn, is connected with internal and external cables to the main panel in the working area of the vehicle used for the logging work. The length of the external cable (25 m) can be increased to several hundred meters if necessary. The wall of the sealed cylinder has a recess opposite to the sensitive surface of the semiconductor detector; the bottom of the recess is covered with a 200-μ-thick beryllium foil. Openings for two radioactive sources are provided in the walls of the recess. After their assembly and after evacuation, all the components are in a steel tube with a diameter of 100 mm and a length of 1800 mm. Vacuum is maintained with the aid of a cryostatic absorption pump. The probe is pressed to the borehole walls with the aid of a steel cable which is led to the surface. One liquid nitrogen filling lasts for 12-14 h of operation. The borehole probe was tested in 1974 in dry boreholes of one of the Central Asian ore sites. When analyses were made in the various ranges, γ-radiation sources made of ^{57}Co or ^{241}Am were used; the sources had an activity which produced a pulse rate of $(6-8)\cdot 10^3$ pulses/sec in the electronic circuits.

Figure 2 is a view of the equipment developed.

The energy scale of the analyzer was calibrated before and after the measurements. The amplitude spectra were pointwise recorded in 1-m intervals to a depth of 18 m (Fig. 3). Though not all the peaks of total absorption can be reliably identified, the spectrum indicates the presence of elements such as antimony (26 keV), barium, and possibly, cesium (31-32 keV), several rare-earth elements (at 44 and 50 keV), elements of the iridium–osmium group (62-65 keV), and lead (75 keV) at the corresponding depths in the borehole.

The evaluation of the results has led to the relative concentrations of certain elements at various depths, as indicated in Fig. 4. A first utilization of the borehole equipment with semiconductor detectors for x-ray radiation has proved definite advantages over logging with other types of detectors, particularly when investigations of complex ore bodies with a complicated composition are made.

LITERATURE CITED

1. V. N. Mitov et al., in: Geophysical Equipment [in Russian], No. 46, Nedra, Moscow (1971), p. 50.
2. Yu. P. Lyubavin et al., in: Geophysical Equipment [in Russian], No. 48, Nedra, Moscow (1972), p. 71.
3. S. A. Baldin et al., Applied Spectrometry with Semiconductor Detectors [in Russian], Atomizdat, Moscow (1974).

MEETING ON THE DESIGN OF LARGE THERMONUCLEAR TOKAMAKS

É. I. Kuznetsov

The successful growth of studies in controlled thermonuclear fusion indicates that in the next few years machines will be built which will substantially approach demonstration thermonuclear reactiors, i.e., systems in which controlled thermonuclear reactions will take place with fusion of deuterium and tritium and the release of energy comparable to the energy delivered to the plasma from outside. Of the various experimental thermonuclear machines the one most studied at present is a quasistationary closed system – the Tokamak. A few years ago stable confinement of a hot plasma in a closed magnetic trap was first attained in Tokamaks. At that time work was being done on these systems only in the USSR; however, now about 20 Tokamaks are working in different countries and more than ten are in the design and construction stage.

The IAEA, with the cooperation of the State Committee on Atomic Energy of the USSR, has organized a discussion on the four designs for demonstration thermonuclear reactors of Tokamak type: the European (European Economic Community countries), American, Soviet, and Japanese. More than 100 specialists from Belgium, Great Britain, Italy, the Netherlands, the USSR, the USA, France, the Federal Republic of Germany, Sweden, and Japan took part in this international meeting (Dubna, June 4-11, 1975), where, along with detailed consideration of the construction of the different systems of these machines, there were discussions on the design of future thermonuclear power stations, and the problems and prospects for thermonuclear power.

The sizes of the proposed machines, JET (EÉC), TFTR (USA), DTRT (USSR), and JT-60 (Japan), are determined by the physical and engineering problems which it is proposed to solve with these machines on the way to building thermonuclear power reactors in the future. The most compact in size (major and minor radii of the plasma 2.48 and 0.85 m, respectively) is the American machine. The European and Japanese machines will have about the same dimensions (major radius of the plasma about 3 m, minor radius 1.25 and 1 m, respectively). The major and minor radii of the plasma in the Soviet machine are 5 and 2 m, respectively. The discharge current in the various machines is 1-6 MA and the longitudinal magnetic field is 3.5-5.2 T. One of the basic characteristics of thermonuclear machines with magnetic containment of the plasma is the product of the plasma density and the confinement time, $n\tau$. This quantity, together with the ion temperature, determines the range of plasma parameters required to ensure positive energy yield from a thermonuclear reactor. For the different machines $n\tau$ lies between 10^{13} and 10^{14} cm^{-3} sec, while the average ion temperature lies between 5 and 15 keV.

The differences in the technical and design solutions and in the choice of plasma parameters are determined by the set of problems which are expected to be solved on each machine. The authors of the JT-60 design have set themselves the most immediate, mainly physical, problems which must be solved to build a thermonuclear reactor. As opposed to the other three machines, here there is no plan to work with tritium. The task of the American design for a test thermonuclear reactor is to achieve high thermonuclear temperatures and to study the so-called two component Tokamak regime, where the fusion reaction takes place between nuclei of the main initially produced plasma and fast particles injected into the plasma from without (in this case a value of $n\tau$ of order 10^{13} cm^{-3} sec is sufficient).

The joint European Tokamak project is the most complete of the remaining efforts and the task for this machine is to obtain and study a plasma with parameters which ensure a self sustaining thermonuclear reaction ($n\tau \approx 10^{14}$ cm^{-3} sec). An extensive program of physical and engineering studies is planned for the Soviet demonstration Tokamak. This machine is intended both for producing the plasma parameters needed

Translated from Atomnaya Énergiya, Vol. 39, No. 6, pp. 439-440, December, 1975.

for a self sustaining thermonuclear reaction and for long operation with a deuterium–tritium plasma. Plans include neutron physics studies, studies of sputtering of the discharge chamber walls by alpha particles, and determination of the tritium breeding coefficients for various blanket modules (breeding zones).

It should be noted that the plasma parameters of DTRT are practically the same as those for a hybrid power reactor, i.e., a thermonuclear reactor with a blanket containing depleted or natural uranium for energy production from fissionable materials as well.

Since Ohmic heating of plasma cannot produce thermonuclear temperatures, additional heating methods are planned for all these machines. The discussions were mostly centered on the neutral beam injection problem, adiabatic compression, and RF heating of the plasma, as well as heating by plasma instabilities (i.e., the question of whether supplementary heating techniques lead to deterioration of the confinement conditions). Large scale experiments are required to make a final choice of plasma heating methods.

The problem of building vacuum chambers and choosing wall materials for the experimental machines and future thermonuclear reactors must be solved taking into account such factors as embrittlement due to neutron irradiation and sputtering due to charged particles from the plasma. Also important is the prevention of localized energy deposition in various parts of the chamber. We note that solution of many of these problems requires research analogous to that carried out for building fast breeder reactors, in connection with which an idea was proposed for a thermonuclear reactor as a source of 14-MeV neutrons especially intended for materials study and solution of engineering and technological problems.

In particular, the problems of radiation protection in experiments with D–T plasmas and of systems for recovering and preventing leakage of tritium during regular operation and emergencies were discussed. The design solutions chosen must ensure normal operating conditions for the experimenters and technicians.

Construction on all four machines will begin in the early 1980's and, if positive results are obtained, a decision will have to be made as regards building test thermonuclear power reactors. During the meeting conceptual designs for pure (with tritium breeding) and hybrid thermonuclear Tokamak reactors developed in the USSR, the USA, and Japan were discussed. It was noted that in the first stage of development of thermonuclear reactors, hybrid reactors may seem more economically advantageous than pure fusion reactors. The size and electrical power of such thermonuclear Tokamak reactors do not differ greatly. The major radius is taken to be 10–15 m, and the minor, from 3 to 5 m. The electrical power in most designs is taken to be 2000–2500 MW. The discussions showed that technical and engineering studies are needed already to ensure the development of economically advantageous commercial thermonuclear power stations that have a minimal effect on the environment. Those groups having experience in the design of nuclear power stations with thermal and fast reactors must certainly be drawn into this work.

The meeting showed that international collaboration in discussions on the design of large thermonuclear Tokamaks is very useful and can make a number of improvements for future study and use in these designs.

SEMINAR "THE FUTURE OF FISSION AND FUSION BREEDERS"

G. A. Eliseev and A. S. Kochenov

The Seminar took place in the beginning of 1975 at the I. V. Kurchatov Institute of Atomic Energy. The Seminar has been organized jointly by the State Committee on Science and Technology of the USSR and the International Institute of System Analysis IISA (Austria, Luxemburg). Besides Soviet scientists, the Seminar was attended by Prof. W. Hefele (IISA), Prof. G. L. Kulcinski (University of Wisconsin), Prof. J. P. Holdren (University of California), and Dr. H. Kessler (Carlsruhe Nuclear Research Center, FRG).

Inaugurating the Seminar, Academician M. A. Styrikovich welcomed the initiative of the International Institute of System Analysis and pointed out the importance of system analysis research in the analysis of the global energy problem and in particular in the comparison of the prospects of fission and fusion breeders for future power engineering. W. Hefele reported on a tentative comparative evaluation of breeders of both types carried out in cooperation with C. Starr [1]. The analysis was based on the following propositions: 1) the natural reserves of chemical fuels will be essentially exhausted in the next 40-50 years; 2) the time needed to master new energy sources is on the order of 25-30 years so that the fundamentals of power engineering of the 21st century must be laid now; 3) the use of either fission or fusion breeders can offer practically unlimited energy resources.

W. Hefele noted that the report [1] provoked lively interest and much sound criticism especially among specialists in thermonuclear fusion. The IISA is now preparing a new report in which the above criticism and recently obtained information are taken into account.

In the course of a discussion of the problem as a whole, the participants of the Seminar came to a unanimous conclusion that most difficulties encountered on the way to either atomic or thermonuclear power are due to specific demands imposed on structural materials, to the necessity of ensuring reliable protection from ejection of radioactive materials in normal reactor operation and in emergency situations, and finally, to the problem of disposal of radioactive wastes. The availability of raw fuel and the high share of fuel in the final cost of the produced energy evidently present no problem. The participants came to the conclusion that a comprehensive comparative analysis of fission and fusion breeders is impossible for the time being as the two systems are on different levels of historical development. The task of system analysis should thus be not the choice of some particular direction in the development of global power engineering, but a thorough investigation of all unsolved problems in all directions and the suggestion of optimum ways for their solution. This should cover the entire cycle from the production of raw materials and the availability of fuel and construction materials to the distribution of energy and the processing and disposal of wastes.

System analysis of the future prospects of atomic and thermonuclear energy should take into account geographical characteristics of the various regions of the world. For example, small countries may find the use of large power plants unacceptable. States that have no facilities for burial of large amounts of radioactive wastes will obviously prefer "pure" systems. In large countries, such as the United States or the Soviet Union, the choice of a particular type of power plant may depend on the specific location of the power system. Even preliminary considerations indicate that such problems as fuel doubling time and the provision of construction materials are to different degrees critical for the two types of breeders. The problem of construction materials has been nearly solved for fission breeders. Fast breeder reactors are already operating in several countries. It must however be noted that the fuel doubling time of these reactors is considerably longer than the time which will be probably needed for the expansion of atomic power in the next century (≤ 5 years) [2]. Reduction of fuel doubling time requires the reactors to operate at much higher energy-intensity conditions and thus uses better heat-resistant materials and nuclear fuel of higher density (as compared with UO_2).

Translated from Atomnaya Énergiya, Vol. 39, No. 6, pp. 440-441, December, 1975.

The fuel doubling time is not a limiting factor for thermonuclear breeders. On the other hand, the problem of structural materials, in particular for the "first wall," is now very acute. Niobium, which in several preliminary designs was considered as the basic construction material, proved to be disappointing from the point of view of activation.

The probability of ejection of radioactive materials in fission breeders is mainly determined by emergency situations not only in the reactor proper but also in fuel processing plants. Obviously, this probability can be reduced to a reasonable minimum at the cost of additional capital investments. The same is also true of the problem of radioactive wastes burial.

The total radioactivity of thermonuclear breeders, and thus also the probability of radioactive pollution of the environment, can be significantly reduced by using construction materials based on weakly activating elements (vanadium, aluminum, etc.). One must however consider the practical feasibility of producing on the basis of these elements materials possessing the necessary mechanical strength and radiation resistance (as well as their availability).

The participants of the Seminar agreed that both plutonium fission breeders and thermonuclear breeders based on D–T fusion reactions with tritium regeneration would provide mankind with an almost unlimited source of energy. For future global power it is important that at least one of the indicated alternatives becomes practically realizable. The principle of diversity must be followed in this case of safeguard against erroneous decisions. The problem of providing extensive fuel regeneration is so important that the necessity of further progress in both directions arouses no doubt.

LITERATURE CITED

1. W. Hafele and C. Starr, J. Brit. Nucl. Energy Soc., No. 4 (1974).
2. A. P. Aleksandrov, in: Twenty Years of Atomic Power Engineering [in Russian], Atomizdat, Moscow (1974).

RADIATION EFFECTS OF NUCLEAR PLANT DISCHARGES INTO WATER

Yu. V. Sivintsev

The Symposium of the International Atomic Energy Agency (IAEA) on Radiation Effects of Nuclear Power Plant Discharges into Water was held on June 30-July 4 in Otaniemi near Helsinki. The Symposium was attended by 143 specialists from 28 countries and three international organizations – the IAEA, the European Economic Community (EEC), and the Euratom. The symposium heard and debated 33 reports: eight from the United States, four each from the Soviet Union and Japan, three each from Great Britain and France, two from the International Laboratory of Sea Water Radioactivity Studies (Monaco), and one each from Austria, the GDR, Netherlands, Egypt, Israel, India, Italy, Finland, and the FRG.

The reports treated various aspects of the problem which plays an important role in modern nuclear power engineering and radioecology. Discussed in detail were the behavior of stable and radioactive isotopes of various elements in the water environment, the critical paths of radionuclides into physical, chemical, and biological systems, methods of radiation monitoring and evaluating the effects of radiation exposure on humans and hydrobionta, the radiological capacity of water reservoirs, and the behavior of plutonium and other transuranium elements in water. The special interest in the last problem is due to the absence of stable isotopes of transuranium elements in the environment which can lead to a particularly high concentration of such isotopes in certain chains of ecosystems and the creation of radiation hazards for man and other living organisms. A recent (February 1974) report of the US Environmental Protection Agency evaluated the consequences of the discharge of such radionuclides from atomic plants in the USA. Assuming that the fraction of plutonium escaping into the environment is $P = 10^{-7}$, the relative contribution of transuranium elements in the natural background is small, but becomes dominant if $P = 10^{-6}$.

The reports presented at the Symposium described the results of simulation experiments and of the studies of actual water ecosystems.

Experimental laboratory studies of plutonium kinetics in hydrobionta have been carried out at the International Laboratory in Monaco. An important advantage was the use of ^{237}Pu whose γ spectrum can be easily recorded (five lines near 100 keV). The measurement of ^{237}Pu in shrimp organisms proved that the concentration factor (CF) is $(0.9\text{-}4.1) \cdot 10^3$, and that 30-60% of the accumulated plutonium is discarded into water in molting. This indicates that this process can be an important source of this element in the environment. An analysis of the curves showing the secretion of radionuclides of sea organisms shows that the effective half-lives of Pu(VI), mercury, and cadmium are the same (to within the experimental error). These data show that at least in hydrobionta plutonium behaves as other heavy metals (S. Fowler).

Experimental investigations of sorption–desorption of Pu(III), (IV) and (VI) and Am(III) by sediments in a laboratory model of a river estuary revealed the drastic effect of plutonium valency and the pH and salinity of the medium. In sea water, plutonium and americium quickly turn into a colloidal form probably as a result of combination with sodium carbonate. Discussing the results of these investigations, H. Hammet (France) stressed the importance of Pu(VII) studies as this form will be a dominant component in liquid wastes in case of emergency discharges from radiochemical plants ($T_{1/2}$ of the transition to Pu(VI) is several weeks).

Radioecological research at the Flat Rock Nuclear Center (USA) provided extensive data on the behavior of plutonium in a chain of settling ponds. Since 1953 this Center worked on nuclear fuel, processing 2400 kg of ^{239}Pu on the average annually. A two-stage liquid radioactive waste processing system, with decontamination factors of 10-100 and 10^4, respectively, ensures high recovery of ^{239}Pu from water. The average concentration of ^{239}Pu in discharge waters in 1974 was 1.8 pCi/liter. For 22 years of the plant operation,

Translated from Atomnaya Énergiya, Vol. 39, No. 6, pp. 441-443, December, 1975.

the discharge waters added 75 mCi of ^{239}Pu. It has been estimated that an additional 135 mCi has been accumulated on the plant territory. An analysis of the ^{239}Pu content in the various links of the ecosystem indicates that the concentration factor is 10^4-10^5 for primary phytoplankton, 10^4 for edible algae, and 10^3 for zooplankton. The accumulation of ^{239}Pu is much lower at higher trophic levels: the CF in freshwater fish of the carp family is 0.9-8, and in vascular plants even as low as 10^{-1}-10^{-2}. Assuming conservatively that ^{239}Pu concentration due to this plant is 0.01 pCi/liter of drinking water, and that 10,000 people consumed such water for 20 years, M. Thompson arrived at the conclusion that such plutonium levels present no danger for either man or other biosystems.

The Division of Radiological and Ecological Research of the Argonne National Laboratory (USA) presented the materials of natural investigations of the behavior of plutonium and other long-lived radionuclides in Lake Michigan which provide data on biological transport, seasonal variations, and the staying time of ^{239,240}Pu, ^{241}Am, and ^{137}Cs in the lake, and on the rate of inflow of these radionuclides in the sediments. Inspite of the fact that no less than eight nuclear reactors are operating on the shores of Lake Michigan, the total intensity of long-lived radionuclides discharged into the water is much lower than that coming from global fallout. The results of investigations indicate that at present ^{239,240}Pu and ^{137}Cs are mostly in an ionized form and that their effective half-life in Lake Michigan is 3-4 years (100 years for ^{90}Sr). This indicates a practically equilibrium state in the given ecosystem and a significant biogeochemical similarity of plutonium and cesium properties. The activity of radionuclides in lake water is 5-4% of the total inflow of ^{239}Pu and 3-2.5% of ^{137}Cs. It is interesting to note the agreement of these data for ^{239}Pu in lake (M. Walgren and J. H. Marshall) and sea (J. H. Hetherington et al) water.

Food-chain investigations revealed that ^{239,240}Pu and ^{137}Cs strongly concentrate in phytoplankton (average CF $5.7 \cdot 10^3$ and $3.7 \cdot 10^3$, respectively) and that the concentration of ^{90}Sr is considerably lower (CF = 40). In edible fish the CF is 4-20 for ^{239,240}Pu, 160-420 for ^{137}Cs, and 15-67 for ^{90}Sr.

The ratio of the concentration in higher trophic levels to the concentration in phytoplankton is ~ 3 for ^{137}Cs, ~ 0.3 for ^{90}Sr, and $\sim 10^{-3}$ for ^{239,240}Pu. This indicates that there is a marked inverse dependence between the concentration of ^{239,240}Pu in the studied hydrobionta and their trophic level. It has been found that the numerical value of CF is strongly related to Q-sol content in plankton samples (expressed in percent of raw weight) and in the range from 10^2-10^4 can be expressed as $CF = 200\ Q^{1.4}$ for $0.6 \leq Q \leq 15\%$.

Out of global fallout, 97% of the total ^{239,240}Pu activity and 95% of total ^{137}Cs activity has been received by the sediment. A study of the distribution revealed a pronounced peak of activity of the above nuclides at a depth of 2-6 cm (at different plants). From this it was possible to estimate the sediment deposition rate. This has been found as 0.015-0.5 cm/year (4.8-96.3 mg/cm^2 year). The deposition rate and the concentration of ^{239}Pu and ^{137}Cs in bottom sediments are in good correlation with each other.

Workers of the Radiobiological Laboratory of Ministry of Agriculture, Food, and Fisheries of Great Britain have studied the behavior of plutonium in the Irish Sea in comparison with other long-lived radionuclides discharged from the Windscale Radiochemical Plant. It has been found that the rate of plutonium discharge into the Irish Sea is 40-150 Ci/month ($\sim$1000 times the global fallout), more than 90% of it settling near the discharge point. The total plutonium activity in the Irish Sea waters is of the order 50-60 Ci (nearly 4% of the cumulative discharge of the previous years), and its content in "critical path" foods does not exceed 2% of the permissible effective level.

The behavior of ^{239}Pu and of long-lived fragments of ^{144}Ce, ^{137}Cs, and ^{106}Ru in sea water and sediment is distinguished by considerable similarity of these radionuclides with respect to their concentration contours in filtered sea water, to the practically constant ratio of their relative activities, and to variation with depth in sediments (up to 24-28 cm). The concentration of ^{239}Pu in sediments is very high and in a region up to 110 cm from the discharge point the CF ranges from $(22\text{-}7) \cdot 10^4$ to $(2\text{-}0.1) \cdot 10^4$. The concentration in hydrobionta is at least one order of magnitude less: $3 \cdot 10^3$ in algae, $2 \cdot 10^3$ in the soft parts of mollusks, and 30 in fresh fish.

J. Miettinen et al. (Finland) discussed the results of the determination of ^{239}Pu + ^{240}Pu content in water samples, sediment, mollusks, algae, and fish at one of the seashore stations on the Gulf of Finland. Gamma spectrometry measurements proved that fish has 0.04-0.14, mollusks 0.6, algae 5, and sediments up to 0.18 pCi/kg of raw weight. These values are basically the same as the results of biosample measurements in the Great Lakes of the USA published by V. E. Noshkin in a series of reports of the USA Atomic Energy Commission and in a well-known paper [Health Physics, 22, 537 (1972)]. The sole exception is plutonium content in algae (one order of magnitude higher than in Lake Michigan). This can be explained by the low

exchange rate of the Baltic Sea waters. According to A. G. Trusov et al. (USSR) the same conclusion can be drawn from the analysis of ^{90}Sr concentration in the Gulf of Finland waters: if the specific activity of ^{90}Sr in the oceans is taken as 1.00, the activity in the Mediterranean Sea is 1.5, in the North Sea 3.2, and in the Black Sea 4.0, and in the Baltic Sea 6.

The concluding report has been prepared by a large number of American specialists and in fact attempted to justify the admissibility of deep-sea burial of long-lived radioactive wastes. Its main conclusions met with critical remarks on the part of delegates of India, the USSR, Japan, and other countries.

In the final analysis, the results of the IAEA Symposium can be summed up as follows.

1. None of the 33 presented reports cited examples of any radiation damage to ecosystem elements in view of the existing discharges from nuclear plants into water. This once more confirms the fact that nuclear power (as compared with other kinds of human activity) presents little danger both for mankind and the environment.

2. The construction of nuclear power plants, which is expanding in almost all countries, necessitates the continuation and expansion of radioecological research in specific geographic regions. The Symposium heard highly specialized reports on these topics by research workers of many countries. The possibility of conducting such research with low radionuclide concentration in the environment makes the locality of atomic power plants a natural proving ground with little danger for man and the biosphere. The study of critical paths and "radiation resistance" of various parts of real ecosystems becomes especially important in this connection.

3. The Symposium has been presented with interesting and abundant data on the behavior of plutonium in water media. Plutonium and other transuranium elements which have no stable natural isotopes should remain at the center of attention for the next decades since further development of nuclear power based on fission reactors is impossible without the transition to fast breeder reactors and extensive use of plutonium. The accompanying increase of plutonium influx into the environment and its concentration in some links of the ecosystem can be critical for future nuclear power. Continuing accumulation of objective data in this field is an exceedingly important and acute task.

SEVENTH ALL-UNION CONFERENCE ON THE PHYSICS OF INTERACTION OF CHARGED PARTICLES WITH SINGLE CRYSTALS

A. G. Kadmenskii

The Conference took place in Moscow on May 26-28, 1975. The topic of discussion at this and the preceding conferences were the relatively recently discovered effects of channeling and shadowing in the motion of fast charged particles in single crystals and phenomena associated with these effects. The Conference was attended by nearly 200 scientists of various Soviet cities who represented universities and research institutes of the Academy of Sciences of the USSR and other Soviet Republics, and also several ministries and departments. Papers have also been presented by prominent scientists from the USA, GDR, Poland, Mongolia, and Yugoslavia. The 93 reports read at the Conference touched upon various aspects of this rapidly developing subject. All reports can be arbitrarily divided into three major groups. First, the study of orientational effects of the motion of heavy charged particles (protons, ions) in single crystals; second, works associated with the motion of light charged particles (electrons, positrons) and radiation in single crystals; and third, the application of orientational effects in the study of nuclear, atomic, solid state, and other problems in single crystals. Such a classification takes into account not only the kind of particle but also the different form of description of the motion of heavy and light particles in single crystals. After the work of J. Linhard (1965) on the channeling of heavy particles, the basic model of description is the classical model of statistical equilibrium in the phase space of transverse coordinates and particle momenta in the crystal (the amount of transversality relative to the direction of atomic nucleus for axial channeling and relative to the atomic plane for planar channeling). Such a description can also be used for high-energy electrons but the main approach to this case is a quantum mechanical treatment.

The study of channeling and shadowing effects of heavy particles now proceeds in two directions. The method of kinetic equations for channeling particles, developed on the basis of the Linhard model by Danish (Banderoop, Andersen, and others) and Soviet (M. A. Kumakhov, V. V. Beloshitskii, et al.) workers, is extensively used for calculating dechanneling and the elements of angular shadow-pattern distributions. Such calculations have been reported by, for example, M. A. Kumakhov, V. V. Beloshitskii, et al. (Moscow) and by V. S. Andreev et al. (Sverdlovsk). On the other hand, experimental and theoretical results have been reported which indicate that axial and planar channeling are associated phenomena. Thus, the prevalent formalism of kinetic equations does not describe certain effects of particle channeling. Important work on this subject has been carried out by Yu. V. Bulgakov, V. I. Shul'ga et al. (Moscow) who studied the behavior of crystal transparency in the transition region between axial and planar channeling where the transparency has been experimentally observed to vary nonmonotonically with the angle of particle incidence in relation to the close-packed axis. This effect has been explained by the presence of additional focusing by ordered atomic chains of the particle moving in the axial channel.

The ordered arrangement of atomic chains is manifested experimentally in the azimuthal dependence of the elastic scattering cross section of channeling particles in the axial channel ("back shadow"). This has been most clearly demonstrated in a study of the spectra of back-scattered particles entering an axial channel with the same transverse energy ($E_{\perp 0} \geq 0.5E_{\perp cr}$, where $E_{\perp cr}$ is the Lindhard critical energy), but with different starting azimuths [E. I. Sirotinin, A. S. Rudnev, et al. (Moscow)].

Finally, computer simulation of angular distributions of particles passing through a thin single crystal under axial channeling conditions [A. G. Kadmenskii et al. (Moscow)] proved that for $E_{\perp 0} \geq 0.2E_{\perp cr}$ angular distributions show a regular azimuthal structure that coincides with the principal direction of crystallographic planes passing through the studied crystallographic axis. It has been found that these angular

Translated from Atomnaya Énergiya, Vol. 39, No. 6, pp. 443-444, December, 1975.

distributions are far from being in statistical equilibrium in the Lindhard sense, and that the transverse energy distribution also differs from the predictions of the Lindhard model of statistical equilibrium for an axial channel.

All these facts will undoubtedly stimulate further development of the theory of orientational phenomena.

Considerable progress has been made in the important problem of the mechanisms and magnitude of energy loss by channeling ions. A. F. Burenkov et al. (Moscow, Minsk) calculated the energy loss of a channeling particle taking into account the band structure of the electron energy spectrum in crystals. The ratio of the energy loss in motion through an axial channel to the energy loss of a particle moving in a nonoriented direction has been found to be a nonmonotonic function of the particle energy and is essentially different from 1/2 as predicted by the Lindhard rule of equipartition of energy losses into distant and near collisions. An experimental study of average relative energy losses for various tungsten axes and planes, carried out by the thick-target method [E. I. Sirotinin, A. S. Rudnev, A. F. Tulinov et al. Moscow], has found that for all orientations the figures are ≥ 1.5 and ~ 0.35, respectively, for crystals escaping from the surface layers and from greater depths.

Channeling of electrons and positrons is actively studied in Tomsk, Kharkov, and Moscow. Of particular interest are attempts to analyze the bound state of an electron moving in channeling conditions, and the bremsstrahlung of such an electron in the planar and axial cases [N. P. Kalashnikov, et al. (Moscow); S. A. Vorob'ev, V. V. Kaplin, et al. (Tomsk)].

The field of application of orientational effects increases from year to year. Widely known are the results of measurements of the lifetime of excited nuclei in nuclear reactions in single crystal targets, and the localization of impurity atoms in the crystalline lattice. Yu. V. Melikov, P. E. Vorotnikov, N. G. Chechenin, et al. (Moscow) reported on the measurement of ^{236}U fission time as a function of excitation energy in a wide range of energies. The obtained results indicate that the level density of the studied nucleus has in the investigated energy range a discontinuity which cannot be explained by existing theoretical models. Considerable advances have been made in the determination of the site of impurities (oxygen, carbon) in semiconductor crystals by Yu. Yu. Kryuchkov, N. V. Slavin, et al. (Tomsk), who used high-energy α particles.

The calculation of the three-dimensional distribution of particles in a channel and of its variation with depth makes it possible now to find the depth distribution of impurity ions and defects in a crystal by the method of particle backscattering. Interesting work in this direction has been jointly described by a group of Soviet and GDR scientists.

Investigations of the dynamics of phase transitions in single crystals and of the structure of heteroepitaxial films [A. A. Puzanov, et al. (Sverdlovsk)] proved that the application of charged particle beams in such studies can provide new information, which greatly surpasses the capabilities of traditional methods (e. g., x-ray methods).

New possibilities in atomic studies have been discovered by German scientists (H. Otto, et al.). They succeeded in recording together with a proton diffraction pattern, a circle representing the cross section of the Kossel cone of the characteristic x-ray radiation of the crystal atoms. Of special interest is the new approach to the study of dynamic interaction of ions with the aid of channeling which has been put forward by D. Hammel (USA). If a collimated beam of molecular H_2^+ ions enters a thin single crystal in the direction of the close-packed axis, the molecule disintegrates inside the crystal, but protons continue to move in a correlated form in adjacent channels. The angular and energy distributions of particles escaping the crystal carry important information about the interaction of such protons with the medium.

EXHIBITIONS

EXHIBITION "RADIOISOTOPE STATIC-ELECTRICITY NEUTRALIZERS" AT THE EXHIBITION OF ACHIEVEMENTS OF THE NATIONAL ECONOMY OF THE USSR

K. A. Nekrasov

This Exhibition was held from Sept. 1-Oct. 15, 1975. Radioisotope static-electricity neutralizers are intended to remove electric charge from electrified materials during their processing in various technological installations. This problem has become especially important in recent years with the increasing amounts of artificial and synthetic materials being processed and the intensification of existing technological processes. The radioisotope neutralizers produced by Soviet industry constitute the most effective means of combating static electrical charges. By comparison with earlier electrical and inductive neutralizers these have a number of important advantages: They contain no electrical supply source, they are portable, convenient in assembly, operation, and servicing, they are very reliable, operate for a long time without repair, and are entirely safe to use in fire-hazard sites.

The scientific-research institutes, together with industrial organizations, have developed and started routine production of radioisotope neutralizers based on radioactive isotopes such as ^{239}Pu, ^{147}Pm, and tritium. In recent years the production of radioisotope neutralizers has greatly increased: In 1964 about 800 of these devices were in use, now there are more than 14,000. The neutralizers are used in the textile, polygraphic, rubber-technology, chemical, and a variety of other branches of industry. The materials of the exhibition revealed that in the textile and polygraphic industries of Moscow alone some 80 undertakings were now equipped with radioisotope static-electricity neutralizers. The exhibition presented full-scale samples of the following models NSÉ-200A, NSÉ-400A, NRI-5, NRI-7N, NR-5N, NR-8N, NR-11N, NR-11V, NR-12N, NR-13N, NR-13V, NR-14V, NR-1, 2, NR-3, 4, NR-6, NR-9V, NR-9N, NR-10V and NR-10N, and also the new forms NTSÉ-15 and NTSÉ-16 (with a tritium source of radiation) developed by the Institute of Nuclear Studies, Academy of Sciences of the Ukrainian SSR. The annular economic effect due to the introduction of the tritium neutralizers is 2.5-3 thousand rubles. The time required to cover the capital outlay is 3-6 months. The NTSÉ neutralizers create no radiation and may therefore be used in the production of motion-picture photographic materials.

The M. V. Lomonosov Moscow Institute of fine chemical technology exhibited radioisotope neutralizers PRIN-2 and PRIN-3, which greatly increase efficiency in the removal of static electrical charges. The Exhibition gave a leading place to the use of radioisotope neutralizers in various branches of industry. The Leningrad "Red Triangle" Industrial Corporation uses radioisotope neutralizers based on ^{239}Pu for removing static electrical charges from the surface of fabric being processed in a gluing machine. The neutralizer consists of a cassette accommodating 15-20 ^{239}Pu sources; it is stable, long-lasting, easy to service, and safe in operation; it prevents fire from developing. The economic effect gained by the use of this neutralizer is 5000 rubles per year. In the technological equipment of the Rose Lyuksemburg "Red Rose" Moscow Silk Corporation there are 129 radioisotope static-electricity neutralizers; 40 devices of the NRI-3 and NRI-5 type are used in the warp machines, which greatly improves the quality of the warps in the warping process; 89 devices of the NSE-200A and NSE-400A type are used in the sorting of the raw materials and in finishing the fabric. The economic effect averages 1500 rubles per year for one instrument.

In the P. Zibertas Order of the Workers' Red Banner Silk Corporation, NSÉ radioisotope neutralizers of the NRI types were installed in five weaving machines in 1974; this reduced the breaking of the warps, increased labor efficiency by 1.8%, and improved warp quality. The servicing zone was increased and so was the output of the weavers. An annual economy of 64.7 thousand rubles was achieved.

Translated from Atomnaya Énergiya, Vol. 39, No. 6, pp. 444-445, December, 1975.

In the Busevsk Glass-Fiber Factory, as a result of the use of NSÉ-140 and NSÉ-350 neutralizers in the warp machines a break-free technological process of warping the fibers was achieved in the production of glass cloth. This ensured a high quality of the glass cloth so produced. The NSÉ-140 and NSÉ-350 neutralizers are placed very close to the moving fiber. The use of 18 neutralizers of the NSÉ-400A and NSÉ-200A types in a single technological line for the finishing of glass cloth reduced the static electrical voltage to 2000-3000 V/cm^2 (up to 8000 being tolerated). The efficient reduction of charge prevents explosions and fires in the room used for purifying the glass cloth from paraffin in benzene vapor.

The Exhibition showed that radioisotope static-electricity neutralizers are widely employed in explosion-hazardous production processes of the petrochemical and oil-refining industries, for the water-free degassing of rubbers, the production of adhesive tape, in the manufacture of polypropylene, and in the gluing of fabrics. The economic effect obtained from the introduction of radioisotope static-electricity neutralizers in the undertakings of the Ministry for the Petrochemical Industry was more than 500 thousand rubles a year.

The Sverdlovsk Plastics Factory has also installed 25 radioisotope neutralizers, which have completely removed static electric charges from polymer films, greatly improving the quality of the manufacture as well as aiding safety precautions in the work rooms, while still observing the health and hygiene radiation-safety norms. The neutralizers are installed on machines producing hard films of polyvinyl chloride and transparent adhesive polyvinyl chloride protective films, and also on machines used for producing diagrams on polyethylene. The factory uses 21 systems of NSÉ and NR neutralizers, which almost entirely remove static electric charges from the surface of artificial leathers. Before the introduction of the neutralizers the static electric voltage amounted to an average of 15-28 kV/cm^2; afterwards it fell to 0.02-0.4 kV/cm^2.

In the Voronezh Branch of the All-Union Scientific-Research Institute of Synthetic Rubber there are six neutralizers of the NR-7N and NSÉ-400A types in the water-free degassing installations (two-roll drying apparatus). According to the static electrical charge present, one, two, or three neutralizers may be employed. The electrical voltage falls from 1000-1500 to 100-400 V/cm^2 and thus eliminates the danger of igniting the solvent vapor.

The Chekhov Polygraphic Corporation uses 108 NSÉ-400 and 40 NSÉ-200 neutralizers in the high and low rotary printing machines PRL-3 and PGL, and in the high printing machines "Viktoriya" and "Planeta T-2D."

The section concerned with ensuring radiation safety in the use of radioisotope static-electricity neutralizers exhibited various products of the Scientific-Research Institute of Labor Hygiene and Prevention of Illness. Instruments for measuring the static electric charge on materials being processed were demonstrated: a portable spark-safe static meter (the SIP), a remote-control spark-safe electrostatic meter (the DÉS), an electrostatic voltage meter (the INÉP-20d), an installation for studying the electrifiability of chemical fibers of the IÉV-2 type, and an instrument for measuring the electrostatic field (the INÉP-1).

SELF-SHIELDING FACILITY FOR THE MODIFICATION OF TISSUE AND POLYMER FILMS WITH AN ELECTRON ACCELERATOR BASED ON THE RUP-400 X-RAY EQUIPMENT

I. I. Buslaev, N. G. Kon'kov,
O. N. Kochetov, and S. Yu. Krylov

The present-day state of high-powered accelerator technology permits its even more widespread use for the industrial irradiation of materials for the purposes of imparting new properties to them, modification of textile materials, strengthening of coverings, etc. Electron accelerators at energies of 0.3-1.5 MeV find the most widespread application for these purposes. The achievement of a number of radiation processes can be economically advantageous only by the use of an accelerator with an energy of order 0.4 MeV. Similar accelerators are used also for scientific research. Papers [1, 2] describe an electron accelerator constructed on the basis of the RUP-400 x-ray facility. In the All-Union Scientific-Research Institute of Radiation Technology, a facility has been developed and constructed with an electron accelerator based on the series-produced RUP-400-5-1 x-ray apparatus at a nominal energy of 350 keV. The facility is designed for laboratory and semi-industrial investigations on radiation modification, with a beam of accelerated electrons, of cotton tissues and polymer films; it can be used also for strengthening coverings, initiation of reactions in the gas phase, etc. In the case when a target is installed, the accelerator can serve as a source of powerful bremsstrahlungen.

The facility (see Fig. 1) consists of an accelerator with a vacuum system and a scanning device 1, a local biological shield 2 with opening protective panels 3, a control desk 4, where the accelerator power supplies and scanning systems are assembled, all the control elements and the automation and locking systems. The accelerator in the transformer-unit 5 of the RUP-400 x-ray facility with an improved 1.5 VPV2-400 x-ray tube. The beam of electrons, after passing through the focusing lens, arrives in the field of the magnet 6 of the scanning device and then is incident on the outlet window 7.

The biological shield provides easy access to all units of the facility. It is made from lead, with a thickness of 15-45 mm in a steel cladding. The facility is made self-shielding and it can be assembled without any major problems in almost any production or laboratory location.

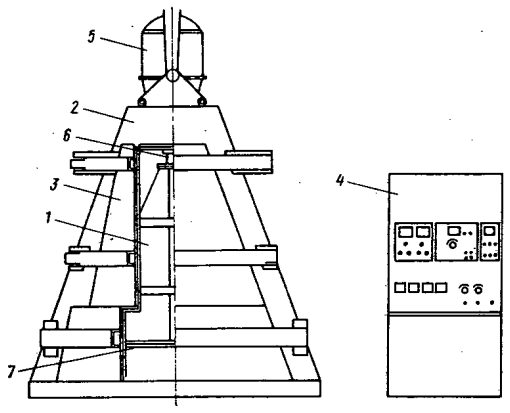

Fig. 1. Diagram of equipment based on the RUP-400-5-1.

The required vacuum in the tube and the electron guide is achieved by means of a magnetic electric-discharge pump. Initial pumping-out of the system is carried out with a mechanical pump with a nitrogen trap. The scanning device is of the electromagnetic scanning type with a sawtooth field. The power supply of the scanning device is a thyrister square wave voltage inverter. The lens focusing is armored and of short focus. The feed current is pulsed with a frequency of 25 Hz. The outlet window of the accelerator is made of titanium foil, 20-50 μ thick and is cooled by compressed air. The power supply system allows the energy of the beam of accelerated electrons to be varied from the control desk, independently of the current and the length of the sweep band. The automation and locking system switches off the

Translated from Atomnaya Énergiya, Vol. 39, No. 6, p. 446, December, 1975.

accelerator in the case of vacuum impairment in the tube, in the absence of cooling air, and in the absence of a deployed beam. The accelerator cannot be switched on with open or incompletely closed protective panels.

For passing the material being irradiated below the scanning device, a system of rollers without drive is used, which allows the material to be irradiated in three layers with a distance between layers of not more than 15 mm. In order to introduce the material into the irradiation zone and to remove it, there are two labyrinth slits with a width of 10 mm. The characteristics of the facility are:

Nominal energy of accelerated electrons, keV	350
Limits of energy control, keV	200-400
Max. current of extracted beam of electrons, mA	1.5
Freq. of variation of deflecting field, Hz	1000
Length of sweep band, cm	30-100
Nonuniformity of current density along sweep band, %	±10
Required power, kW	7
Supply voltage, V	220/380
Freq., Hz	50
Air flow rate, liter/sec	15
Dimensions of facility, m	2.5 × 2.5 × 3.7
Mass of facility, kg	5000

LITERATURE CITED

1. D. M. Margolin and L. A. Vasil'ev, in: Problems of Physical Chemistry [in Russian], No. 3, Moscow (1963), p. 134.
2. L. V. Chepel' et al., in: Radiation Chemistry [in Russian], Atomizdat, Moscow (1972), p. 501.

P. Ya. Antropov

THE FUEL AND POWER POTENTIAL OF THE EARTH*

Reviewed by Yu. I. Klimov

This book is a summary of fundamental research and correlates much material on sources of oil, gas, coal, and nuclear energy resources. It includes a general survey of the fuel and power potential of the earth and describes the geological concepts pertaining to the fuel and power potential. Special attention is paid to a survey of the oil and gas bearing regions of the earth including three divisions: the main oil and gas regions of the USSR (the Eastern region of European Russia, West Siberia, Central Asia and Kazakhstan); the main oil and gas regions of the capitalist and developing countries (the Near and Middle East, Africa, and America); and shelves and seas. About 40% of the book is a survey of uranium deposits in the capitalist and developing countries (Europe, Asia, Africa, America, Australia, and New Zealand).

This book acquires a special value because of the recently developed tensions in the fuel and power balance in a number of Western countries. Unfortunately, the material on which the book is based is largely limited to data published up to 1970. Owing to the energy crisis of 1973-1974, there have recently been a large number of publications, especially on nuclear energy resources, the promising role of which in the energy available to mankind is exceedingly important.

On the basis of his material, the author looks with optimism on the problem of energy supply. The book will certainly be of use to specialists in fuel and power resources.

*Izd. VINITI, Moscow (1974).

Translated from Atomnaya Énergiya, Vol. 39, No. 6, p. 447, December, 1975.

V. A. Artsybashev and G. A. Ivanyukovich

DENSITY GAMMA–GAMMA LOGGING IN ORE DEPOSITS*

Reviewed by E. M. Filippov

At present, x-ray radiometric logging (XRL) and selective gamma–gamma logging (GGLS) are extensively used to study ore boreholes. The depth of investigation of the rocks and ores by these methods is small, of the order of 1 mm for XRL and 3-5 cm for GGLS. This constitutes one of their important disadvantages. Therefore the successful use of these methods depends on combination with deeper nuclear methods. One such method is density gamma–gamma logging (GGLD) which has a depth of about 8-15 cm. It is described in this book. The book is written by well-known specialists who have a good knowledge of the subject and have made a definite contribution to its development. In a brief and clear form they have set out all the main topics of one-probe GGLD.

The 1st and 2nd chapters contain the necessary information on the physical basis of GGLD, the construction of deep devices, and the commercially produced radiometric apparatus which can be used in GGLD. The 3rd chapter deals with calibration of the apparatus, and describes a monitor and calibration device developed by the authors and the method of using it. The 4th chapter deals with the influence of disturbing factors on the results of GGLD. The next chapter gives basic information on the method of measurement with GGLD apparatus. The 6th and last chapter discusses the main principles necessary for interpretation of logging diagrams obtained by the method.

The book is not without its faults.

On p. 6 the authors advocate registration of scattered radiation by scintillation counters of the maximum possible size. In determining the densities of ores and rocks, one usually measures the scattered radiation with energies of at most 300-400 keV. To register such radiation the optimum scintillators have diameters and lengths of 20-40 mm. Even for good spectrometry of gamma radiation in the 100-400 keV range, it is not recommended that NaI(Tl) scintillators should be used with dimensions greater than 48 × 50 mm (see, for example, "Applied Spectrometry of Ionizing Radiations" by E. L. Stolyarova).

On p. 19 the authors recommend that GGLD measurements should be made by compound screens with thin parts near the source and thick parts near the detector. In fact these screens should be just the other way around. This follows directly from the physics of interaction of radiation with matter: absorption of harder primary radiation always needs thicker screens than radiation scattered by the medium being measured. To support their conclusions the authors usually refer to a special experiment, which must evidently have been incorrectly performed.

On pp. 17-18, Fig. 5b gives the threshold gamma spectrum, not the integral spectrum as stated by the authors. For the integral spectrum the curves should not tend to zero, as in this figure, but to some asymptote.

Curve 4 in Fig. 9 clearly corresponds to a completely exposed layer of absorbent.

The division of probes into 2π and 4π is especialy mathematical and the terms are wrongly used. These probes should more correctly be called probes with sectorial and circular coverage.

It would have been more logical to put §3 of Chap. 2 into the 3rd chapter.

There are no references to the specialist book by G. D. Varvarin and E. M. Filippov, "The Density Gamma–Gamma Method in Geophysics" and the monograph by E. M. Filippov, "Nuclear Geophysics."

*Atomizdat, Moscow (1975).

Translated from Atomnaya Énergiya, Vol. 39, No. 6, p. 447, December, 1975.

The authors discuss only the one-probe method of GGLD. Astonishingly enough, in application to ore boreholes they have done quite a lot of original work on the two-probe GGLD method. A description of this method would not have made the book much longer, and would have undoubtedly been an improvement.

These criticisms are of detail, and do not spoil the general impression of a book written by authors who know what they are talking about. The publication of the book is very timely, because practical workers and even some researchers have recently been taking a not altogether correct view of GGLD.

The book will be useful to practical engineers and to research workers, as well as students of nuclear geophysics.

INDEX

SOVIET ATOMIC ENERGY

Volumes 38-39, 1975

SOVIET ATOMIC ENERGY
Volumes 38-39, 1975

(A translation of Atomnaya Énergiya)

E

F

G

I

K

L

M

N

O

P

R

S

SOVIET ATOMIC ENERGY

Volumes 38-39, 1975

(A translation of Atomnaya Energiya)

Volume 38, Number 1 January, 1975

Volume 38, Number 2 February, 1975

Volume 38, Number 3 March, 1975

Volume 38, Number 4 April, 1975

Engl./Russ.

Volume 38, Number 6 June, 1975

Volume 39, Number 1 July, 1975

Volume 39, Number 2 August, 1975

Volume 39, Number 3 September, 1975

Volume 39, Number 4 October, 1975

Engl./Russ.

Volume 39, Number 5 November, 1975

Volume 39, Number 6 December, 1975

The Plenum/China Program

Research in the medical, life, environmental, chemical, physical, and geological sciences from the People's Republic of China

The 15 major scientific journals published in China since the Cultural Revolution are being made available by Plenum in authoritative, cover-to-cover English translations under the Plenum/China Program imprint.

These important journals contain papers prepared by China's leading scholars and present original research from prestigious Chinese institutes and universities. Their editorial boards are affiliated with such organizations as the Chinese Chemical Society, the Academia Sinica in Peking and its Institutes, and the Chinese Microbiological Society.

The English editions are prepared by scientists and researchers, and all translations are reviewed by experts in each field.

Journal Title	No. of Issues	Subscription Price
Acta Astronomica Sinica	2	$65
Acta Botanica Sinica	4	$95
Acta Entomologica Sinica	4	$95
Acta Genetica Sinica	2	$65
Acta Geologica Sinica	2	$75
Acta Geophysica Sinica	4	$95
Acta Mathematica Sinica	4	$75
Acta Microbiologica Sinica	2	$55
Acta Phytotaxonomica Sinica	4	$125
Acta Zoologica Sinica	4	$125
Geochimica	4	$110
Huaxue Tongbao — Chemical Bulletin	6	$95
Kexue Tongbao — Science Bulletin	12	$175
Scientia Geologica Sinica	4	$125
Vertebrata PalAsiatica	4	$95

For further information, please contact the Publishers.

SEND FOR YOUR FREE EXAMINATION COPIES

plenum
PLENUM PUBLISHING CORPORATION
227 West 17 Street, New York, N.Y. 10011
In United Kingdom 8 Scrubs Lane, Harlesden, London, NW10 6SE, England

Declassified and Approved For Release 2013/09/24 : CIA-RDP10-02196R000400060005-0